UC San Diego
UC San Diego Electronic Theses and Dissertations

Title
Interrogating Hippo Pathway Regulation Using Novel Chemical Probes

Permalink
https://escholarship.org/uc/item/2kf7n9nn

Author
Fu, Vivian

Publication Date
2020

Peer reviewed|Thesis/dissertation

eScholarship.org Powered by the California Digital Library
University of California

UNIVERSITY OF CALIFORNIA SAN DIEGO

Interrogating Hippo Pathway Regulation Using Novel Chemical Probes

A dissertation submitted in partial satisfaction of the
requirements for the degree Doctor of Philosophy

in

Biomedical Sciences

by

Vivian Wei-Ming Fu

Committee in charge:

Professor Kun-Liang Guan, Chair
Professor Alexandra Newton, Co-Chair
Professor Gen-Sheng Feng
Professor Jorge Silvio Gutkind
Professor Scott Lippman
Professor Paul Mischel

2020

©
Vivian Wei-Ming Fu, 2020
All rights reserved.

The Dissertation of Vivian Wei-Ming Fu is approved, and it is acceptable in quality and form for publication on microfilm and electronically:

_____

_____

_____

_____

_____

_____
Co-Chair

_____
Chair

University of California San Diego
2020

DEDICATION

In memory of Martin K. Belles, a lifelong mentor and friend,
who lit an 8th grader's first sparks of scientific curiosity
with college-level teachings of explosive nucleosynthesis,
and whose eloquent candor, pursuit of excellence, and passion for life
(still) inspire me beyond words.

EPIGRAPH

“To copy the truth can be a good thing, but to invent the truth is better, much better.”

-Giuseppe Verdi

TABLE OF CONTENTS

Signature Page……..…iii

Dedication……iv

Epigraph……v

Table of Contents……..…vi

List of Figures and Tables……viii

Acknowledgements…….....ix

Vita…….....x

Abstract of the Dissertation……xi

Chapter 1: Introduction to the Hippo Pathway……1

1.1 Overview of the Hippo Pathway……..……..1

1.2 Upstream Signals Regulating the Hippo Pathway…….……....5

1.3 The Hippo Pathway in Organ Regeneration and Homeostasis……..9

1.4 Hippo Pathway Deregulation in Cancer……....16

1.5 Future Inquiries……20

1.6 Acknowledgements……..21

1.7 References……23

Chapter 2: Characterization of VT01454 as an inhibitor of YAP-driven cancer……..…...33

2.1 Introduction……...33

2.1.1 The Hippo Pathway as a Therapeutic Target…….....34

2.1.2 Current Small-Molecule YAP-TEAD Inhibitors……..35

2.2 Results……...37

2.3 Discussion……40

2.4 Experimental Procedures……....41

2.5 Acknowledgements……..45

2.6 References……63

Chapter 3: Target Identification and Mechanism of Action for the YAP Inhibitor VT01454……..66

3.1 Introduction……66

3.1.1 Affinity-Based, Bioorthogonal Methods for Small-Molecule Target Deconvolution……..66

3.1.2 Introduction to Phosphoinositide Metabolism……69

3.1.3 Phosphoinositol-4-Kinase (PI4K) family, the Sac1 phosphatase, and phosphoinositol-4-phosphate (PI4P) metabolism……69

3.1.4 Phosphoinositide Transfer Proteins alpha and beta (PITPα/β)……...71

3.2 Results……...73

3.3 Discussion……82

3.4 Future Inquiries……83

3.5 Experimental Procedures……85

3.6 Acknowledgements……92

3.7 References……..…105

Chapter 4: Conclusion……112

4.1 Conclusion and Future Directions……...112

4.2 References……..…115

LIST OF FIGURES AND TABLES

Figure 1.1: The Hippo Pathway integrates various signals to regulate YAP/TAZ activity……..…..22

Table 2.1: Structures of Compounds Reported to Modulate Hippo Pathway Activity…….46

Figure 2.1: Microcolin B is a YAP inhibitor…….....47

Figure 2.2: VT01454 induces YAP phosphorylation through core Hippo pathway components……..48

Figure 2.3: VT01454 exhibits potent and specific cytotoxicity in YAP-dependent uveal melanoma cell lines…….....50

Figure S2.1: Chemical library screen for YAP inhibitors……..53

Figure S2.2: MCB induces selective cytotoxicity in YAP-dependent uveal melanoma cell lines…….55

Figure S2.3: LCMS Reports of Intermediate 4, Intermediate 5, and Compound 6……..57

Figure 3.1: PITPα/ß are the major biochemical targets of VT01454……93

Figure 3.2: PITPα/ß are the major functional targets of VT01454 that mediate YAP phosphorylation…….95

Figure 3.3: A plasma membrane pool of PI4P regulates YAP phosphorylation……97

Figure 3.4: BioID using P4M-SidMx2 as bait identifies MAP4K6 and MAP4K7 as PI4P-proximal proteins……....99

Figure S3.1: Trifunctional 545-biotin-azide click reaction and streptavidin pulldown……100

Figure S3.2: VT01454 has no effect on PI3P and PI(4,5)P2 localization……101

Figure S3.3: Partial List of Mass Spectrometric Analyses for Target Identification and BioID……104

Figure 4.1: Summarizing Model Depicting Mechanism of Action for a Novel YAP Inhibitor……114

ACKNOWLEDGEMENTS

I'd first like to thank my thesis advisor and mentor Dr. Guan for his unending patience with my scientific development, for giving me the opportunity to embark on a high-risk and ultimately high-reward project, and for giving me the creative space and freedom in driving and executing a project whose critical points of breakthrough largely took place outside of the lab's traditional wheelhouse.

I'd like to thank all past and present members of the Guan lab for their support as some of the friendliest and most easygoing colleagues I've had the pleasure of working with thus far. In particular, I want to thank Guangbo Liu for spearheading the chemical library screen that singled out Microcolin B, Audrey Hong for her technical help as a scientist and for her emotional support as a friend, Matt Franklin for lending his expertise in imaging (and in free-food-hunting across the building), Jenna Jewell who was my first mentor even before I joined the lab, and Zhipeng Meng for being my last mentor and for being not only a walking encyclopedia of scientific knowledge (really, he could give the Lehninger textbook a run for its money), but also for becoming a wonderful friend over the years.

I'd also like to thank my collaborators: Esther Kemper for singlehandedly ensuring 2 years ago that my project wasn't going to die, the Dixon lab for fantastic scientific discussions at our joint lab meetings, Vivace Therapeutics, and the Gerwick lab; and last but certainly not least, I'd like to thank my thesis committee for their long-term mentorship and valuable scientific input over the years.

Finally, I'd like to thank all of my friends, former mentors, and family whose direct, indirect, and oftentimes long-distance support have kept me sane over the last five years. To my Dharma family at Chung Tai Zen Monastery – thank you for inspiring me to live with compassion, clarity, and mindfulness. To my yoga guru Sherry – thank you for teaching me "the gift that I can give myself for the rest of my life." To my parents, two of my biggest blessings in life whose fierce lifelong support empowered me to pursue classical training as a violin performance major, subsequently start a biochemistry degree from scratch, and ultimately embark on a PhD program – thank you for all that you did to foster the fearless pursuit of my passions in each stage of life, for encouraging me to reinvent my perceived failures as singular opportunities for intensive growth, and for being my point of entry to leading a more meaningful existence through the Buddhist teaching. To David, who is now an honorary Hippo pathway expert after 3 years of late-night lab runs and countless discussions of the YAP mobility shift on my gels – thank you for exuding light, optimism,

and patience ~~even~~ especially at my rock-bottoms, for inspiring me to realize the best version of myself, and for re-humanizing an often-robotized scientist-in-desperation with hugs, cupcakes, and belly laughs. You are my sunshine.

Chapter 1 Section 1.3 “The Hippo Pathway in Organ Regeneration and Homeostasis” is a partial reprint of the material as it appears in Current Opinion in Cell Biology; Fu, V., Plouffe, SW., Guan, K-L. Elsevier Publishing Group, 2017. The dissertation author was the primary author of this paper.

Chapters 2 and 3 are currently being prepared for submission for publication of the material. Fu, V., Liu, G-B., Kemper, EK., Li, F-L, Mayfield, JE., Peng, X., Konradi, AW., Tang, TT., Dixon, JE., Cravatt, BF., Gerwick, WH., Guan, K-L. The dissertation author was the primary investigator and author of this material.

VITA

2009-2014 Bachelor of Arts, Rice University

2014-2020 Doctor of Philosophy, University of California San Diego

PUBLICATIONS

Fu, V., Liu, G-B., Kemper, E., Li, F-L, Mayfield, J., Tang, T., Meng, ZM., Cravatt, B., Guan, K-L. Interrogation of Hippo Pathway Regulation using Novel Chemical Probes, manuscript in preparation.

Fu, V., Guan, K-L. Tales from the Cryptkeeper: New Roles for Lats1/2 in Wnt-driven Homeostasis. Cell Stem Cell. 26: 612-614

Jewell, JL., Fu, V., Hong, A., Yu, F-X., Meng, D., Melick, C., Wang, H., Lam, WM., Yuan, H-X., Taylor, S., Guan, K-L. (2019) GPCR signaling inhibits mTORC1 via PKA phosphorylation of Raptor. eLife. 8: e43038

Fu, V., Plouffe, SW., Guan, K-L. (2017) The Hippo pathway in organ development, homeostasis, and regeneration. Current Opinion in Cell Biology. 49: 99–107

Fu, V., Moroishi, T., Guan, K-L. (2016) Glycoholics Anonymous: Cancer Sobers up with mTORC1. Cancer Cell. 29: 432-434

FIELDS OF STUDY

Major Field: Biomedical Sciences
Studies in Pharmacology
Professor Kun-Liang Guan

ABSTRACT OF THE DISSERTATION

Interrogating Hippo Pathway Regulation Using Novel Chemical Probes

By

Vivian Wei-Ming Fu

Doctor of Philosophy in Biomedical Sciences

University of California San Diego, 2020

Professor Kun-Liang Guan, Chair
Professor Alexandra Newton, Co-Chair

We herein describe a PITPα/β-PI4KIIIα-MAP4K signaling axis that modulates the Hippo pathway in response to plasma membrane PI4P levels. Our study highlights a novel role for PITPα/β in regulating the Hippo kinase cascade through the identification of VT01454, a small-molecule inhibitor and Microcolin B analog that induces YAP phosphorylation. We characterize VT01454 as both a potent and specific YAP inhibitor, use bio-orthogonal methods to identify PITPα/β as the unequivocal targets of VT01454, and functionally validate the role of PITPα/β in Hippo signaling by genetic deletion in HEK293A cells. Finally, we demonstrate that VT01454 inhibition of PITPα/β regulates the Hippo pathway by modulation of a plasma membrane pool of PI4P, and that MAP4K6/7 are potential PI4P-interacting proteins.

Chapter 1: Introduction to the Hippo Pathway

1.1 Overview of the Hippo Pathway

The Hippo pathway is a universal governor of organ size, tissue homeostasis, and regeneration. Its evolutionary conservation as a fundamental mechanism supporting multicellularity has sparked considerable interest in understanding its physiological function and molecular regulation. Two decades of intense research has established the Hippo pathway as a cardinal regulator of organ size and tissue homeostasis, and expanded the Hippo kinase cascade into a complex signaling network integrating diverse signals such as cell adhesion and polarity, soluble factors, stress signals, and mechano-transduction (Yu and Guan, 2013). The same cellular properties both regulating and regulated by the Hippo pathway (e.g. cell proliferation, survival, competition, among others) also define tumorigenesis upon their dysregulation. The impact of the deregulated Hippo pathway on cancer development is thus of little surprise, and warrants continued investigation of the functions and regulatory mechanisms of this pathway to identify new therapeutic targets.

1.1.1 The Hippo Pathway in Drosophila

Discovery of the Hippo pathway in *Drosophila* was a pivotal point of entry to understanding the molecular mechanisms that govern organ growth during development and regeneration. In 1995, two studies independently observed that deleting the *Warts (wts)* gene induced a dramatic overgrowth phenotype in multiple *Drosophila* tissues (Justice et al., 1995, Xu et al., 1995). A flurry of genetic studies that followed further identified *Salvador (sav), Hippo (hpo),* and *Mob as tumor suppressor (mats)* as equally consequential mutants that likewise resulted in tissue overgrowth, phenocopying the effects of the *wts* mutant clone. This striking organ size phenotype elicited by *hpo, wts, sav,* and *mats* mutations was unprecedented in previously established developmental pathways. Thus, upon elucidating their genetic and physical interaction, Hpo, Wts, Sav, and Mats were grouped into a new signaling module coined the “Hippo” pathway, owing to the hippopotamus-like appearance of the *hpo* mutant organs. *Yorkie (yki)*, the Hippo pathway’s leading functional effector, was later identified in a screen for Wts-interacting proteins (Huang et

al., 2005). Briefly, the Hpo-Sav complex phosphorylates and activates the Wts-Mats complex, which in turn phosphorylates and inhibits Yki, a transcriptional coactivator that regulates gene transcription by binding its key partner and transcription factor Scalloped (Sd) (Goulev et al., 2008, Wu et al., 2008, Zhang et al., 2008, Zhao et al., 2008), thereby mediating the Hippo pathway's biological functions.

1.1.2 The Mammalian Hippo Pathway

Mammalian Orthologs of the Hippo pathway

The Hippo pathway is highly conserved in mammals (Figure 1.1). The mammalian orthologs of *Hpo, Sav, Wts, and Mats,* and *Yki* are Mammalian Sterile 20-like kinases 1 and 2 (MST1/2, also called STK4/3), Salvador homolog 1 (SAV1), large tumor suppressor 1 and 2 (LATS1/2), and MOB kinase activator 1A and 1B (MOB1A/B), which regulate the downstream effectors Yes-associated protein (YAP) and transcriptional co-activator with PDZ-binding motif (TAZ, also called WWTR1). Much like Yki, the transcriptional coactivators YAP/TAZ are unable to directly bind DNA, and instead bind the TEAD family of transcription factors (TEAD1-4, orthologs of Sd). The transcriptional activity of YAP/TAZ is regulated in the nucleus by Vestigial-like family member 4 (VGLL4), which directly competes with YAP/TAZ for TEAD binding and results in inhibition of YAP-regulated transcription (Zhang et al., 2014a).

Transcriptional Regulation by YAP/TAZ

YAP and TAZ drive the transcriptional output of the Hippo pathway by binding to and activating the TEAD1-4 transcription factors. Mechanistically, YAP/TAZ recruit components of either the SWI/SNF chromatin remodeling complex or the NCOA6 histone methyltransferase complex to stimulate TEAD transcriptional activity (Qing et al., 2014, Skibinski et al., 2014). Of note, the YAP/TAZ-TEAD complex can also act as transcription co-repressors by recruiting the NuRD histone deacetylate complex, targeting additional genes such as DDIT4 (Kim et al., 2015) and Trail or ΔNp63 (Valencia-Sama et al., 2015).

The YAP/TAZ-TEAD complex transcriptionally activates a host of genes reviewed in detail elsewhere (Zhu et al., 2015). Recent deep sequencing efforts have attempted to elucidate YAP/TAZ transcriptional activity on a genome-wide scale, leading to unanticipated functions of YAP/TAZ in

transcriptional regulation. Though YAP/TAZ had previously been associated with TEAD binding at promoter regions of their target genes (Lian et al., 2010), recent ChIP-seq (chromatin immunoprecipitation combined with deep sequencing) studies in multiple cancer and non-transformed cell lines revealed that the majority of YAP/TAZ-TEAD complexes in fact bind to distal enhancer regions to activate gene transcription (Zanconato et al., 2015, Stein et al., 2015, Galli et al., 2015). De novo motif analyses at YAP/TAZ peaks identified a significant enrichment of the AP-1 transcription factor consensus motif at YAP-binding regions, suggesting that YAP/TAZ-TEAD and AP-1 cooperate to activate target genes in a synergistic manner (Stein et al., 2015, Zanconato et al., 2015). Consistent with this notion, AP-1 enhances YAP/TAZ-induced mammary epithelial cell growth, while YAP/TAZ deletion abrogates AP-1-driven tumorigenesis (Zanconato et al., 2015). In a separate study using global chromatin occupancy analyses, YAP was found to control transcriptional pause release by interacting with and recruiting the Mediator complex to enhancers, which in turn recruits the CDK elongating kinase (Galli et al., 2015). Furthermore, treatment with a CDK9 kinase inhibitor prevented YAP-driven hepatomegaly, corroborating the global chromatin analysis data.

Collectively, these genome-wide studies delineate a model for YAP/TAZ-regulated gene expression, where TEAD mediates YAP/YAZ binding to distal enhancers as well as promoters and YAP/TAZ in turn cooperate with AP-1 and/or additional regulators to stimulate de novo transcription initiation and enhance transcription elongation, thereby stimulating target gene expression. Given the role of YAP/YAZ in stem cell development and tissue homeostasis, future ChIP-seq analyses of YAP/TAZ-TEAD in stem or primary tissue progenitor cells would provide significant insight into the mechanisms by which a YAP/TAZ-mediated transcriptional program coordinates downstream gene expression to regulate organ development and homeostasis (Meng et al., 2016).

Regulatory Mechanisms of YAP Activity and the Core Hippo Kinases

LATS1/2 serve as the most direct level of control for YAP activity through inhibitory phosphorylation. YAP contains 5 phosphorylation sites harboring LATS1/2 target consensus motifs (HxRxxS). Phosphorylation of YAP on serine-127 (S127) initiates a 14-3-3 binding site, leading to cytoplasmic sequestration upon 14-3-3 binding. Phosphorylation on serine-381 (S381) induces a second phosphorylation event by casein kinase (CK1δ/ε) while stimulating a phosphodegron, leading to the

recruitment of $SCF^{beta\text{-}TRCP}$ E3 ligase and subsequent ubiquitination and proteasomal degradation of YAP (Zhao et al., 2010). Thus, LATS1/2 regulates both YAP subcellular localization and protein stability, enabling fine spatiotemporal control of its transcriptional activity. It is worth noting that YAP/TAZ can also be phosphorylated by other kinases such as cyclin-dependent kinase 1 (CDK1), Jun N-terminal kinases (JNK), homeodomain-interacting protein kinases (HIPK), ABL, and Src family tyrosine kinases (Varelas, 2014), suggesting that YAP/TAZ can be regulated by Hippo-pathway-independent mechanisms.

MST1/2 in turn serve as direct activators of LATS1/2, regulating their kinase activity through several mechanisms. First, MST2 phosphorylates LATS1 at its C-terminus hydrophobic domain on threonine-1079 (T1079), stimulating autophosphorylation of its activation loop to increase its kinase activity (Tamaskovic et al., 2003, Stegert et al., 2004). Second, MST1/2 phosphorylate MOB1, enhancing MOB1 binding to the LATS1/2 autoinhibitory domain (Callus et al., 2006, Chan et al., 2005, Praskova et al., 2008). Phosphorylated MOB1 allosterically promotes LATS1/2 autophosphorylation at serine-909 (S909) of its activation loop, which is required for LATS1/2 activation following its initial phosphorylation at T1079. MST1/2 additionally phosphorylate SAV1, which acts as a scaffold for MST1/2 in promoting LATS1/2 recruitment and phosphorylation (Callus et al., 2006, Tapon et al., 2002). Two groups of mitogen-activated protein kinase kinase kinase kinases (MAP4Ks), MAP4K1/2/3/5 (homologs of *Drosophila* Happyhour) and MAP4K4/6/7 (homologs of *Drosophila* Misshapen), were recently discovered as additional core Hippo components acting in parallel to MST1/2 to directly phosphorylate and activate LATS1/2 at its hydrophobic motif (Meng et al., 2015). Finally, neurofibromin 2 (NF2) can directly interact with and recruit LATS1/2 to the plasma membrane for phosphorylation by the MST1/2-SAV1 complex (Yin et al., 2013). It is worth noting that there may be additional kinases (particularly STE20 family members) that can activate LATS1/2 in a tissue-specific and upstream signal-specific manner.

While numerous studies have identified various components of the peripheral Hippo network, the upstream regulation of MST1/2 and the MAP4Ks remains an ongoing area of inquiry. The TAO kinases (TAOK1/2/3) phosphorylate and activate MST1/2 at their activation loop (T183 for MST1 and T180 for MST2) (Boggiano et al., 2011, Poon et al., 2011), while other reports have also shown that MST1/2 can autophosphorylate and dimerize, thereby enhancing activation loop phosphorylation (Praskova et al., 2008, Glantschnig et al., 2002). The Ras-related GTPase RAP2 was recently reported to bind and activate

MAP4K4/6/7 in response to ECM rigidity (Meng et al., 2018). Most recently, our lab delineated a mechanism in which the striatin (STRN)-interacting phosphatase and kinase (STRIPAK) complex regulates MST1/2 and MAP4Ks through inactivating binding by protein phosphatase 2A catalytic subunit (PP2AC) (Chen et al., 2019). Given the Hippo pathway's extensive implications in tumorigenesis, continuing to decode the front lines of its molecular regulation is an area of considerable therapeutic potential and interest.

1.2 Upstream Signals Regulating the Mammalian Hippo Pathway

The core Hippo kinases regulate YAP/TAZ in response to a myriad of upstream intra- and extracellular signals. While peripheral components of the Hippo network generally mediate these signals by modulating the phosphorylation status of the core Hippo kinases, there are also a number of other proteins that directly regulate YAP localization or activation independently of LATS kinase activity (Yu and Guan, 2013). Here we summarize the major upstream signals regulating the Hippo pathway, and the respective peripheral Hippo components transducing each specific cue to the core kinase cascade.

1.2.1 Soluble factors

GPCR Signaling Regulates YAP/TAZ

Tissue growth requires both nutrient uptake, which is regulated by growth-stimulating cues, as well as hormonal signals, which are transduced through autocrine, paracrine, and endocrine mechanisms. As YAP/TAZ primarily serve to promote cell growth, it had long been speculated that mitogenic hormones and growth factors might regulate the Hippo pathway as a mechanism of controlling tissue growth. G-protein-coupled-receptors (GPCR) are the largest family of membrane receptors that transduce a host of diverse physiological and pathological responses. A major breakthrough in the Hippo field came with the discovery that ligands signaling through GPCRs coupled to $G\alpha_{12/13}$ or $G\alpha_{q/11}$ (e.g. estrogen, thrombin, angiotensin II, lysophosphatidic acid [LPA], sphingosine-1-phosphate [S1P]) activate YAP/TAZ, while ligands signaling through $G\alpha_s$-coupled GPCRs (e.g. epinephrine and glucagon) and protein kinase A (PKA) can repress YAP/TAZ activity (Yu et al., 2012). Curiously, protein kinase C (PKC) activation by $G\alpha_{q/11}$ can both activate

and inhibit YAP/TAZ via conventional or novel PKC, respectively (Gong et al., 2015), thus explaining cell-type specific responses to PKC activation. A series of subsequent studies further demonstrated that GPCR regulation of the Hippo pathway is in fact a universal cellular response to hormonal cues (Miller et al., 2012, Mo et al., 2012, Yu et al., 2013, Gong et al., 2015, Zhou et al., 2015). It is worth noting that GPCR regulation of the Hippo pathway not only demonstrated YAP/TAZ modulation by an array of hormonal signals, but also showcased their capacity to mediate a wide range of physiological regulations and thus their potential for therapeutic targeting by GPCR agonists or inhibitors.

Wnt/β-catenin Pathway Ligands

Crosstalk between the Hippo and Wnt signaling pathways has been extensively studied and summarized by recent reviews (Hansen et al., 2015, Piccolo et al., 2014). In particular, Wnt5a/b are among the GPCR ligands involved in Hippo pathway regulation, and normally activate noncanonical Wnt signaling by binding to the Frizzled receptors, which are class F GPCRs (Anastas and Moon, 2013). A recent study demonstrated that Wnt induced YAP activation through the Frizzled receptors, $G\alpha_{12/13}$, the Rho GTPases, and LATS1/2, while another study revealed APC as a scaffold protein for SAV1 and LATS1 with *Apc* deletion resulting in YAP activation (Park et al., 2015, Cai et al., 2010). Furthermore, Wnt5a/b regulation of YAP/TAZ appears to be required for noncanonical Wnt signaling in mediating cell differentiation and migration, as well as antagonizing canonical Wnt/β-catenin activation (Park et al., 2015).

Epidermal Growth Factor (EGF)

While several reports have shown that EGF and insulin regulate YAP activity through Ras-Raf-MAPK signaling and phosphoinositide-dependent-kinase (PDK1) (Fan et al., 2013, Reddy and Irvine, 2013), other studies reported no significant effects of EGF and IGF on YAP activity, as well as unaffected YAP activity in the presence of PI3K/AKT inhibitors and PDK1-null cells (Zhao et al., 2007, Yu et al., 2012). These inconsistencies could be due to cell-type-dependency or other experimental discrepancies, and warrant further study for clarification.

1.2.2 Cell Adhesion and Polarity

Physical attachment to the extracellular matrix (ECM) is vital to cell growth and survival. Cell attachment to the ECM activates the Rho GTPases or the FAK-Src-PI3K pathway, either of which induce YAP dephosphorylation and nuclear localization (Zhao et al., 2012, Kim and Gumbiner, 2015), and disrupting F-actin antagonizes the effects of cell attachment on both aforementioned phenotypes. Conversely, cell detachment induces YAP phosphorylation and inhibition, ultimately leading to LATS1/2-dependent anoikis (Zhao et al., 2012). It is worth noting that cells expressing a constitutively active YAP exhibited higher levels of survival upon detachment, suggesting that cancer cells with high YAP activity might metastasize by escaping anoikis.

Another critical attribute to cell growth, particularly in epithelium, is cell polarity. Epithelial cells adhere to one another through cell-cell junctions, and these junctions divide the plasma membrane into an apical and basolateral domain with the help of various polarity complexes, thereby establishing apical-basal polarity. Many of these polarity complexes contain known peripheral regulators of the Hippo network such as NF2 (Merlin in *Drosophila*). Furthermore, several adherens and tight junction proteins such as angiomotin (AMOT), protein tyrosine phosphatase nonreceptor type 14 (PTPN14), and α-catenin, can regulate the Hippo pathway by sequestering YAP/TAZ at tight junctions (Yu and Guan, 2013) (Figure 1.1). Consistent with this notion, disrupting adherens and tight junctions in cell culture by extracellular calcium depletion induces YAP/TAZ nuclear localization (Cordenonsi et al., 2011). Thus, cell adhesion and intercellular junction formation serve as additional mechanisms regulating YAP/TAZ activity.

1.2.3 Physical Cues: Cell Contact and Mechanical Signals

Cells in solid tissues communicate with both neighboring cells and the ECM to sense and interpret physical cues from their environment, and cell-cell contact was in fact the first signal discovered to regulate the Hippo pathway (Zhao et al., 2007). In this study, cells cultured at low density exhibited primarily nuclear YAP/TAZ, thereby promoting target gene transcription and cell proliferation, while cells cultured at high density showcased cytoplasmic YAP/TAZ that corresponded to growth inhibition. Mechanistically, cells grown at or past confluence also produced more tight junctions and adherens junctions, both of which mediated LATS activation and subsequent YAP phosphorylation. Under basal conditions, healthy cells cease to proliferate upon physical contact with a neighboring cell. Loss of contact inhibition is a hallmark of

oncogenic transformation; thus, regulation of YAP/TAZ by cell density implicated a critical role for the Hippo pathway not only in contact inhibition but also in tumorigenesis (Ota and Sasaki, 2008, Zhao et al., 2007).

Mechanical cues such as ECM stiffness and cell geometry potently regulate YAP/TAZ, as do related mechanical forces like stretching and edge/curvature changes (Aragona et al., 2013). ECM stiffness controls YAP/TAZ localization through cytoskeletal tension (Dupont, 2016, Driscoll et al., 2015), primarily mediated by the Rho GTPases as well as F-actin capping and severing proteins. The Rho GTPases and F-actin may also serve as a physical checkpoint of cell growth and fate determination during mechano-induced stem cell differentiation (Aragona et al., 2013). Indeed, activating YAP/TAZ by increasing substrate rigidity significantly enhances differentiation of human pluripotent stem cells into motor neuron cells, suggesting a potential application of engineered substrates to generate differentiated cell types of interest (Sun et al., 2014). Interestingly, cell geometry has been posited as a mechanism explaining Hippo pathway regulation by cell density: at low density, cells are more spread out and therefore flatter, leading to YAP activation; in contrast, cells at high density must grow into a rounder and more compact geometric constraint, leading to YAP inactivation (Aragona et al., 2013, Wada et al., 2011).

1.2.4 Cellular Metabolic Status

The transcriptional activity of YAP/TAZ is most widely recognized for promoting cell growth and proliferation, both of which are energy-consuming processes. YAP/TAZ activity must therefore be restricted by regulatory checkpoints governed by metabolic status, and such a mechanism is illustrated in AMPK regulation of Hippo signaling. Under conditions of energy stress, such as glucose deprivation, activated AMPK directly phosphorylates YAP at serine-61 (S61) and serine-94 (S94), abolishing the YAP-TEAD interaction and consequently TEAD-mediated gene transcription (Mo et al., 2015, Wang et al., 2015). Energy stress also induces LATS1/2 kinase activity in both an AMPK-dependent and -independent manner. Finally, active AMPK phosphorylates AMOTL1 at serine-793, which further promotes YAP phosphorylation by LATS1/2 (DeRan et al., 2014). Apart from AMPK, glucose itself may also activate YAP/TAZ through phosphofructokinase, which promotes YAP-TEAD binding (Enzo et al., 2015). In addition to energy stress, metabolic strain from inhibiting cholesterol synthesis likewise inhibits YAP activity. This is accomplished

indirectly through the Rho GTPases, which require the geranylgeranyl pyrophosphate produced by the mevalonate pathway for proper activation (Sorrentino et al., 2014).

Oxygen plays a critical role in cell metabolism, and its availability – or lack thereof – likewise regulates YAP/TAZ activity. Under hypoxic conditions, hypoxia-inducible factor 1 (HIF1) induces expression of the E3 ubiquitin ligases SIAH1/2. SIAH1/2 destabilize LATS2 by promoting its ubiquitination and subsequent degradation, thereby activating YAP (Ma et al., 2015). HIF1 can also directly induce TAZ transcription (Xiang et al., 2014), and YAP interacts with stabilizes HIF1 to promote HIF1-induced gene transcription (Ma et al., 2015).

1.3 The Hippo Pathway in Organ Regeneration and Homeostasis

A growing body of work has advanced our understanding of Hippo pathway regulation of cell proliferation, differentiation, and spatial patterning not only in organ development but also upon injury-induced regeneration. The pathway's central role in stem cell biology thus implicates its potential for therapeutic manipulation in mammalian organ regeneration. Here we review differential roles of the Hippo pathway in the development and homeostasis of various organs.

1.3.1 Brain/Central Nervous System

Brain development requires a rigorous balance between the expansion of neural progenitors and the production of post-mitotic neurons and glial cells, and disrupting this equilibrium leads to structural abnormalities and dysfunction in the nervous system (Lavado et al., 2013). Several lines of evidence have implicated YAP in the regulation of neural stem cell (NSC) behavior. For instance, YAP is reported to interact with Smad to mediate bone morphogenetic protein (BMP) suppression of NSC differentiation and mediate Sonic hedgehog-induced neural progenitor proliferation (Alarcón et al., 2009). During murine brain development, neurofibromatosis 2 (NF2) suppresses YAP activity to promote differentiation of guidepost cells in the corpus callosum (Lavado et al., 2013). In the developing central nervous system (CNS), downregulation of YAP is correlated with neural cell cycle exit, which is required for their terminal differentiation (Zhang et al., 2012). Furthermore, in Drosophila, yki is critical for maintaining neuroepithelial

cells in an undifferentiated state, while YAP knockdown reduces neuron production in zebrafish embryos (Zhang et al., 2011, Jiang et al., 2009). Together, these observations support an indispensable role for YAP in neural progenitor proliferation and differentiation.

Moreover, there is sufficient evidence that YAP plays an important role during brain development, and dysregulation of YAP can have severe consequences on brain size. One study identified a YAP-positive subpopulation of early, pre-migratory neural crest mesenchymal cells, and demonstrated that YAP expression was inversely correlated with human neuronal differentiation (Hindley et al., 2016). Furthermore, YAP acted synergistically with retinoic acid signaling to regulate neural crest fate and migration. In Drosophila, yki was recently linked to neuroblast biology downstream of the energy-sensing Lkb1 and AMPK kinases, where lkb1 restricted yki activity in larval neuronal cells in the central brain and ventral nerve cord (VNC) independently of wts (Gailite et al., 2015). The Hippo pathway was most recently shown to restrict Drosophila brain size by modulating larval neuroblasts, where depletion of upstream kinases tao-1, hpo, or wts by RNAi led to a significant increase in brain volume; deletion of hpo or tao-1, or mutation of wts, in VNC neuroblasts also significantly increased clonal volume(Poon et al., 2016).

Given the Hippo pathway's critical role in brain development, its recent association with several neurodevelopmental diseases is perhaps unsurprising. During brain development, NSCs coordinate cell cycle entry and exit with developmental timing to ensure that the correct neuron type and number are specified in a strict temporal sequence. NSC deregulation can thus give rise to either an under-sized or oversized brain, and microcephaly is one such disorder resulting in an undersized brain along with other developmental complications. Microcephaly is associated with mutations in Cyclin-dependent kinase 5 regulatory subunit 2 (CDK5RAP2), and MST1 was recently identified as a CDK5RAP2 interaction partner, while CDK5RAP2 was also found to regulate YAP/TAZ, suggesting a potential role for the Hippo pathway in CDK5RAP2-associated microcephaly (Sukumaran et al., 2017). Another neurodevelopmental disease linked to the Hippo pathway is hydrocephalus, a disease characterized by enlarged cerebrospinal fluid (CSF)-filled ventricles, severe mental retardation, and motor dysfunction. Hydrocephalus is caused by abnormal generation and maturation of the ependymal cells that line the ventricular surface, and a recent study demonstrated that YAP was required for generating ependymal cells and maintaining structural integrity of the ventricular system. Nervous system-specific deletion of YAP led to severe hydrocephalus

phenotypes in mice, and Yap overexpression rescued a lysophosphatidic acid-induced model of hydrocephalus (Park et al., 2016). These results highlight a novel function of YAP in maintaining tissue junctions during normal development and after fetal brain injury, thereby suggesting its potential as a therapeutic target for certain neurodevelopmental diseases.

1.3.2 Heart

Organ size is especially critical during heart development: the heart must be sufficiently large to generate a physiological cardiac output, yet not so large as to inhibit cardiac outflow, as is the case with cardiomyopathies (Heallen et al., 2011). The Hippo pathway plays a well-established role in the developmental control of mammalian cardiac size. Deletion of MST1/2 or LATS1/2 increases cardiomyocyte proliferation during mouse embryogenesis, and overexpression of a constitutively active YAP in either the embryonic or post-natal mouse heart increases cardiomyocyte proliferation and cardiac size (Heallen et al., 2011, Xin et al., 2011, von Gise et al., 2012). YAP and TAZ play redundant roles in cardiac growth, and dual deletion of both proteins leads to dose-dependent cardiomyopathy (Xin et al., 2013). While cardiomyocytes retain some regenerative capacity at birth, this capacity is largely lost during postnatal development, during which the Hippo pathway inhibits cardiomyocyte proliferation to limit cardiac regeneration in the adult heart (Heallen et al., 2011, Heallen et al., 2013).

Though its role in cardiac size control has been well-established, the mechanism by which the Hippo pathway restricts cardiac growth has yet to be fully elucidated. Recent work has shown that the murine FAT tumor suppressor homolog 4 (FAT4) restricts cardiomyocyte proliferation through a non-canonical mechanism involving the scaffold protein Angiomotin-like 1 (AMOTL1), independent of LATS1/2-mediated YAP phosphorylation (Ragni et al., 2017). AMOTL1 physically interacts with both YAP and FAT4, and this FAT4 complex sequesters YAP in the cytoplasm, thereby preventing excessive YAP-mediated cardiac growth.

The Hippo pathway's regulation of cardiac development has also garnered interest in the potential roles that the pathway might play in cardiac regeneration following injury. For instance, SAV knockout adult cardiomyocytes have been shown to increase proliferative capacity and expression levels of YAP target genes, many of which are normally expressed in the fetal mammalian heart, including components of the

dystrophin–glycoprotein complex (DGC), a complex critical for cardiac regeneration (Morikawa et al., 2015). Indeed, it was more recently shown that the DGC inhibits cardiomyocyte proliferation through direct interaction of one of its components, dystroglycan 1 (DAG1) with YAP. Specifically, Hippo-mediated YAP phosphorylation promotes the interaction between DAG1 and YAP, and the DGC and Hippo pathway cooperatively inhibits YAP nuclear localization to prevent its transcriptional activity (Morikawa et al., 2017). Finally, a recent study by Tian et al. explored the use of microRNAs (miRNAs) in Hippo-mediated cardiac regeneration. The authors identified the microRNA cluster miR302–367 as a Hippo pathway inhibitor that mediated cardiomyocyte proliferation during development via repression of MST1, LATS2, and MOB1B. Importantly, administration of miR302–367 following induced myocardial infarction reactivated the cardiomyocyte cell cycle and reduced scar formation, thus providing a proof-of-concept for microRNA-based approaches to transiently induce cardiac regeneration following injury (Tian et al., 2015). These collective studies hold exciting implications for the therapeutic harnessing of the Hippo pathway in promoting transient regeneration during cardiac development or upon injury.

1.3.3 Liver

Adult liver cells are normally quiescent, yet the liver possesses a striking capacity for regeneration following surgical resection or injury, during which fully differentiated adult hepatocytes emerge from quiescence to divide and proliferate (Ponder, 1996). The Hippo pathway is already a well-established regulator of liver size: MST1/2 are required for maintaining quiescence in the adult liver and their dual deletion leads to YAP activation, liver overgrowth, and hepatocellular carcinoma (HCC) (Zhou et al., 2009). Early studies already established that YAP overexpression in the liver similarly leads to liver overgrowth and HCC in mice (Camargo et al., 2007, Dong et al., 2007, Yimlamai et al., 2015). Furthermore, YAP is partly responsible for regulating the transcriptional program associated with the fetal-to-adult switch during liver maturation, through modulation of transcriptional regulators of hepatocyte specification and function including hepatocyte nuclear factor 4 (HNF4a) and forkhead box A2 (FOXA2) (Zhang et al., 2010, Alder et al., 2014).

In addition to its role in restricting YAP/TAZ to prevent overgrowth, the Hippo pathway may also play a role in liver fibrosis. Hepatic stellate cells (HSCs) are activated in response to liver damage and are

the major cell type involved in liver fibrosis. Recent work has shown that YAP/TAZ are overexpressed in fibrotic liver and activated HSCs, suggesting that elevated levels of YAP/TAZ play a role in HSC activation. Interestingly, omega-3 polyunsaturated fatty acids (ω−3 PUFAs) inhibited HSC activation and CCl4-induced liver fibrosis by promoting YAP/TAZ degradation (Zhang et al., 2016). Another recent study demonstrated that YAP activation selectively eliminates damaged hepatocytes by switching cell fate from proliferation to migration/apoptosis in response to cell stresses such as ethanol damage in both liver sinusoidal epithelial cells and hepatocytes (Miyamura et al., 2017).

During liver development, hepatoblasts arising from the endoderm develop into mature hepatocytes or biliary epithelial cells. Recent work has shown that LATS1/2 are redundantly required for differentiation and maturation during mouse liver development in both the biliary epithelial and hepatocyte lineages (Yi et al., 2016). Deletion of LATS1/2 resulted in perinatal lethality, excess biliary epithelial proliferation, and a failure of hepatoblast maturation, while YAP overexpression repressed the transcriptional network associated with normal hepatocyte maturation (Yi et al., 2016). Thus, this study demonstrates the appreciable fine-tuning of YAP activity required in regulating the balance between organ growth and differentiation in the liver.

1.3.4 Intestine

The gut epithelium must maintain its integrity and function amidst constant microbial and environmental threats. Indeed, intestinal epithelial cells (IECs) have evolved the capacity for rapid regeneration upon insult and harbor an appropriately short half-life to do so: the small intestinal epithelia, for instance, turn over completely every 4–5 days (Hong et al., 2016). While YAP/TAZ are not required for normal intestinal turnover (Azzolin et al., 2014), their upstream regulators MST1/2 and SAV1 are indispensable for intestinal homeostasis. For example, mice harboring conditional knockouts of MST1/2 in IECs exhibit drastic changes in intestinal architecture, including disorganized villi, epithelial dysplasia, and adenomas (Zhou et al., 2011). Furthermore, mice with SAV1-deficient small and large intestines display higher levels of polyp formation and enlarged crypt structures (Cai et al., 2010). In light of the considerable body of work on Hippo in intestinal homeostasis, a comprehensive survey can be found in a more extensive recent review (Hong et al., 2016).

Crosstalk between the Hippo pathway and Wnt/β-catenin signaling is central to the regulation of intestinal regeneration and homeostasis (Hong et al., 2016). Several studies have demonstrated that the Hippo and Wnt pathways are intimately tied in regulation and function, yet the exact mechanistic role of YAP in Wnt signaling is still a subject of debate. Recent work identified the lysine methyltransferase suppressor of variegation 3–9-Enhancer of zeste-Trithorax domain 7 (SETD7) as an important cross-regulator between the two pathways in intestinal regeneration (Oudhoff et al., 2016). SETD7 was shown to be required for Wnt-mediated intestinal regeneration, and its control over Wnt signaling in turn required YAP (Oudhoff et al., 2016).

In the colon, inflammatory cytokine prostaglandin E2 (PGE2) plays an important role in regeneration and tumorigenesis (Kim et al., 2017). Recent work has shown that PGE2 positively regulates YAP expression in the mouse colon and human colon cancer cells, creating a positive feedback loop that then promoted colon regeneration following colitis in vivo.

1.3.5 Lung

During lung development, temporal coordination of proliferation and differentiation is critical for proper organization of the complex branch structures comprising the airway epithelia. Loss of YAP in the lung epithelium is sufficient to cause defective lung development (Mahoney et al., 2014), while deleting MST1/2 in the developing lung results in alveolar defects independent of YAP localization (Chung et al., 2013), indicating that the Hippo pathway plays a critical role in regulating lung development. Consistent with these findings, recent work has shown that loss of MST1/2 in the lung epithelium results in neonatal lethality from lung defects in mice; analysis of the mutant lungs revealed denser lung architecture, reduced airway space, and increased proliferation, all reflective of disrupted lung epithelial differentiation (Lin et al., 2015). Genetic deletion of one allele of YAP, or one allele of both YAP and TAZ, is sufficient to rescue the lethality seen from loss of MST1/2, thereby supporting a conserved MST1/2-YAP/TAZ axis regulating lung growth during development (Lin et al., 2015).

Furthermore, the precise regulation of YAP localization is critical for distal–proximal patterning in the terminal differentiation of both human and mouse lung epithelium. Nuclear YAP is required for progenitor specification, while cytoplasmic YAP is a marker for proximal airway maturation; thus, YAP

localization is intricately coordinated with airway epithelial cell fate (Mahoney et al., 2014). Building upon this notion, Szymaniak et al. recently outlined a polarity-directed mechanism of YAP regulation by Crumbs protein homolog 3 (CRB3) in airway epithelial cell fate (Szymaniak et al., 2015). In mouse and human airway epithelia, CRB3 controls apical-basal polarity and promotes interaction between LATS1/2 and YAP at apical junctions to increase YAP phosphorylation and cytoplasmic retention, thereby initiating airway progenitor differentiation.

1.3.6 Breast

The mammary epithelium undergoes various developmental phases: ductal elongation in the virgin mammary gland, proliferation and differentiation during pregnancy, and post-lactation-induced epithelial cell death (Chen et al., 2014). Though the Hippo pathway has had longstanding associations with breast cancer, its role in mammary gland development has remained poorly understood until recent years. The Hippo pathway is dispensable in the virgin gland and is specifically required during pregnancy, when mammary epithelia undergo rapid proliferation and differentiation (Chen et al., 2014). Surprisingly, Yap hyper-activation alone is insufficient to drive hyperplasia, only leading to failed terminal differentiation of the mammary epithelia. These observations parallel the role of the Hippo pathway in the intestine, where YAP is dispensable for intestinal development but required for injury-induced regeneration. Thus, the temporally restricted roles of the Hippo pathway suggest it is particularly important during times of robust tissue growth and morphogenesis (Chen et al., 2014).

Recent work has continued to advance our understanding of the Hippo pathway's role in mammary development. Britschgi et al. identified LATS1 and LATS2 as regulators of human breast epithelial cell fate using a high-content, image-based short hairpin RNA (shRNA) screen (Britschgi et al., 2017). The authors found that LATS1/2 deletion promoted a luminal phenotype via expansion of bipotent and luminal progenitors. Interestingly, LATS1/2 deletion stabilized both YAP/TAZ and the estrogen receptor alpha (ERα), suggesting non-canonical crosstalk between the Hippo pathway and ERα signaling that may have far-reaching implications in cell fate and development in other tissue types. Another recent study delineated a mechanism of Hippo-mediated regulation of breast epithelial cell fate, where poly(rC)-binding proteins

(PCBPs) form a complex with the Hippo pathway components SAV1, MST1/2, and LATS1 to suppress YAP/TAZ activity (Li et al., 2016).

1.4 Hippo Pathway Deregulation in Cancer

While the Hippo pathway quickly attracted broad attention due to its remarkable potency in regulating organ size, its dysregulation was just as much an area of fascination, since uncontrolled proliferation is a hallmark of tumorigenesis. Indeed, an abundance of translational and clinical studies has established both oncogenic and tumor suppressive roles for YAP/TAZ and the core Hippo components across various types and stages of tumorigenesis.

1.4.1 Liver Cancer

The Hippo pathway is extensively implicated in liver cancer initiation and progression, owing to its remarkable role in liver size control. Vanguard studies found that overexpressing YAP in transgenic mice induced rapid and aberrant tissue expansion in the liver, quickly resulting in hepatomegaly; sustained YAP overexpression accordingly led to hepatic tumor formation (Dong et al., 2007, Camargo et al., 2007). YAP-induced liver cancer seems largely dependent on a TEAD-mediated transcription program, as evidenced by suppression of YAP-induced hepatomegaly and tumorigenesis by a dominant-negative TEAD that sequesters both YAP/TAZ (Liu-Chittenden et al., 2012).

Consistent with the notion that YAP hyperactivity can drive hepatic transformation, deleting core Hippo components produces phenotypes akin to YAP overexpression. Conditional knockouts of MST1/2 and SAV1 in mouse liver led to dramatic liver enlargement, accumulation of oval cells, and formation of lesions characteristic of hepatocellular carcinoma (HCC) (Song et al., 2010, Lee et al., 2010, Lu et al., 2010). Likewise, *Mob1A/1B* deletion in the liver led to cholangiocyte and oval cell hyperplasia, and *Mob1A/1B* knockout livers not only hyperproliferate but also undergo dedifferentiation and show increasing EMT potential, all of which collectively metamorphose into liver cancer (Nishio et al., 2016).

The oncogenic role of YAP overexpression in HCC is an area of increasing clinical significance and therapeutic interest. *Yap* gene amplification is required for sustained tumor growth and cancer progression

in mouse liver carcinomas *(Zender et al., 2006)*, and ectopic YAP expression alone is enough to induce malignant transformation of an immortalized hepatocyte cell line (Xu et al., 2009). In humans, many HCC specimens frequently harbor *YAP* gene amplifications, and YAP itself has been identified as an independent prognostic marker for HCC and other cancer types. Furthermore, YAP and TAZ overexpression in HCC correlate with poor differentiation, increased tumor aggressiveness, and shortened overall survival (Zhao et al., 2007, Xu et al., 2009, Xiao et al., 2015, Guo et al., 2015). Finally, *TAZ* knockdown in HCCs inhibited proliferation and metastasis both in vitro and in vivo (Xiao et al., 2015). Due to the inefficacy of current chemotherapeutics, surgical resection and liver transplantation represent the only curative treatments for HCC thus far. Further elucidating the role of the Hippo pathway in liver cancer may therefore present more potent and effective therapeutic options in the future.

1.4.2 Colorectal Cancer

Over 80% of human colon cancers and their derived cell lines exhibit YAP overexpression, and a number of early *in vivo* and later clinical studies have implicated the Hippo pathway in intestinal overgrowth and tumorigenesis. YAP overexpression in transgenic mice resulted in loss of differentiation and severe dysplasia along the intestinal epithelium (Camargo et al., 2007). MST1/2 deletion increased YAP nuclear accumulation and dephosphorylation in the intestinal epithelium, as well as adenoma growth in the distal colon by 13 weeks, all of which correlated with Notch and β-catenin pathway activation (Zhou et al., 2011). Supporting these observations, YAP silencing in high-YAP-expressing colon cancer cell lines reduced Notch and β-catenin signaling, thereby inhibiting cell proliferation and survival. A separate study showed that Sav1 deletions in mice resulted in crypt hyperplasia, which proved reversible upon YAP deletion. Furthermore, Sav1-knockout mice exhibited colonic polyps and epithelial hyperplasia characteristic of pre-colorectal cancer (CRC) lesions, all by 13 months of age (Cai et al., 2010).

Crosstalk between the Hippo and Wnt signaling pathways may also regulate different stages of CRC, though YAP appears to take on either an oncogenic or tumor-suppressive role, depending on the genomic and cellular context of the tumor. For instance, a recent study suggested that the loss of adenomatous polyposis coli (APC) in CRC works synergistically with YAP-induced suppression of Paneth cell differentiation to promote tumorigenesis, as YAP was found in its active, nuclear state in adenomas of

an *Apc*-mutant background (Gregorieff et al., 2015). However, a separate study showed that loss of *Yap* led to Wnt hyperactivation, hyperplasia, and microadenomas, and that a minor subset of human tumors exhibiting complete loss of *YAP* were associated with stage IV disease, suggesting that YAP took on a tumor suppressive role in this context (Barry et al., 2013).

Clinically, higher YAP or TAZ expression in patients correlates with poorer prognosis (i.e. shortened overall survival times) (Zhou et al., 2011, Yuen et al., 2013, Wang et al., 2013). A YAP-activated gene signature was likewise associated with poor prognosis and reduced rates of disease-free survival in a retrospective study of colorectal cancer (CRC) patient cohorts with stage I-III disease (Lee et al., 2015). In a similar vein, decreased LATS1 expression has also been detected in some cases of CRC (Wierzbicki et al., 2013).

1.4.3 Pancreatic Cancer

Pancreatic deletion of MST1/2 disrupts pancreatic architecture and produces metaplastic lesions resembling those of pancreatic cancer (George et al., 2012). Furthermore, TAZ overexpression in pancreatic cancer cells increase their metastatic potential, while knockdown of YAP abrogated cell migration and invasion (Yang et al., 2015, Xie et al., 2015). Recent studies using Kras-driven models of pancreatic ductal adenocarcinoma (PDAC) showed that YAP deletion inhibited proliferation of Kras mutant cells both *in vitro* and *in* vivo, suggesting that YAP is necessary for disease progression (Zhang et al., 2014b). Furthermore, another study in the same model revealed spontaneous *YAP* amplification as a resistance mechanism upon Kras inactivation (Kapoor et al., 2014). Clinically, human pancreatic tumor specimens also show significantly higher levels of YAP/TAZ expression, especially in metastatic lesions, relative to the surrounding healthy pancreatic tissue, and expression levels correlate with poor patient prognosis (Diep et al., 2012, Xie et al., 2015, Yang et al., 2015).

1.4.4 Breast Cancer

Multiple studies have correlated YAP/TAZ expression levels with breast cancer initiation, progression, and metastasis. Immunohistochemical analysis of breast cancer tissues, particularly in those with aggressive and invasive phenotypes, demonstrate significant overexpression of YAP/TAZ as well as

nuclear localization (Chan et al., 2008, Díaz-Martín et al., 2015, Wang et al., 2012). YAP/TAZ overexpression elevates the invasive and migratory potential of MCF10A, a nontumorigenic cell line, and knocking down either YAP or TAZ inhibited the aforementioned phenotypes both *in vitro* and *in vivo (Wang et al., 2012, Chan et al., 2008, Lei et al., 2008, Overholtzer et al., 2006)*.

Several lines of evidence suggest that TAZ expression and activity may potentiate cancer stem cell (CSC) renewal and drive breast cancer development. TAZ knockdown and overexpression respectively induced luminal cell differentiation in basal cells and basal cell characteristics in luminal cells, suggesting that TAZ promotes lineage switching in the mammary epithelium (Skibinski et al., 2014). Furthermore, TAZ expression and activity may drive more aggressive basal-like breast cancers, as TAZ appears to enrich a CSC population to mediate the formation of high-grade tumors, and is itself required for breast cancer cell renewal and tumorigenic potential (Cordenonsi et al., 2011). On the other hand, YAP may be required for tumor formation but is insufficient in and of itself for oncogenic transformation. *In vivo* YAP hyperactivity in mammary epithelia induces terminal differentiation but is insufficient for hyperplastic induction. Furthermore, loss of YAP suppressed polyoma middle T oncogene (PyMT)-mediated tumor induction but was ineffectual in virgin mammary glands (Chen et al., 2014). Thus, YAP may act cooperatively with other oncogenic determinants of breast cancer (e.g. BRCA1 and p53) to potentiate cellular transformation (Overholtzer et al., 2006).

Together, YAP and TAZ also mediate other breast cancer determining factors such as Leukemia inhibitory factor reception (LIFR) whose expression level directly correlates with improved overall survival in breast cancer patients. Loss of LIFR in nonmetastatic breast cancer increases metastatic potential, while restoring LIFR in tumors was found to suppress metastasis by promoting YAP phosphorylation (Chen et al., 2012). G protein–coupled estrogen receptor (GPER) is highly upregulated in invasive ductal carcinoma, as compared with adjacent normal tissue, and drives breast cancer cell migration and tumor growth. The effects of estrogen on breast cancer cells were found to be partly mediated through GPER stimulation and a TAZ-driven transcriptional program (Zhou et al., 2015). Furthermore, YAP/TAZ interaction with TGFβ also promotes a metastatic transcriptional program in breast cancer cells (Hiemer et al., 2014). Taken together, while YAP/TAZ appear to be critical towards breast cancer initiation, progression, and metastasis, they

behave in a context-dependent manner and require additional genetic alterations to cooperatively induce oncogenic transformation.

1.4.5 Uveal Melanoma

Uveal melanoma (UM) is the most common adult intraocular tumor arising from melanocytes in the iris, ciliary body, or choroid, with high metastatic rates and poor prognosis thereafter. Over 80% of UM cases exhibit somatic mutations in either GNAQ or GNA11, and overexpression of active $G_{q/11}$ is sufficient to drive transformation of healthy melanocytes, suggesting a critical role for these mutations in disease development (Van Raamsdonk et al., 2010, Van Raamsdonk et al., 2009). Though ERK signaling was originally thought to mediate the mechanism of melanocyte transformation, later studies revealed that hyperactive and constitutively nuclear YAP mediated $G_{q/11}$ transformation and oncogenesis through LATS inhibition (Yu et al., 2014) or disrupted AMOT-YAP interactions (Feng et al., 2014). Furthermore, functional studies demonstrated the therapeutic potential of targeting YAP for UM treatment using verteporfin, a compound that abrogates the YAP-TEAD interface, thereby inhibiting UM tumor growth *in vivo* (Feng et al., 2014, Yu et al., 2014).

1.5 Future Inquiries

Several key areas of further inquiry remain in spite of the rapid advancements made in the Hippo signaling field. First, the molecular mechanisms regulating MST1/2 and MAP4K activity, and whether both regulatory arms respond to overlapping or different upstream signals, remain an ongoing area of research. Though many upstream signals regulating LATS1/2 phosphorylation and kinase activity have already been identified, neither MST1/2 and MAP4K phosphorylation nor their kinase activity appear to be strongly modulated by any extracellular cues. Recent work from our lab has identified the Ras-related GTPase RAP2 as a key transducer of ECM rigidity signals by binding to and activating MAP4K4/6/7, suggesting that MST1/2 and the MAP4Ks can be differentially regulated by separate signals (Meng et al., 2018), and another recent study delineated a mechanism in which the striatin (STRN)-interacting phosphatase and

kinase (STRIPAK) complex regulates MST1/2 and MAP4Ks through inactivating binding by protein phosphatase 2A catalytic subunit (PP2AC) (Meng et al., 2018, Chen et al., 2019).

Second, it is still unclear where the Hippo pathway components (excluding YAP) are localized in mammalian cells. A previous report suggested a working model in which active Merlin/NF2 recruits Wts/LATS to the plasma membrane (Yin et al., 2013), while another study showed that multiple *Drosophila* components are organized into distinct complexes at apical junctions in the wing disc (Sun et al., 2015). Further work is needed to fully clarify the spatial-functional relationships among mammalian Hippo components as well as the exact localization of LATS1/2 activation. Third, the mechanism by which YAP becomes deregulated in cancer is still unclear. Though YAP/TAZ activation has been observed in a wide spectrum of human cancers, actual mutations in Hippo pathway genes are relatively few compared to other pathways. Further work is needed to fully address this paradox, which may suggest that the Hippo pathway is simply regulated by other cancer-driving pathways. Finally, the true mechanism of organ size sensing has yet to be uncovered. Though a diverse array of signals has now been reported to regulate the Hippo pathway *in vitro*, none of them have yet demonstrated a prominent role in organ size control *in vivo*. Identifying this signal(s) will unravel a long-sought-after question in developmental biology.

1.6 Acknowledgements

Section 1.3 “The Hippo Pathway in Organ Regeneration and Homeostasis” is a partial reprint of the material as it appears in Current Opinion in Cell Biology; Fu, V., Plouffe, SW., Guan, K-L. Elsevier Publishing Group, 2017. The dissertation author was the primary author of this paper.

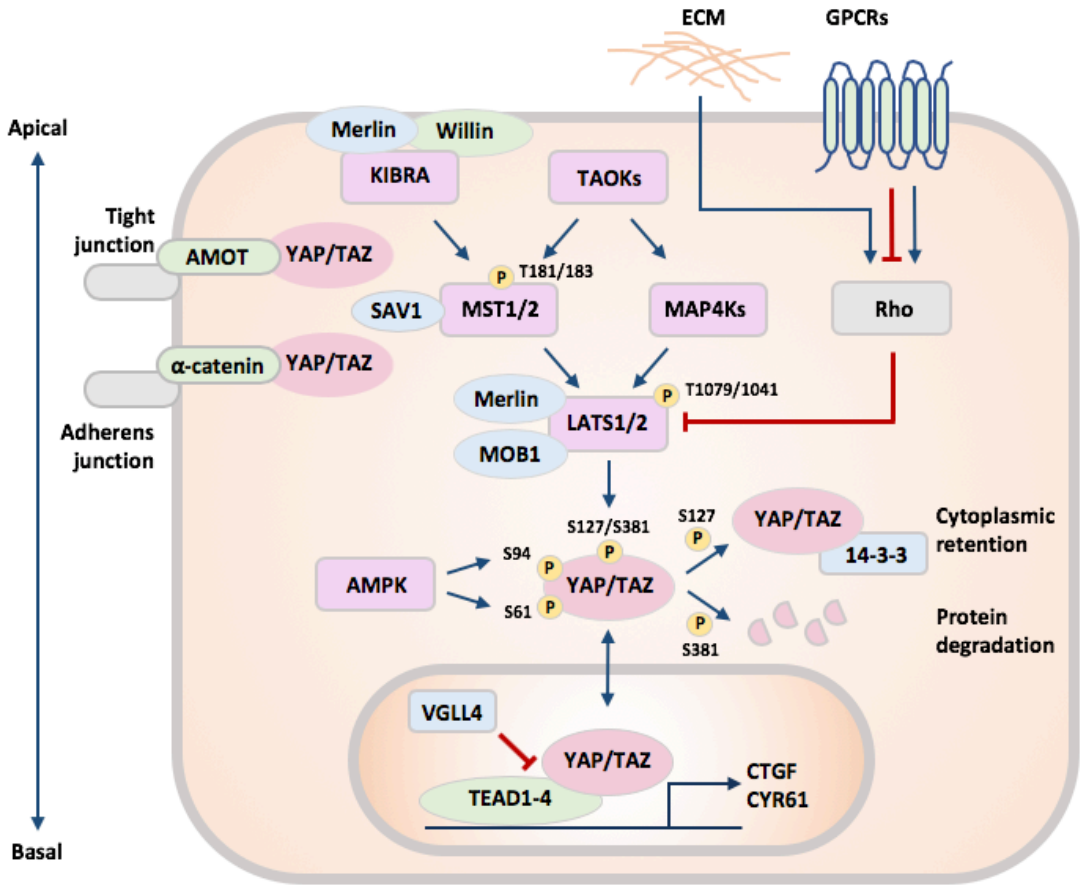

Figure 1.1: The Hippo pathway integrates various signals to regulate YAP/TAZ activity. The core Hippo pathway comprises kinase cascade MST1/2 and LATS1/2. MST proteins, activated by upstream signals, phosphorylate and activate LATS proteins directly, as well as activating their scaffold proteins MOB1 and SAV1. MAP4Ks also phosphorylate and activate the LATS proteins in parallel to MST1/2. Activated LATS proteins phosphorylate YAP and TAZ at multiple sites, inducing 14-3-3-mediated cytoplasmic retention and protein degradation. YAP and TAZ function as transcriptional co-activators of TEAD proteins to induce expression of genes involved in cell proliferation and apoptosis. Merlin, Willin and KIBRA form a complex that recruit MSTs and LATS to the apical plasma membrane, thereby activating LATS proteins. AMOT sequesters YAP and TAZ at tight junctions, while α-catenin sequesters YAP and TAZ at adherens junctions to prevent their nuclear translocation. Activated AMPK phosphorylates LATS as well as YAP to disrupts the YAP1–TEAD complex. The Hippo pathway is further regulated by ECM stiffness and mechanotransduction through Rho GTPases. GPCRs mediate many extracellular signals to either activate or inhibit LATS via Rho GTPase. AMOT, Angiomotin; AMPK, AMP-activated protein kinase; ECM, extracellular matrix; GPCRs, G protein-coupled receptors; LATS, large tumour suppressor; LKB1, liver kinase B1; MAP4K, mitogen-activated protein kinase kinase kinase kinase; MOB1, Mob1 homologue; MST, mammalian ste20-like kinase; P, phosphorylation of indicated amino acid residue; SAV1, salvador family WW domain-containing protein 1; TAZ, transcriptional co-activator with PDZ-binding motif; TEAD, TEA domain family member; TAOK, thousand and one amino acid protein kinase; YAP1, Yes-associated protein 1.

1.7 References

ALARCÓN, C., ZAROMYTIDOU, A. I., XI, Q., GAO, S., YU, J., FUJISAWA, S., BARLAS, A., MILLER, A. N., MANOVA-TODOROVA, K., MACIAS, M. J., SAPKOTA, G., PAN, D. & MASSAGUÉ, J. 2009. Nuclear CDKs drive Smad transcriptional activation and turnover in BMP and TGF-beta pathways. *Cell,* 139**,** 757-69.

ALDER, O., CULLUM, R., LEE, S., KAN, A. C., WEI, W., YI, Y., GARSIDE, V. C., BILENKY, M., GRIFFITH, M., MORRISSY, A. S., ROBERTSON, G. A., THIESSEN, N., ZHAO, Y., CHEN, Q., PAN, D., JONES, S. J. M., MARRA, M. A. & HOODLESS, P. A. 2014. Hippo signaling influences HNF4A and FOXA2 enhancer switching during hepatocyte differentiation. *Cell Rep,* 9**,** 261-271.

ANASTAS, J. N. & MOON, R. T. 2013. WNT signalling pathways as therapeutic targets in cancer. *Nat Rev Cancer,* 13**,** 11-26.

ARAGONA, M., PANCIERA, T., MANFRIN, A., GIULITTI, S., MICHIELIN, F., ELVASSORE, N., DUPONT, S. & PICCOLO, S. 2013. A mechanical checkpoint controls multicellular growth through YAP/TAZ regulation by actin-processing factors. *Cell,* 154**,** 1047-1059.

AZZOLIN, L., PANCIERA, T., SOLIGO, S., ENZO, E., BICCIATO, S., DUPONT, S., BRESOLIN, S., FRASSON, C., BASSO, G., GUZZARDO, V., FASSINA, A., CORDENONSI, M. & PICCOLO, S. 2014. YAP/TAZ incorporation in the β-catenin destruction complex orchestrates the Wnt response. *Cell,* 158**,** 157-70.

BARRY, E. R., MORIKAWA, T., BUTLER, B. L., SHRESTHA, K., DE LA ROSA, R., YAN, K. S., FUCHS, C. S., MAGNESS, S. T., SMITS, R., OGINO, S., KUO, C. J. & CAMARGO, F. D. 2013. Restriction of intestinal stem cell expansion and the regenerative response by YAP. *Nature,* 493**,** 106-10.

BOGGIANO, J. C., VANDERZALM, P. J. & FEHON, R. G. 2011. Tao-1 phosphorylates Hippo/MST kinases to regulate the Hippo-Salvador-Warts tumor suppressor pathway. *Dev Cell,* 21**,** 888-95.

BRITSCHGI, A., DUSS, S., KIM, S., COUTO, J. P., BRINKHAUS, H., KOREN, S., DE SILVA, D., MERTZ, K. D., KAUP, D., VARGA, Z., VOSHOL, H., VISSIERES, A., LEROY, C., ROLOFF, T., STADLER, M. B., SCHEEL, C. H., MIRAGLIA, L. J., ORTH, A. P., BONAMY, G. M., REDDY, V. A. & BENTIRES-ALJ, M. 2017. The Hippo kinases LATS1 and 2 control human breast cell fate via crosstalk with ERα. *Nature,* 541**,** 541-545.

CAI, J., ZHANG, N., ZHENG, Y., DE WILDE, R. F., MAITRA, A. & PAN, D. 2010. The Hippo signaling pathway restricts the oncogenic potential of an intestinal regeneration program. *Genes Dev,* 24**,** 2383-8.

CALLUS, B. A., VERHAGEN, A. M. & VAUX, D. L. 2006. Association of mammalian sterile twenty kinases, Mst1 and Mst2, with hSalvador via C-terminal coiled-coil domains, leads to its stabilization and phosphorylation. *FEBS J,* 273**,** 4264-76.

CAMARGO, F. D., GOKHALE, S., JOHNNIDIS, J. B., FU, D., BELL, G. W., JAENISCH, R. & BRUMMELKAMP, T. R. 2007. YAP1 increases organ size and expands undifferentiated progenitor cells. *Curr Biol,* 17**,** 2054-60.

CHAN, E. H., NOUSIAINEN, M., CHALAMALASETTY, R. B., SCHÄFER, A., NIGG, E. A. & SILLJÉ, H. H. 2005. The Ste20-like kinase Mst2 activates the human large tumor suppressor kinase Lats1. *Oncogene,* 24**,** 2076-86.

CHAN, S. W., LIM, C. J., GUO, K., NG, C. P., LEE, I., HUNZIKER, W., ZENG, Q. & HONG, W. 2008. A role for TAZ in migration, invasion, and tumorigenesis of breast cancer cells. *Cancer Res,* 68**,** 2592-8.

CHEN, D., SUN, Y., WEI, Y., ZHANG, P., REZAEIAN, A. H., TERUYA-FELDSTEIN, J., GUPTA, S., LIANG, H., LIN, H. K., HUNG, M. C. & MA, L. 2012. LIFR is a breast cancer metastasis suppressor upstream of the Hippo-YAP pathway and a prognostic marker. *Nat Med,* 18**,** 1511-7.

CHEN, Q., ZHANG, N., GRAY, R. S., LI, H., EWALD, A. J., ZAHNOW, C. A. & PAN, D. 2014. A temporal requirement for Hippo signaling in mammary gland differentiation, growth, and tumorigenesis. *Genes Dev,* 28**,** 432-7.

CHEN, R., XIE, R., MENG, Z., MA, S. & GUAN, K. L. 2019. STRIPAK integrates upstream signals to initiate the Hippo kinase cascade. *Nat Cell Biol,* 21**,** 1565-1577.

CHUNG, C., KIM, T., KIM, M., SONG, H., KIM, T. S., SEO, E., LEE, S. H., KIM, H., KIM, S. K., YOO, G., LEE, D. H., HWANG, D. S., KINASHI, T., KIM, J. M. & LIM, D. S. 2013. Hippo-Foxa2 signaling pathway plays a role in peripheral lung maturation and surfactant homeostasis. *Proc Natl Acad Sci U S A,* 110**,** 7732-7.

CORDENONSI, M., ZANCONATO, F., AZZOLIN, L., FORCATO, M., ROSATO, A., FRASSON, C., INUI, M., MONTAGNER, M., PARENTI, A. R., POLETTI, A., DAIDONE, M. G., DUPONT, S., BASSO, G., BICCIATO, S. & PICCOLO, S. 2011. The Hippo transducer TAZ confers cancer stem cell-related traits on breast cancer cells. *Cell,* 147**,** 759-72.

DERAN, M., YANG, J., SHEN, C. H., PETERS, E. C., FITAMANT, J., CHAN, P., HSIEH, M., ZHU, S., ASARA, J. M., ZHENG, B., BARDEESY, N., LIU, J. & WU, X. 2014. Energy stress regulates hippo-YAP signaling involving AMPK-mediated regulation of angiomotin-like 1 protein. *Cell Rep,* 9**,** 495-503.

DIEP, C. H., ZUCKER, K. M., HOSTETTER, G., WATANABE, A., HU, C., MUNOZ, R. M., VON HOFF, D. D. & HAN, H. 2012. Down-regulation of Yes Associated Protein 1 expression reduces cell proliferation and clonogenicity of pancreatic cancer cells. *PLoS One,* 7**,** e32783.

DONG, J., FELDMANN, G., HUANG, J., WU, S., ZHANG, N., COMERFORD, S. A., GAYYED, M. F., ANDERS, R. A., MAITRA, A. & PAN, D. 2007. Elucidation of a universal size-control mechanism in Drosophila and mammals. *Cell,* 130**,** 1120-33.

DRISCOLL, T. P., COSGROVE, B. D., HEO, S. J., SHURDEN, Z. E. & MAUCK, R. L. 2015. Cytoskeletal to Nuclear Strain Transfer Regulates YAP Signaling in Mesenchymal Stem Cells. *Biophys J,* 108**,** 2783-93.

DUPONT, S. 2016. Role of YAP/TAZ in cell-matrix adhesion-mediated signalling and mechanotransduction. *Exp Cell Res,* 343**,** 42-53.

DÍAZ-MARTÍN, J., LÓPEZ-GARCÍA, M., ROMERO-PÉREZ, L., ATIENZA-AMORES, M. R., PECERO, M. L., CASTILLA, M., BISCUOLA, M., SANTÓN, A. & PALACIOS, J. 2015. Nuclear TAZ expression associates with the triple-negative phenotype in breast cancer. *Endocr Relat Cancer,* 22**,** 443-54.

ENZO, E., SANTINON, G., POCATERRA, A., ARAGONA, M., BRESOLIN, S., FORCATO, M., GRIFONI, D., PESSION, A., ZANCONATO, F., GUZZO, G., BICCIATO, S. & DUPONT, S. 2015. Aerobic glycolysis tunes YAP/TAZ transcriptional activity. *EMBO J,* 34**,** 1349-70.

FAN, R., KIM, N. G. & GUMBINER, B. M. 2013. Regulation of Hippo pathway by mitogenic growth factors via phosphoinositide 3-kinase and phosphoinositide-dependent kinase-1. *Proc Natl Acad Sci U S A,* 110**,** 2569-74.

FENG, X., DEGESE, M. S., IGLESIAS-BARTOLOME, R., VAQUE, J. P., MOLINOLO, A. A., RODRIGUES, M., ZAIDI, M. R., KSANDER, B. R., MERLINO, G., SODHI, A., CHEN, Q. & GUTKIND, J. S. 2014.

Hippo-independent activation of YAP by the GNAQ uveal melanoma oncogene through a trio-regulated rho GTPase signaling circuitry. *Cancer Cell,* 25**,** 831-45.

GAILITE, I., AERNE, B. L. & TAPON, N. 2015. Differential control of Yorkie activity by LKB1/AMPK and the Hippo/Warts cascade in the central nervous system. *Proc Natl Acad Sci U S A,* 112**,** E5169-78.

GALLI, G. G., CARRARA, M., YUAN, W. C., VALDES-QUEZADA, C., GURUNG, B., PEPE-MOONEY, B., ZHANG, T., GEEVEN, G., GRAY, N. S., DE LAAT, W., CALOGERO, R. A. & CAMARGO, F. D. 2015. YAP Drives Growth by Controlling Transcriptional Pause Release from Dynamic Enhancers. *Mol Cell,* 60**,** 328-37.

GEORGE, N. M., DAY, C. E., BOERNER, B. P., JOHNSON, R. L. & SARVETNICK, N. E. 2012. Hippo signaling regulates pancreas development through inactivation of Yap. *Mol Cell Biol,* 32**,** 5116-28.

GLANTSCHNIG, H., RODAN, G. A. & RESZKA, A. A. 2002. Mapping of MST1 kinase sites of phosphorylation. Activation and autophosphorylation. *J Biol Chem,* 277**,** 42987-96.

GONG, R., HONG, A. W., PLOUFFE, S. W., ZHAO, B., LIU, G., YU, F. X., XU, Y. & GUAN, K. L. 2015. Opposing roles of conventional and novel PKC isoforms in Hippo-YAP pathway regulation. *Cell Res,* 25**,** 985-8.

GOULEV, Y., FAUNY, J. D., GONZALEZ-MARTI, B., FLAGIELLO, D., SILBER, J. & ZIDER, A. 2008. SCALLOPED interacts with YORKIE, the nuclear effector of the hippo tumor-suppressor pathway in Drosophila. *Curr Biol,* 18**,** 435-41.

GREGORIEFF, A., LIU, Y., INANLOU, M. R., KHOMCHUK, Y. & WRANA, J. L. 2015. Yap-dependent reprogramming of Lgr5(+) stem cells drives intestinal regeneration and cancer. *Nature,* 526**,** 715-8.

GUO, Y., PAN, Q., ZHANG, J., XU, X., LIU, X., WANG, Q., YI, R., XIE, X., YAO, L., LIU, W. & SHEN, L. 2015. Functional and clinical evidence that TAZ is a candidate oncogene in hepatocellular carcinoma. *J Cell Biochem,* 116**,** 2465-75.

HANSEN, C. G., MOROISHI, T. & GUAN, K. L. 2015. YAP and TAZ: a nexus for Hippo signaling and beyond. *Trends Cell Biol,* 25**,** 499-513.

HEALLEN, T., MORIKAWA, Y., LEACH, J., TAO, G., WILLERSON, J. T., JOHNSON, R. L. & MARTIN, J. F. 2013. Hippo signaling impedes adult heart regeneration. *Development,* 140**,** 4683-90.

HEALLEN, T., ZHANG, M., WANG, J., BONILLA-CLAUDIO, M., KLYSIK, E., JOHNSON, R. L. & MARTIN, J. F. 2011. Hippo pathway inhibits Wnt signaling to restrain cardiomyocyte proliferation and heart size. *Science,* 332**,** 458-61.

HIEMER, S. E., SZYMANIAK, A. D. & VARELAS, X. 2014. The transcriptional regulators TAZ and YAP direct transforming growth factor β-induced tumorigenic phenotypes in breast cancer cells. *J Biol Chem,* 289**,** 13461-74.

HINDLEY, C. J., CONDURAT, A. L., MENON, V., THOMAS, R., AZMITIA, L. M., DAVIS, J. A. & PRUSZAK, J. 2016. The Hippo pathway member YAP enhances human neural crest cell fate and migration. *Sci Rep,* 6**,** 23208.

HONG, A. W., MENG, Z. & GUAN, K. L. 2016. The Hippo pathway in intestinal regeneration and disease. *Nat Rev Gastroenterol Hepatol,* 13**,** 324-37.

HUANG, J., WU, S., BARRERA, J., MATTHEWS, K. & PAN, D. 2005. The Hippo signaling pathway coordinately regulates cell proliferation and apoptosis by inactivating Yorkie, the Drosophila Homolog of YAP. *Cell,* 122**,** 421-34.

JIANG, Q., LIU, D., GONG, Y., WANG, Y., SUN, S., GUI, Y. & SONG, H. 2009. yap is required for the development of brain, eyes, and neural crest in zebrafish. *Biochem Biophys Res Commun,* 384**,** 114-9.

JUSTICE, R. W., ZILIAN, O., WOODS, D. F., NOLL, M. & BRYANT, P. J. 1995. The Drosophila tumor suppressor gene warts encodes a homolog of human myotonic dystrophy kinase and is required for the control of cell shape and proliferation. *Genes Dev,* 9**,** 534-46.

KAPOOR, A., YAO, W., YING, H., HUA, S., LIEWEN, A., WANG, Q., ZHONG, Y., WU, C. J., SADANANDAM, A., HU, B., CHANG, Q., CHU, G. C., AL-KHALIL, R., JIANG, S., XIA, H., FLETCHER-SANANIKONE, E., LIM, C., HORWITZ, G. I., VIALE, A., PETTAZZONI, P., SANCHEZ, N., WANG, H., PROTOPOPOV, A., ZHANG, J., HEFFERNAN, T., JOHNSON, R. L., CHIN, L., WANG, Y. A., DRAETTA, G. & DEPINHO, R. A. 2014. Yap1 activation enables bypass of oncogenic Kras addiction in pancreatic cancer. *Cell,* 158**,** 185-197.

KIM, H. B., KIM, M., PARK, Y. S., PARK, I., KIM, T., YANG, S. Y., CHO, C. J., HWANG, D., JUNG, J. H., MARKOWITZ, S. D., HWANG, S. W., YANG, S. K., LIM, D. S. & MYUNG, S. J. 2017. Prostaglandin E. *Gastroenterology,* 152**,** 616-630.

KIM, M., KIM, T., JOHNSON, R. L. & LIM, D. S. 2015. Transcriptional co-repressor function of the hippo pathway transducers YAP and TAZ. *Cell Rep,* 11**,** 270-82.

KIM, N. G. & GUMBINER, B. M. 2015. Adhesion to fibronectin regulates Hippo signaling via the FAK-Src-PI3K pathway. *J Cell Biol,* 210**,** 503-15.

LAVADO, A., HE, Y., PARÉ, J., NEALE, G., OLSON, E. N., GIOVANNINI, M. & CAO, X. 2013. Tumor suppressor Nf2 limits expansion of the neural progenitor pool by inhibiting Yap/Taz transcriptional coactivators. *Development,* 140**,** 3323-34.

LEE, K. P., LEE, J. H., KIM, T. S., KIM, T. H., PARK, H. D., BYUN, J. S., KIM, M. C., JEONG, W. I., CALVISI, D. F., KIM, J. M. & LIM, D. S. 2010. The Hippo-Salvador pathway restrains hepatic oval cell proliferation, liver size, and liver tumorigenesis. *Proc Natl Acad Sci U S A,* 107**,** 8248-53.

LEE, K. W., LEE, S. S., KIM, S. B., SOHN, B. H., LEE, H. S., JANG, H. J., PARK, Y. Y., KOPETZ, S., KIM, S. S., OH, S. C. & LEE, J. S. 2015. Significant association of oncogene YAP1 with poor prognosis and cetuximab resistance in colorectal cancer patients. *Clin Cancer Res,* 21**,** 357-64.

LEI, Q. Y., ZHANG, H., ZHAO, B., ZHA, Z. Y., BAI, F., PEI, X. H., ZHAO, S., XIONG, Y. & GUAN, K. L. 2008. TAZ promotes cell proliferation and epithelial-mesenchymal transition and is inhibited by the hippo pathway. *Mol Cell Biol,* 28**,** 2426-36.

LI, F., BULLOUGH, K. Z., VASHISHT, A. A., WOHLSCHLEGEL, J. A. & PHILPOTT, C. C. 2016. Poly(rC)-Binding Protein 2 Regulates Hippo Signaling To Control Growth in Breast Epithelial Cells. *Mol Cell Biol,* 36**,** 2121-31.

LIAN, I., KIM, J., OKAZAWA, H., ZHAO, J., ZHAO, B., YU, J., CHINNAIYAN, A., ISRAEL, M. A., GOLDSTEIN, L. S., ABUJAROUR, R., DING, S. & GUAN, K. L. 2010. The role of YAP transcription coactivator in regulating stem cell self-renewal and differentiation. *Genes Dev,* 24**,** 1106-18.

LIN, C., YAO, E. & CHUANG, P. T. 2015. A conserved MST1/2-YAP axis mediates Hippo signaling during lung growth. *Dev Biol,* 403**,** 101-13.

LIU-CHITTENDEN, Y., HUANG, B., SHIM, J. S., CHEN, Q., LEE, S. J., ANDERS, R. A., LIU, J. O. & PAN, D. 2012. Genetic and pharmacological disruption of the TEAD-YAP complex suppresses the oncogenic activity of YAP. *Genes Dev,* 26**,** 1300-5.

LU, L., LI, Y., KIM, S. M., BOSSUYT, W., LIU, P., QIU, Q., WANG, Y., HALDER, G., FINEGOLD, M. J., LEE, J. S. & JOHNSON, R. L. 2010. Hippo signaling is a potent in vivo growth and tumor suppressor pathway in the mammalian liver. *Proc Natl Acad Sci U S A,* 107**,** 1437-42.

MA, B., CHEN, Y., CHEN, L., CHENG, H., MU, C., LI, J., GAO, R., ZHOU, C., CAO, L., LIU, J., ZHU, Y., CHEN, Q. & WU, S. 2015. Hypoxia regulates Hippo signalling through the SIAH2 ubiquitin E3 ligase. *Nat Cell Biol,* 17**,** 95-103.

MAHONEY, J. E., MORI, M., SZYMANIAK, A. D., VARELAS, X. & CARDOSO, W. V. 2014. The hippo pathway effector Yap controls patterning and differentiation of airway epithelial progenitors. *Dev Cell,* 30**,** 137-50.

MENG, Z., MOROISHI, T. & GUAN, K. L. 2016. Mechanisms of Hippo pathway regulation. *Genes Dev,* 30**,** 1-17.

MENG, Z., MOROISHI, T., MOTTIER-PAVIE, V., PLOUFFE, S. W., HANSEN, C. G., HONG, A. W., PARK, H. W., MO, J. S., LU, W., LU, S., FLORES, F., YU, F. X., HALDER, G. & GUAN, K. L. 2015. MAP4K family kinases act in parallel to MST1/2 to activate LATS1/2 in the Hippo pathway. *Nat Commun,* 6**,** 8357.

MENG, Z., QIU, Y., LIN, K. C., KUMAR, A., PLACONE, J. K., FANG, C., WANG, K. C., LU, S., PAN, M., HONG, A. W., MOROISHI, T., LUO, M., PLOUFFE, S. W., DIAO, Y., YE, Z., PARK, H. W., WANG, X., YU, F. X., CHIEN, S., WANG, C. Y., REN, B., ENGLER, A. J. & GUAN, K. L. 2018. RAP2 mediates mechanoresponses of the Hippo pathway. *Nature,* 560**,** 655-660.

MILLER, E., YANG, J., DERAN, M., WU, C., SU, A. I., BONAMY, G. M., LIU, J., PETERS, E. C. & WU, X. 2012. Identification of serum-derived sphingosine-1-phosphate as a small molecule regulator of YAP. *Chem Biol,* 19**,** 955-62.

MIYAMURA, N., HATA, S., ITOH, T., TANAKA, M., NISHIO, M., ITOH, M., OGAWA, Y., TERAI, S., SAKAIDA, I., SUZUKI, A., MIYAJIMA, A. & NISHINA, H. 2017. YAP determines the cell fate of injured mouse hepatocytes in vivo. *Nat Commun,* 8**,** 16017.

MO, J. S., MENG, Z., KIM, Y. C., PARK, H. W., HANSEN, C. G., KIM, S., LIM, D. S. & GUAN, K. L. 2015. Cellular energy stress induces AMPK-mediated regulation of YAP and the Hippo pathway. *Nat Cell Biol,* 17**,** 500-10.

MO, J. S., YU, F. X., GONG, R., BROWN, J. H. & GUAN, K. L. 2012. Regulation of the Hippo-YAP pathway by protease-activated receptors (PARs). *Genes Dev,* 26**,** 2138-43.

MORIKAWA, Y., HEALLEN, T., LEACH, J., XIAO, Y. & MARTIN, J. F. 2017. Dystrophin-glycoprotein complex sequesters Yap to inhibit cardiomyocyte proliferation. *Nature,* 547**,** 227-231.

MORIKAWA, Y., ZHANG, M., HEALLEN, T., LEACH, J., TAO, G., XIAO, Y., BAI, Y., LI, W., WILLERSON, J. T. & MARTIN, J. F. 2015. Actin cytoskeletal remodeling with protrusion formation is essential for heart regeneration in Hippo-deficient mice. *Sci Signal,* 8**,** ra41.

NISHIO, M., SUGIMACHI, K., GOTO, H., WANG, J., MORIKAWA, T., MIYACHI, Y., TAKANO, Y., HIKASA, H., ITOH, T., SUZUKI, S. O., KURIHARA, H., AISHIMA, S., LEASK, A., SASAKI, T., NAKANO, T., NISHINA, H., NISHIKAWA, Y., SEKIDO, Y., NAKAO, K., SHIN-YA, K., MIMORI, K. & SUZUKI, A. 2016. Dysregulated YAP1/TAZ and TGF-β signaling mediate hepatocarcinogenesis in Mob1a/1b-deficient mice. *Proc Natl Acad Sci U S A,* 113**,** E71-80.

OTA, M. & SASAKI, H. 2008. Mammalian Tead proteins regulate cell proliferation and contact inhibition as transcriptional mediators of Hippo signaling. *Development,* 135**,** 4059-69.

OUDHOFF, M. J., BRAAM, M. J. S., FREEMAN, S. A., WONG, D., RATTRAY, D. G., WANG, J., ANTIGNANO, F., SNYDER, K., REFAELI, I., HUGHES, M. R., MCNAGNY, K. M., GOLD, M. R., ARROWSMITH, C. H., SATO, T., ROSSI, F. M. V., TATLOCK, J. H., OWEN, D. R., BROWN, P. J. & ZAPH, C. 2016. SETD7 Controls Intestinal Regeneration and Tumorigenesis by Regulating Wnt/β-Catenin and Hippo/YAP Signaling. *Dev Cell,* 37**,** 47-57.

OVERHOLTZER, M., ZHANG, J., SMOLEN, G. A., MUIR, B., LI, W., SGROI, D. C., DENG, C. X., BRUGGE, J. S. & HABER, D. A. 2006. Transforming properties of YAP, a candidate oncogene on the chromosome 11q22 amplicon. *Proc Natl Acad Sci U S A,* 103**,** 12405-10.

PARK, H. W., KIM, Y. C., YU, B., MOROISHI, T., MO, J. S., PLOUFFE, S. W., MENG, Z., LIN, K. C., YU, F. X., ALEXANDER, C. M., WANG, C. Y. & GUAN, K. L. 2015. Alternative Wnt Signaling Activates YAP/TAZ. *Cell,* 162**,** 780-94.

PARK, R., MOON, U. Y., PARK, J. Y., HUGHES, L. J., JOHNSON, R. L., CHO, S. H. & KIM, S. 2016. Yap is required for ependymal integrity and is suppressed in LPA-induced hydrocephalus. *Nat Commun,* 7**,** 10329.

PICCOLO, S., DUPONT, S. & CORDENONSI, M. 2014. The biology of YAP/TAZ: hippo signaling and beyond. *Physiol Rev,* 94**,** 1287-312.

PONDER, K. P. 1996. Analysis of liver development, regeneration, and carcinogenesis by genetic marking studies. *FASEB J,* 10**,** 673-82.

POON, C. L., LIN, J. I., ZHANG, X. & HARVEY, K. F. 2011. The sterile 20-like kinase Tao-1 controls tissue growth by regulating the Salvador-Warts-Hippo pathway. *Dev Cell,* 21**,** 896-906.

POON, C. L., MITCHELL, K. A., KONDO, S., CHENG, L. Y. & HARVEY, K. F. 2016. The Hippo Pathway Regulates Neuroblasts and Brain Size in Drosophila melanogaster. *Curr Biol,* 26**,** 1034-42.

PRASKOVA, M., XIA, F. & AVRUCH, J. 2008. MOBKL1A/MOBKL1B phosphorylation by MST1 and MST2 inhibits cell proliferation. *Curr Biol,* 18**,** 311-21.

QING, Y., YIN, F., WANG, W., ZHENG, Y., GUO, P., SCHOZER, F., DENG, H. & PAN, D. 2014. The Hippo effector Yorkie activates transcription by interacting with a histone methyltransferase complex through Ncoa6. *Elife,* 3.

RAGNI, C. V., DIGUET, N., LE GARREC, J. F., NOVOTOVA, M., RESENDE, T. P., POP, S., CHARON, N., GUILLEMOT, L., KITASATO, L., BADOUEL, C., DUFOUR, A., OLIVO-MARIN, J. C., TROUVÉ, A., MCNEILL, H. & MEILHAC, S. M. 2017. Amotl1 mediates sequestration of the Hippo effector Yap1 downstream of Fat4 to restrict heart growth. *Nat Commun,* 8**,** 14582.

REDDY, B. V. & IRVINE, K. D. 2013. Regulation of Hippo signaling by EGFR-MAPK signaling through Ajuba family proteins. *Dev Cell,* 24**,** 459-71.

SKIBINSKI, A., BREINDEL, J. L., PRAT, A., GALVÁN, P., SMITH, E., ROLFS, A., GUPTA, P. B., LABAER, J. & KUPERWASSER, C. 2014. The Hippo transducer TAZ interacts with the SWI/SNF complex to regulate breast epithelial lineage commitment. *Cell Rep,* 6**,** 1059-1072.

SONG, H., MAK, K. K., TOPOL, L., YUN, K., HU, J., GARRETT, L., CHEN, Y., PARK, O., CHANG, J., SIMPSON, R. M., WANG, C. Y., GAO, B., JIANG, J. & YANG, Y. 2010. Mammalian Mst1 and Mst2 kinases play essential roles in organ size control and tumor suppression. *Proc Natl Acad Sci U S A,* 107**,** 1431-6.

SORRENTINO, G., RUGGERI, N., SPECCHIA, V., CORDENONSI, M., MANO, M., DUPONT, S., MANFRIN, A., INGALLINA, E., SOMMAGGIO, R., PIAZZA, S., ROSATO, A., PICCOLO, S. & DEL

SAL, G. 2014. Metabolic control of YAP and TAZ by the mevalonate pathway. *Nat Cell Biol,* 16**,** 357-66.

STEGERT, M. R., TAMASKOVIC, R., BICHSEL, S. J., HERGOVICH, A. & HEMMINGS, B. A. 2004. Regulation of NDR2 protein kinase by multi-site phosphorylation and the S100B calcium-binding protein. *J Biol Chem,* 279**,** 23806-12.

STEIN, C., BARDET, A. F., ROMA, G., BERGLING, S., CLAY, I., RUCHTI, A., AGARINIS, C., SCHMELZLE, T., BOUWMEESTER, T., SCHÜBELER, D. & BAUER, A. 2015. YAP1 Exerts Its Transcriptional Control via TEAD-Mediated Activation of Enhancers. *PLoS Genet,* 11**,** e1005465.

SUKUMARAN, S. K., STUMPF, M., SALAMON, S., AHMAD, I., BHATTACHARYA, K., FISCHER, S., MÜLLER, R., ALTMÜLLER, J., BUDDE, B., THIELE, H., TARIQ, M., MALIK, N. A., NÜRNBERG, P., BAIG, S. M., HUSSAIN, M. S. & NOEGEL, A. A. 2017. CDK5RAP2 interaction with components of the Hippo signaling pathway may play a role in primary microcephaly. *Mol Genet Genomics,* 292**,** 365-383.

SUN, S., REDDY, B. V. & IRVINE, K. D. 2015. Localization of Hippo signalling complexes and Warts activation in vivo. *Nat Commun,* 6**,** 8402.

SUN, Y., YONG, K. M., VILLA-DIAZ, L. G., ZHANG, X., CHEN, W., PHILSON, R., WENG, S., XU, H., KREBSBACH, P. H. & FU, J. 2014. Hippo/YAP-mediated rigidity-dependent motor neuron differentiation of human pluripotent stem cells. *Nat Mater,* 13**,** 599-604.

SZYMANIAK, A. D., MAHONEY, J. E., CARDOSO, W. V. & VARELAS, X. 2015. Crumbs3-Mediated Polarity Directs Airway Epithelial Cell Fate through the Hippo Pathway Effector Yap. *Dev Cell,* 34**,** 283-96.

TAMASKOVIC, R., BICHSEL, S. J., ROGNIAUX, H., STEGERT, M. R. & HEMMINGS, B. A. 2003. Mechanism of Ca2+-mediated regulation of NDR protein kinase through autophosphorylation and phosphorylation by an upstream kinase. *J Biol Chem,* 278**,** 6710-8.

TAPON, N., HARVEY, K. F., BELL, D. W., WAHRER, D. C., SCHIRIPO, T. A., HABER, D. & HARIHARAN, I. K. 2002. salvador Promotes both cell cycle exit and apoptosis in Drosophila and is mutated in human cancer cell lines. *Cell,* 110**,** 467-78.

TIAN, Y., LIU, Y., WANG, T., ZHOU, N., KONG, J., CHEN, L., SNITOW, M., MORLEY, M., LI, D., PETRENKO, N., ZHOU, S., LU, M., GAO, E., KOCH, W. J., STEWART, K. M. & MORRISEY, E. E. 2015. A microRNA-Hippo pathway that promotes cardiomyocyte proliferation and cardiac regeneration in mice. *Sci Transl Med,* 7**,** 279ra38.

VALENCIA-SAMA, I., ZHAO, Y., LAI, D., JANSE VAN RENSBURG, H. J., HAO, Y. & YANG, X. 2015. Hippo Component TAZ Functions as a Co-repressor and Negatively Regulates ΔNp63 Transcription through TEA Domain (TEAD) Transcription Factor. *J Biol Chem,* 290**,** 16906-17.

VAN RAAMSDONK, C. D., BEZROOKOVE, V., GREEN, G., BAUER, J., GAUGLER, L., O'BRIEN, J. M., SIMPSON, E. M., BARSH, G. S. & BASTIAN, B. C. 2009. Frequent somatic mutations of GNAQ in uveal melanoma and blue naevi. *Nature,* 457**,** 599-602.

VAN RAAMSDONK, C. D., GRIEWANK, K. G., CROSBY, M. B., GARRIDO, M. C., VEMULA, S., WIESNER, T., OBENAUF, A. C., WACKERNAGEL, W., GREEN, G., BOUVIER, N., SOZEN, M. M., BAIMUKANOVA, G., ROY, R., HEGUY, A., DOLGALEV, I., KHANIN, R., BUSAM, K., SPEICHER, M. R., O'BRIEN, J. & BASTIAN, B. C. 2010. Mutations in GNA11 in uveal melanoma. *N Engl J Med,* 363**,** 2191-9.

VARELAS, X. 2014. The Hippo pathway effectors TAZ and YAP in development, homeostasis and disease. *Development,* 141**,** 1614-26.

VON GISE, A., LIN, Z., SCHLEGELMILCH, K., HONOR, L. B., PAN, G. M., BUCK, J. N., MA, Q., ISHIWATA, T., ZHOU, B., CAMARGO, F. D. & PU, W. T. 2012. YAP1, the nuclear target of Hippo signaling, stimulates heart growth through cardiomyocyte proliferation but not hypertrophy. *Proc Natl Acad Sci U S A,* 109**,** 2394-9.

WADA, K., ITOGA, K., OKANO, T., YONEMURA, S. & SASAKI, H. 2011. Hippo pathway regulation by cell morphology and stress fibers. *Development,* 138**,** 3907-14.

WANG, L., SHI, S., GUO, Z., ZHANG, X., HAN, S., YANG, A., WEN, W. & ZHU, Q. 2013. Overexpression of YAP and TAZ is an independent predictor of prognosis in colorectal cancer and related to the proliferation and metastasis of colon cancer cells. *PLoS One,* 8**,** e65539.

WANG, W., XIAO, Z. D., LI, X., AZIZ, K. E., GAN, B., JOHNSON, R. L. & CHEN, J. 2015. AMPK modulates Hippo pathway activity to regulate energy homeostasis. *Nat Cell Biol,* 17**,** 490-9.

WANG, X., SU, L. & OU, Q. 2012. Yes-associated protein promotes tumour development in luminal epithelial derived breast cancer. *Eur J Cancer,* 48**,** 1227-34.

WIERZBICKI, P. M., ADRYCH, K., KARTANOWICZ, D., STANISLAWOWSKI, M., KOWALCZYK, A., GODLEWSKI, J., SKWIERZ-BOGDANSKA, I., CELINSKI, K., GACH, T., KULIG, J., KORYBALSKI, B. & KMIEC, Z. 2013. Underexpression of LATS1 TSG in colorectal cancer is associated with promoter hypermethylation. *World J Gastroenterol,* 19**,** 4363-73.

WU, S., LIU, Y., ZHENG, Y., DONG, J. & PAN, D. 2008. The TEAD/TEF family protein Scalloped mediates transcriptional output of the Hippo growth-regulatory pathway. *Dev Cell,* 14**,** 388-98.

XIANG, L., GILKES, D. M., HU, H., TAKANO, N., LUO, W., LU, H., BULLEN, J. W., SAMANTA, D., LIANG, H. & SEMENZA, G. L. 2014. Hypoxia-inducible factor 1 mediates TAZ expression and nuclear localization to induce the breast cancer stem cell phenotype. *Oncotarget,* 5**,** 12509-27.

XIAO, H., JIANG, N., ZHOU, B., LIU, Q. & DU, C. 2015. TAZ regulates cell proliferation and epithelial-mesenchymal transition of human hepatocellular carcinoma. *Cancer Sci,* 106**,** 151-9.

XIE, D., CUI, J., XIA, T., JIA, Z., WANG, L., WEI, W., ZHU, A., GAO, Y., XIE, K. & QUAN, M. 2015. Hippo transducer TAZ promotes epithelial mesenchymal transition and supports pancreatic cancer progression. *Oncotarget,* 6**,** 35949-63.

XIN, M., KIM, Y., SUTHERLAND, L. B., MURAKAMI, M., QI, X., MCANALLY, J., PORRELLO, E. R., MAHMOUD, A. I., TAN, W., SHELTON, J. M., RICHARDSON, J. A., SADEK, H. A., BASSEL-DUBY, R. & OLSON, E. N. 2013. Hippo pathway effector Yap promotes cardiac regeneration. *Proc Natl Acad Sci U S A,* 110**,** 13839-44.

XIN, M., KIM, Y., SUTHERLAND, L. B., QI, X., MCANALLY, J., SCHWARTZ, R. J., RICHARDSON, J. A., BASSEL-DUBY, R. & OLSON, E. N. 2011. Regulation of insulin-like growth factor signaling by Yap governs cardiomyocyte proliferation and embryonic heart size. *Sci Signal,* 4**,** ra70.

XU, M. Z., YAO, T. J., LEE, N. P., NG, I. O., CHAN, Y. T., ZENDER, L., LOWE, S. W., POON, R. T. & LUK, J. M. 2009. Yes-associated protein is an independent prognostic marker in hepatocellular carcinoma. *Cancer,* 115**,** 4576-85.

XU, T., WANG, W., ZHANG, S., STEWART, R. A. & YU, W. 1995. Identifying tumor suppressors in genetic mosaics: the Drosophila lats gene encodes a putative protein kinase. *Development,* 121**,** 1053-63.

YANG, S., ZHANG, L., PUROHIT, V., SHUKLA, S. K., CHEN, X., YU, F., FU, K., CHEN, Y., SOLHEIM, J., SINGH, P. K., SONG, W. & DONG, J. 2015. Active YAP promotes pancreatic cancer cell motility, invasion and tumorigenesis in a mitotic phosphorylation-dependent manner through LPAR3. *Oncotarget,* 6**,** 36019-31.

YI, J., LU, L., YANGER, K., WANG, W., SOHN, B. H., STANGER, B. Z., ZHANG, M., MARTIN, J. F., AJANI, J. A., CHEN, J., LEE, J. S., SONG, S. & JOHNSON, R. L. 2016. Large tumor suppressor homologs 1 and 2 regulate mouse liver progenitor cell proliferation and maturation through antagonism of the coactivators YAP and TAZ. *Hepatology,* 64**,** 1757-1772.

YIMLAMAI, D., FOWL, B. H. & CAMARGO, F. D. 2015. Emerging evidence on the role of the Hippo/YAP pathway in liver physiology and cancer. *J Hepatol,* 63**,** 1491-501.

YIN, F., YU, J., ZHENG, Y., CHEN, Q., ZHANG, N. & PAN, D. 2013. Spatial organization of Hippo signaling at the plasma membrane mediated by the tumor suppressor Merlin/NF2. *Cell,* 154**,** 1342-55.

YU, F. X. & GUAN, K. L. 2013. The Hippo pathway: regulators and regulations. *Genes Dev,* 27**,** 355-71.

YU, F. X., LUO, J., MO, J. S., LIU, G., KIM, Y. C., MENG, Z., ZHAO, L., PEYMAN, G., OUYANG, H., JIANG, W., ZHAO, J., CHEN, X., ZHANG, L., WANG, C. Y., BASTIAN, B. C., ZHANG, K. & GUAN, K. L. 2014. Mutant Gq/11 promote uveal melanoma tumorigenesis by activating YAP. *Cancer Cell,* 25**,** 822-30.

YU, F. X., ZHANG, Y., PARK, H. W., JEWELL, J. L., CHEN, Q., DENG, Y., PAN, D., TAYLOR, S. S., LAI, Z. C. & GUAN, K. L. 2013. Protein kinase A activates the Hippo pathway to modulate cell proliferation and differentiation. *Genes Dev,* 27**,** 1223-32.

YU, F. X., ZHAO, B., PANUPINTHU, N., JEWELL, J. L., LIAN, I., WANG, L. H., ZHAO, J., YUAN, H., TUMANENG, K., LI, H., FU, X. D., MILLS, G. B. & GUAN, K. L. 2012. Regulation of the Hippo-YAP pathway by G-protein-coupled receptor signaling. *Cell,* 150**,** 780-91.

YUEN, H. F., MCCRUDDEN, C. M., HUANG, Y. H., THAM, J. M., ZHANG, X., ZENG, Q., ZHANG, S. D. & HONG, W. 2013. TAZ expression as a prognostic indicator in colorectal cancer. *PLoS One,* 8**,** e54211.

ZANCONATO, F., FORCATO, M., BATTILANA, G., AZZOLIN, L., QUARANTA, E., BODEGA, B., ROSATO, A., BICCIATO, S., CORDENONSI, M. & PICCOLO, S. 2015. Genome-wide association between YAP/TAZ/TEAD and AP-1 at enhancers drives oncogenic growth. *Nat Cell Biol,* 17**,** 1218-27.

ZENDER, L., SPECTOR, M. S., XUE, W., FLEMMING, P., CORDON-CARDO, C., SILKE, J., FAN, S. T., LUK, J. M., WIGLER, M., HANNON, G. J., MU, D., LUCITO, R., POWERS, S. & LOWE, S. W. 2006. Identification and validation of oncogenes in liver cancer using an integrative oncogenomic approach. *Cell,* 125**,** 1253-67.

ZHANG, H., DEO, M., THOMPSON, R. C., UHLER, M. D. & TURNER, D. L. 2012. Negative regulation of Yap during neuronal differentiation. *Dev Biol,* 361**,** 103-15.

ZHANG, H., PASOLLI, H. A. & FUCHS, E. 2011. Yes-associated protein (YAP) transcriptional coactivator functions in balancing growth and differentiation in skin. *Proc Natl Acad Sci U S A,* 108**,** 2270-5.

ZHANG, K., CHANG, Y., SHI, Z., HAN, X., HAN, Y., YAO, Q., HU, Z., CUI, H., ZHENG, L., HAN, T. & HONG, W. 2016. ω-3 PUFAs ameliorate liver fibrosis and inhibit hepatic stellate cells proliferation and activation by promoting YAP/TAZ degradation. *Sci Rep,* 6**,** 30029.

ZHANG, L., REN, F., ZHANG, Q., CHEN, Y., WANG, B. & JIANG, J. 2008. The TEAD/TEF family of transcription factor Scalloped mediates Hippo signaling in organ size control. *Dev Cell,* 14**,** 377-87.

ZHANG, N., BAI, H., DAVID, K. K., DONG, J., ZHENG, Y., CAI, J., GIOVANNINI, M., LIU, P., ANDERS, R. A. & PAN, D. 2010. The Merlin/NF2 tumor suppressor functions through the YAP oncoprotein to regulate tissue homeostasis in mammals. *Dev Cell,* 19**,** 27-38.

ZHANG, W., GAO, Y., LI, P., SHI, Z., GUO, T., LI, F., HAN, X., FENG, Y., ZHENG, C., WANG, Z., CHEN, H., ZHOU, Z., ZHANG, L. & JI, H. 2014a. VGLL4 functions as a new tumor suppressor in lung cancer by negatively regulating the YAP-TEAD transcriptional complex. *Cell Res,* 24**,** 331-43.

ZHANG, W., NANDAKUMAR, N., SHI, Y., MANZANO, M., SMITH, A., GRAHAM, G., GUPTA, S., VIETSCH, E. E., LAUGHLIN, S. Z., WADHWA, M., CHETRAM, M., JOSHI, M., WANG, F., KALLAKURY, B., TORETSKY, J., WELLSTEIN, A. & YI, C. 2014b. Downstream of mutant KRAS, the transcription regulator YAP is essential for neoplastic progression to pancreatic ductal adenocarcinoma. *Sci Signal,* 7**,** ra42.

ZHAO, B., LI, L., TUMANENG, K., WANG, C. Y. & GUAN, K. L. 2010. A coordinated phosphorylation by Lats and CK1 regulates YAP stability through SCF(beta-TRCP). *Genes Dev,* 24**,** 72-85.

ZHAO, B., LI, L., WANG, L., WANG, C. Y., YU, J. & GUAN, K. L. 2012. Cell detachment activates the Hippo pathway via cytoskeleton reorganization to induce anoikis. *Genes Dev,* 26**,** 54-68.

ZHAO, B., WEI, X., LI, W., UDAN, R. S., YANG, Q., KIM, J., XIE, J., IKENOUE, T., YU, J., LI, L., ZHENG, P., YE, K., CHINNAIYAN, A., HALDER, G., LAI, Z. C. & GUAN, K. L. 2007. Inactivation of YAP oncoprotein by the Hippo pathway is involved in cell contact inhibition and tissue growth control. *Genes Dev,* 21**,** 2747-61.

ZHAO, B., YE, X., YU, J., LI, L., LI, W., LI, S., LIN, J. D., WANG, C. Y., CHINNAIYAN, A. M., LAI, Z. C. & GUAN, K. L. 2008. TEAD mediates YAP-dependent gene induction and growth control. *Genes Dev,* 22**,** 1962-71.

ZHOU, D., CONRAD, C., XIA, F., PARK, J. S., PAYER, B., YIN, Y., LAUWERS, G. Y., THASLER, W., LEE, J. T., AVRUCH, J. & BARDEESY, N. 2009. Mst1 and Mst2 maintain hepatocyte quiescence and suppress hepatocellular carcinoma development through inactivation of the Yap1 oncogene. *Cancer Cell,* 16**,** 425-38.

ZHOU, D., ZHANG, Y., WU, H., BARRY, E., YIN, Y., LAWRENCE, E., DAWSON, D., WILLIS, J. E., MARKOWITZ, S. D., CAMARGO, F. D. & AVRUCH, J. 2011. Mst1 and Mst2 protein kinases restrain intestinal stem cell proliferation and colonic tumorigenesis by inhibition of Yes-associated protein (Yap) overabundance. *Proc Natl Acad Sci U S A,* 108**,** E1312-20.

ZHOU, X., WANG, S., WANG, Z., FENG, X., LIU, P., LV, X. B., LI, F., YU, F. X., SUN, Y., YUAN, H., ZHU, H., XIONG, Y., LEI, Q. Y. & GUAN, K. L. 2015. Estrogen regulates Hippo signaling via GPER in breast cancer. *J Clin Invest,* 125**,** 2123-35.

ZHU, C., LI, L. & ZHAO, B. 2015. The regulation and function of YAP transcription co-activator. *Acta Biochim Biophys Sin (Shanghai),* 47**,** 16-28.

Chapter 2: Characterization of VT01454 as an inhibitor of YAP-driven cancer

2.1 Introduction

Over two decades of intensive research has established the Hippo pathway as a universal regulator of organ size and tissue homeostasis, and expanded the Hippo kinase cascade into a complex signaling network integrating an extensive repertoire of signals: soluble factors, cell polarity, mechanical cues, to name a few (Yu and Guan, 2013). The same cellular properties – cell proliferation, survival, competition, among others – that regulate and are regulated by the Hippo pathway also represent hallmarks of tumorigenesis upon their dysregulation (Harvey et al., 2013). Thus, the impact of the deregulated Hippo pathway on cancer development has sparked both basic and translational interest, and warrants continued investigation of the functions and regulatory mechanisms of this pathway to identify new therapeutic targets.

The classical mammalian Hippo pathway comprises the core components mammalian STE20-like protein kinase 1 and 2 (MST1 and MST2) and large tumor suppressor 1 and 2 (LATS1 and LATS2), their respective adaptor proteins salvador homologue 1 (SAV1) and MOB kinase activator 1A and 1B (MOB1A and MOB1B), and Yes-associated protein 1 (YAP1) and its transcriptional co-activator with PDZ-binding motif (TAZ), both of which serve as the pathway's major functional output. The mitogen-activated protein kinase kinase kinase kinases (MAP4Ks) were recently discovered as additional core components acting in parallel to MST1/2 upon Hippo pathway activation (Meng et al., 2015). Together, the MST1/2-Sav1 complex and the MAP4Ks phosphorylate and activate Lats1/2-MOB1A1B, which in turn phosphorylate and inhibit YAP/TAZ.

Hippo pathway deregulation induces tumorigenesis in model organisms and in a wide range of human carcinomas. A recent study analyzing over 9,000 tumors profiled by The Cancer Genome Atlas (TCGA) identified the Hippo pathway as among the top 10 somatically altered canonical signaling pathways in cancer (Sanchez-Vega et al., 2018). Thus, both the Hippo pathway's core and peripheral components – and its primary functional effectors YAP/TAZ – have emerged as attractive therapeutic targets. Indeed, a number of companies and academic institutions have developed small molecular entities targeting YAP/TAZ (and to a lesser extent its upstream kinases) for biochemical and translational use, but for the

most part require additional efforts for therapeutic and clinical relevance (Calses et al., 2019). Thus, there is considerable interest and necessity in advancing the potency, specificity, and clinical viability of small molecules targeting the Hippo pathway.

Here, we report the identification and characterization of VT01454, a novel small-molecule inhibitor and Microcolin B (MCB) analog that induces YAP phosphorylation. We describe the structural optimization of MCB to yield its more potent analog VT01454 and bifunctional probe VT01702, and demonstrate the potency of VT01454 in Hippo pathway activation at low nanomolar concentrations. Additionally, both MCB and VT01454 exhibit selective cytotoxicity against YAP-dependent uveal melanoma (UM) cell lines. Collectively, the data rationalize future use of bio-orthogonal methods to identify the protein target(s) of VT01454 and to further delineate a mechanism of action, both of which would provide grounds for future therapeutic targeting as well as a potentially novel mechanism of Hippo pathway regulation.

2.1.1 The Hippo Pathway as a Therapeutic Target

Therapeutically targeting the Hippo pathway presents a unique set of challenges. Generally speaking, kinases are the most ideal targets for small-molecule therapeutics. Unlike most oncogenic kinase cancer targets, however, the majority of the Hippo kinases (i.e. MST1/2 and LATS1/2) are *bona fide* tumor suppressors (Harvey et al., 2013). This means that inhibiting of any of these components, with the exception of LATS1/2 under the pretext of immunotherapy, would likely increase cell proliferation and be entirely counterproductive in the context of cancer. Thus, the conventional approach of small-molecule kinase inhibition is unlikely to work. While previous studies have identified inhibitors of MST1/2 for the purpose of regenerative medicine (Fan et al., 2016), the rational design of agonists targeting the core Hippo kinases (i.e. restoring loss-of-function) is far more challenging. This leaves YAP and TAZ, along with the TEADs, at the forefront of therapeutic design.

Previous studies have showcased largely indirect methods of targeting the Hippo pathway for YAP inhibition. Statins, for instance, are routinely used to treat hypercholesterolemia and inhibit the conversion of 3-hydroxy-3-methyl-glutaryl-coenzyme A (HMG-CoA) to mevalonate. Mevalonate is a precursor for downstream synthesis of geranylgeranyl pyrophosphate, which is in turn required for Rho GTPase

activation, thereby preventing Rho GTPase inhibition of LATS kinase activity and consequently inhibiting YAP/TAZ (Sorrentino et al., 2014). Dobutamine, a GPCR β-adrenergic receptor (BAR) antagonist, likewise indirectly inhibits YAP transcriptional activity (Bao et al., 2011). In a similar vein, lysophosphatidic acid (LPA) and sphingosine-1-phosphate (S1P), both of which stimulate YAP activity, have also attracted therapeutic interest (Murph and Mills, 2007), and monoclonal antibodies against LPA and S1P have been developed with high specificity and affinity (Fleming et al., 2011, Wojciak et al., 2009).

2.1.2 Current Small-Molecule YAP-TEAD Inhibitors

Key potentially druggable sites in the protein–protein interface between YAP/TAZ and TEAD have recently been identified, as well as a highly conserved TEAD palmitoylation pocket (Noland et al., 2016, Chan et al., 2016, Mesrouze et al., 2017), providing a platform to screen for small molecules targeting the Hippo pathway in cancers. One such small molecule is verteporfin, a porphyrin derivative FDA-approved for the treatment of wet aged-macular degeneration (AMD) (Table 2.1). Verteporfin inhibits YAP activity by abrogating the YAP-TEAD interface (Liu-Chittenden et al., 2012), and has been prominently featured in the Hippo pathway literature owing to its ability to inhibit YAP-induced tumor growth and progression (Yu et al., 2014, Feng et al., 2014).

Despite its known anticancer activities, verteporfin has several drawbacks. First, it is a clinical photosensitizer used to treat macular degeneration, and as such, has poor solubility and bioavailability (Brodowska et al., 2014). Second, verteporfin has low affinity for YAP and is difficult to modify for structure-based optimization. Finally, verteporfin's low affinity for YAP means higher levels of general toxicity, thereby making it an unfavorable drug (Dasari et al., 2017). It is also worth noting that verteporfin is known to induce oligomerization of proteins involved in major cellular processes, including autophagy and cytoskeletal maintenance, among others (Brodowska et al., 2014, Gibault et al., 2016). Taken together, verteporfin has generally served as a valuable research tool, but its viability as a foundation for drug discovery efforts is unclear. Likewise, the compound CA3 was reported as a YAP inhibitor modulating YAP/TEAD transcriptional activity and decreasing YAP expression (Song et al., 2018); however, its mechanism of YAP interaction and inhibition remain unknown.

Several more recent studies from companies and academic institutions alike have also identified and/or patented direct small-molecule inhibitors of YAP and the YAP-TEAD interaction, reviewed in detail elsewhere (Crawford et al., 2018). For instance, the French biotechnology company Inventiva has filed multiple patent applications based on a bis-aryl hydrazine scaffold exhibiting appreciable activity in a TEAD–GAL4 transactivation assay and antiproliferative effects in the NCI-H2052 mesothelioma cell line (albeit at high concentrations), while another group at Massachusetts General Hospital focused on a more defined method of YAP-TEAD inhibition by targeting a palmitoyl binding pocket at the core of all four TEADs essential for TEAD folding, stability, and YAP binding (Table 2.1) (Mesrouze et al., 2017, Noland et al., 2016, Chan et al., 2016). A representative compound was shown to inhibit target gene expression and cell proliferation in the HuH7 liver cell line; however, activity was reported only at relatively high concentrations (30 and 10 μM, respectively) (Crawford et al., 2018).

The nonsteroidal anti-inflammatory drug (NSAID) flufenamic acid binds to the central pocket of TEAD2 but interestingly, does not inhibit YAP-TEAD binding (Table 2.1) (Pobbati et al., 2012). Previous reports showed that flufenamic acid treatment decreased cell growth, TEAD reporter activity, and several Hippo pathway responsive genes by an unknown mechanism of action. More recently, an independent group identified flufenamic acid derivatives containing chloromethyl ketone moieties that bind to the conserved cysteine in the TEAD palmitoyl-binding pocket, thereby inhibiting YAP–TEAD interaction, transcriptional activity, and glioblastoma growth *in vitro* (Table 2.1) (Bum-Erdene et al., 2019).

Finally, cyclic YAP-like peptides represent another emerging class of YAP-TEAD inhibitors. In an early report, Hu and coworkers at Roche employed structure-based design to identify a cyclic YAP-TEAD blocking peptide that could compete with endogenous YAP binding to GST-TEAD1 in cell lysate, with an IC_{50} of 25 nM (Table 2.1) (Zhang et al., 2014), though they were unable to leverage this into a cell-active tool compound. In later studies, Jiao *et al.* found an approach to targeting YAP–TEAD by designing a peptide mimicking Vestigial Like Family Member 4 (VGLL4), known as ‘super-TDU’ (Table 2.1) (Jiao et al., 2014), based on the premise that the VGLL4 represses YAP activity in the nucleus by competitively binding to TEAD (Pobbati et al., 2012). Similar to its endogenous counterpart, the ‘super-TDU’ peptide significantly reduced gastric cell growth *in vitro* and *in vivo* by binding to TEAD in a YAP-competitive manner (Jiao et

al., 2014). While both studies provide proof-of-concept for these types of antagonistic peptides, additional studies are needed to determine their clinically viability and their applicability across other cancer types.

2.2 Results

2.2.1 Phenotypic screening of small molecules that induce YAP phosphorylation

To identify small molecule inhibitors of YAP, we conducted a chemical library screen comprising 152 naturally derived marine compounds (Figure S2.1A), using YAP phosphorylation by mobility shift on a Phostag^{TM} gel as a readout. Among the screened molecules, Microcolin B was found to induce YAP phosphorylation in the micromolar range (Figure 2.1A and 2.1B). Furthermore, overexpression of the YAP-5SA mutant antagonized the effects of VT01454 on YAP phosphorylation (Figure 2.1A), confirming that the inhibitor indeed compromised YAP phosphorylation status.

Microcolin A (Compound **1** of Figure S2.1D) and Microcolin B (Figure 2.1A) are bioactive lipopeptides first isolated from the cyanobacterium *Lyngbya majuscule* (Koehn et al., 1992). The Microcolins possess immunosuppressive, antiproliferative, proapoptotic, and anti-cell adhesion activities (Koehn et al., 1992, Zhang et al., 1997, Zhang and Longley, 1999, Takamatsu et al., 2004). Syntheses and structure-activity relationships for the Microcolins have been reported (Koehn et al., 1994, Mattern et al., 1996, Decicco and Grover, 1996, Mattern et al., 1997, Andrus et al., 1997), as have analogs designed to study their mechanism of action (Mandal et al., 2005). However, no biological macromolecules with high affinity for Microcolins have yet been identified.

2.2.2 Structure-based optimization of Microcolins as YAP inhibitors

To improve the potency of Microcolin B towards YAP, structure–activity relationships (SAR) were explored in a parallel study, and this effort led to various analogs with improved potency and specificity (analogs prepared by Vivace Therapeutics). The primary goals for the SAR studies were: (1) to design analogs with enhanced cellular potency; and (2) to design a bifunctional probe that incorporated a linker

(e.g. an alkyne handle) while retaining its potency, thereby permitting its downstream conversion into various tools useful in experiments aimed towards target identification, such as affinity-based proteomics.

Subsequent screening of Microcolin analogs determined that des-acetyl Microcolin B (Figure S2.1D, compound **4**) (VT00349) is similarly active, and des-acetyl Microcolin A (Figure S2.1D, compound **3**) (VT01454) is 40X more active, but dihydro Microcolin B (Figure S2.1D, compound **5**) (VT00356) is inactive. This structure-activity relationship is similar to that reported for Microcolins using other measures of bioactivity (Koehn et al., 1992, Koehn et al., 1994). The inactivity of compound **5** suggested that compounds **2**, **3**, and **4** may undergo a Michael reaction with a cysteine thiol in a target protein. This in turn suggested that the doubly reactive probe **6** (VT01702) might undergo the hypothesized Michael reaction, as well as a subsequent click chemistry reaction with tracers appropriate for the visualization and capture of a target protein. The probe **6** was prepared and determined to have activity intermediate between (compound **2** or **4**) and compound **3**, and the performance of this reactive probe was deemed sufficient to move forward with additional cellular assays and chemical proteomics for target identification (Figure 3.1). In all subsequent experiments, the compounds used will be henceforth referred to as MCB (Microcolin B/VT00321/compound **2**), VT01454 (des-acetyl Microcolin A/compound **3**), and VT01702 (reactive probe **6**).

2.2.3 VT01454 induces YAP phosphorylation via the core Hippo kinase cascade

While VT00321 treatment in cells induced YAP phosphorylation and cytoplasmic translocation in the micromolar range (Figure 2.1B, S2.1B, S2.1C), treatment with its more potent analog VT01454 induced both aforementioned phenotypes in the low nanomolar range (Figure 2.1C, 2.1D, S2.1B), and their relative potency was consistent with data generated using a firefly luciferase-based TEAD-Binding Reporter (8xTBD) assay (Figure 2.1A and 2.1B).

Lats1/2 are the major direct regulators of YAP phosphorylation status; we thus asked whether VT01454 induced Lats1/2 phosphorylation to inhibit YAP activity. Consistent with this premise, we found that VT01454 treatment led to increased levels of Lats1 phosphorylation (Figure 2.2B). To determine whether VT01454 activity was dependent on Lats1/2 and other upstream core Hippo pathway components, we utilized various Hippo pathway knockout cell lines previously generated in the lab (Plouffe et al., 2016).

While parental HEK293A, Lats1, and Lats2 KO cells exhibited YAP phosphorylation and cytoplasmic translocation upon MCB treatment (Figures 2.2E and 2.2F), Lats1/2 double knockout cells (dKO) were unable to phosphorylate YAP upon both MCB and VT01454 treatment, indicating that these compounds operated in a Lats1/2-dependent manner (Figure 2.2E and 2.2G).

MST1/2 and the MAP4K family of kinases act in parallel to regulate Lats1/2 phosphorylation (Meng et al., 2015). We therefore asked whether either or both regulatory legs were required for VT01454 activity. While VT01454 did not appear to depend on MST1/2 to induce YAP phosphorylation (data not shown), MST1/2/MAP4K1/2/3/4/6/7 knockout (MM-8KO) cells were no longer sensitive to VT01454 (Figure 2.2H and 2.2I). Taken together, these data suggest that VT01454 induced YAP phosphorylation through core Hippo pathway components and warranted further study as a Hippo pathway activator.

2.2.4 VT01454 induces specific and potent cytotoxicity in uveal melanoma cells harboring Gq/11 mutations

To address the specificity of MCB and its analog VT01454 towards YAP, we performed a set of experiments using several uveal melanoma (UM) cell lines. Previous studies have shown that UM cell lines harboring $G_{q/11}$ mutations exhibit YAP hyperactivity, upon which the cancer cells depend for tumorigenesis (Yu et al., 2014). We hypothesized that UM cell lines harboring $G_{q/11}$ mutations (e.g. 92.1, OMM1) would be more sensitive to YAP inhibition compared to their B-raf-mutated counterparts (e.g. OCM1, OCM8), and tested this idea by treating 92.1, OMM1, OCM1, and OCM8 cells with MCB or VT01454 for 24 and 48 hours then imaging the cells for morphological changes. Indeed, we found that both VT01454 and MCB induced selective cytotoxicity in only the $G_{q/11}$-mutant but not the B-raf-mutated cell lines at both the 24 and 48-hour timepoints, based on cell morphology (Figure 2.3A and Figure S2.3A). Consistently, cell viability via trypan blue staining also demonstrated higher degrees of cytotoxicity in the 92.1 and OMM1 cell lines compared to the OCM1 and OCM8 cell lines (Figure 2.3B and Figure S2.3B).

To check for apoptotic induction, cells were stained with Annexin V following 48h of VT01454 treatment, and flow cytometric analysis demonstrated higher levels of apoptotic induction in the 92.1 and OMM1 compared to the OCM1 and OCM8 cell lines (Figure 2.3C and Figure S2.3C). Soft agar colony formation assay is a well-established method to characterize the capacity of transformed cells for

anchorage-independent growth *in vitro*. In alignment with our hypothesis, VT01454 and MCB severely impaired colony formation in 92.1 but not OCM1 cells (Figure 2.3D and Figure S2.3D). Finally, PARP cleavage was assessed as additional indicator of apoptotic induction, and, consistent with our previous observations, 92.1 and OMM1 cells exhibited higher levels of PARP cleavage compared to their OCM1 and OCM8 counterparts (Figure 2.3E).

2.3 Discussion

We herein identify Microcolin B (MCB) as a novel molecule targeting the Hippo pathway, using a phenotypic screen for compounds inducing YAP phosphorylation and inhibition. MCB is a naturally synthesized, bioactive lipopeptide with known immunosuppressive and antiproliferative effects (Zhang et al., 1997). Treating cells with MCB led to YAP phosphorylation and cytoplasmic translocation in a Lats1/2- and MAP4K-dependent manner. Structural optimization was performed on Microcolin B to yield its more potent analog VT01454 and bifunctional probe VT01702 for downstream bioorthogonal applications. VT01454 treatment induced an identical if not enhanced phenotypic profile as its parent compound MCB but at doses in the low nanomolar range, thus demonstrating its improved potency.

Furthermore, MCB and VT01454 induced high levels of cytotoxicity and apoptotic induction in YAP-dependent $G_{q/11}$-mutated but not in B-raf-mutated uveal melanoma cells, demonstrating their high specificity for targeting YAP. These results collectively demonstrate the specificity of VT01454 and analogs in targeting YAP, rationalizing further studies to identify their protein target(s) and delineate mechanism of action. Identifying the putative target(s) of VT01454 and its mechanism of action is not only critical to future optimization of these compounds for any potential clinical applications, but may also reveal previously unknown regulators of the Hippo pathway.

2.4 Experimental Procedures

Synthesis of Microcolin Analogs

Compounds **1-5** were synthesized using previously established methods (Koehn et al., 1994). A detailed synthesis of Compound **6** (VT01702) is described below and LCMS spectra for Intermediate 4, Intermediate 5, and Compound **6** can be found in Figure S2.3.

***tert*-Butyl *N*-[(1*S*)-1-[[(1*S*,2*R*)-2-hydroxy-1-[[(1*S*)-1-[(2*S*,4*S*)-4-hydroxy-2-[(2*S*)-2-methyl-5- oxo-2*H*-pyrrole-1-carbonyl]pyrrolidine-1-carbonyl]-2-methyl-propyl]-methylcarbamoyl] propyl]carbamoyl]-3-methyl-butyl]-*N*-methyl-carbamate (Intermediate 4)**

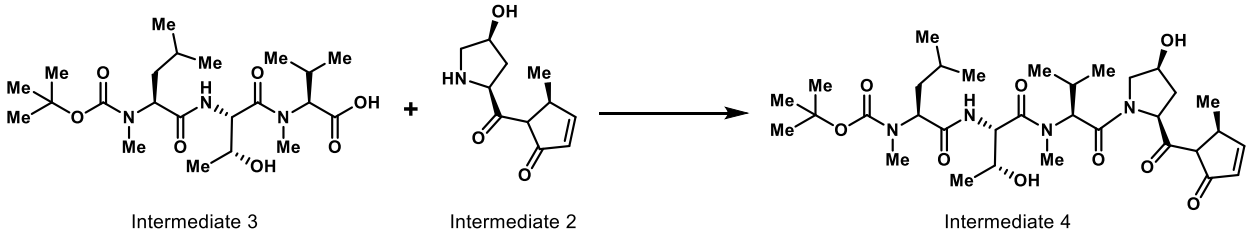

Intermediate **2** was prepared as previously described (Decicco and Grover, 1996). Intermediate **3** was prepared by basic hydrolysis of the O-acetyl threonine analog, which has been previously described (Decicco and Grover, 1996). Intermediate **3** (120 mg, 0.261 mmol, 1.0 eq) and Intermediate **2** (64 mg, 0.26 mmol, 1.0 eq) were dissolved in CH_2Cl_2 (6 mL). To this solution were added $EtN(iPr)_2$ (101 mg, 0.783 mmol, 3.0 eq) and bromo tris(dimethylamino) phosphonium hexafluorophosphate (101 mg, 0.261 mmol, 1.0 eq). The reaction mixture was stirred at 25 °C for 2 hours. The reaction mixture was diluted with water (6 mL), and the resulting mixture was extracted with CH_2Cl_2 (2 x 20 mL). The combined organic layers were dried over Na2SO4, filtered, and evaporated under vacuum. The residue was purified by preparative HPLC using a Waters Xbridge BEH C18 OBD, 130 Angstrom, 5 micrometer, 30 mm x 150 mm column, and 35/65 v/v CH_3CN/H_2O (0.05% ammonium hydroxide) eluent. The pure fractions were combined and evaporated under vacuum. The residue was resuspended in water (10 mL), and the resulting mixture was lyophilized. The title compound (80 mg, 47% yield) was obtained as a white solid. Mass calcd. for $C_{32}H_{53}N_5O_9$ 651.38, m/z found 674.3 [M+Na]+.

(2*S*)-*N*-[(1*S*,2*R*)-2-hydroxy-1-[[(1*S*)-1-[(2*S*,4*S*)-4-hydroxy-2-[(2*S*)-2-methyl-5-oxo-2*H*-pyrrole-1-carbonyl]pyrrolidine-1-carbonyl]-2-methyl-propyl]-methyl-carbamoyl]propyl]-4- methyl-2-(methylamino)pentanamide (Intermediate 5)

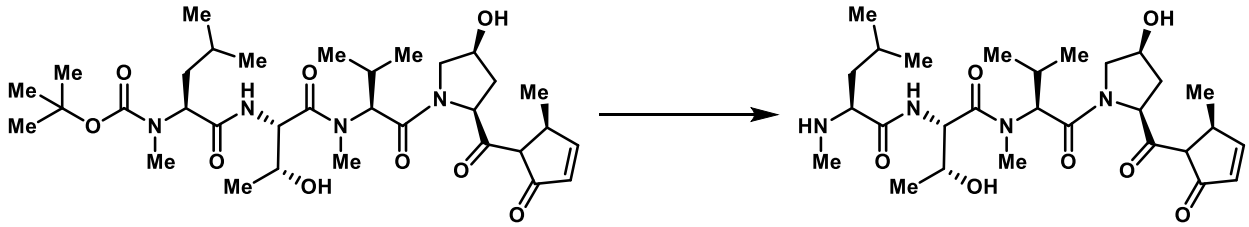

Intermediate 4 Intermediate 5

Intermediate **4** (30 mg, 46 umol, 1.0 eq) was dissolved in dioxane (1 mL) and treated with 4M HCl in dioxane (2 mL) at 0 °C. The reaction mixture was stirred at 0 °C for 2 hours. The mixture was diluted with saturated aqueous $NaHCO_3$ (15 mL), and the resulting mixture was extracted with CH_2Cl_2 (3 x 30 mL). The combined organic layers were dried over Na_2SO_4, filtered, and evaporated under vacuum to obtain the title compound (24 mg, crude) as a yellow oil. Mass calcd. for $C_{27}H_{45}N_5O_7$ 551.33, m/z found 574.2 [M+Na]+.

***N*-[(1*S*)-1-[[(1*S*,2*R*)-2-hydroxy-1-[[(1*S*)-1-[(2*S*,4*S*)-4-hydroxy-2-[(2*S*)-2-methyl-5-oxo-2*H*-pyrrole-1-carbonyl]pyrrolidine-1-carbonyl]-2-methyl-propyl]-methylcarbamoyl] propyl]carbamoyl]-3-methyl-butyl]-*N*-methyl-undec-10-ynamide (Compound 6)**

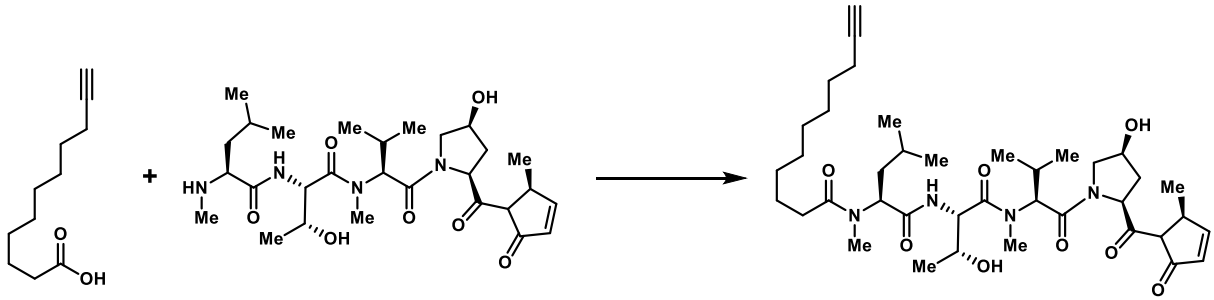

10-undecynoic acid Intermediate 5 Compound **6**

To a solution of Intermediate **5** (24 mg, 43 umol, 1.0 eq) and 10-undecynoic acid (7.9 mg, 44 umol, 1.0 eq) in CH_2Cl_2 (1 mL) at 0 °C were added EtN(*i*Pr)$_2$ (17 mg, 0.13 mmol, 3.0 eq) and bis-(2- oxo-3-oxazolidinyl) phosphinic chloride (11 mg, 44 umol, 1.0 eq). The reaction mixture was warmed to 20 °C, and then stirred at 20 °C for 1 hour. The reaction mixture was diluted with water (10 mL), and the resulting mixture was extracted with CH_2Cl_2 (3 x 30 mL). The combined organic layers were dried over Na_2SO_4, filtered, and evaporated under vacuum. The residue was purified by preparative HPLC using a Waters Xbridge BEH

C18 OBD, 130 Angstrom, 5 micrometer, 30 mm x 150 mm column, and 50/80 v/v CH_3CN/H_2O (0.05% ammonium hydroxide) eluent. The pure fractions were combined and evaporated under vacuum. The residue was re-suspended in water (10 mL), and the resulting mixture was lyophilized. The title compound (5.80 mg, 19% yield) was obtained as a white solid. Mass calcd. for $C_{38}H_{61}N_5O_8$ 715.45, m/z found 738.4 [M+Na]+. ^{1}HNMR (400MHz, $CDCl_3$) δ 7.21 (dd, *J* = 2.0, 6.0 Hz, 1H), 6.84 (d, *J* = 9.0 Hz, 1H), 6.02 (dd, *J* = 1.6, 6.1 Hz, 1H), 5.59 (d, *J* = 8.5 Hz, 1H), 5.16 - 5.06 (m, 1H), 4.95 (d, *J* = 11.0 Hz, 1H), 4.80 - 4.70 (m, 1H), 4.70 - 4.64 (m, 1H), 4.34 (s, 1H), 4.10 - 3.82 (m, 3H), 3.78 - 3.70 (m, 1H), 3.62 - 3.49 (m, 1H), 3.01 (s, 3H), 2.86 (s, 3H), 2.43 - 2.32 (m, 1H), 2.31 - 2.17 (m, 3H), 2.15 - 2.06 (m, 2H), 1.97 (d, *J* = 14.6 Hz, 1H), 1.87 (t, *J* = 2.5 Hz, 1H), 1.72 - 1.63 (m, 1H), 1.49 - 1.43 (m, 2H), 1.49 - 1.42 (m, 1H), 1.39 (d, *J* = 6.8 Hz, 3H), 1.36 - 1.30 (m, 3H), 1.28 - 1.20 (m, 7H), 0.99 (d, *J* = 6.3 Hz, 3H), 0.93 (d, *J* = 6.5 Hz, 3H), 0.91 - 0.84 (m, 4H), 0.83 (d, *J* = 6.5 Hz, 3H), 0.75 (d, *J* = 6.8 Hz, 3H).

Cell Culture

All cell lines were cultured at 37 °C with 5% CO_2. HEK293A cells were cultured in DMEM (GIBCO) with 10% FBS (GIBCO), 100 U ml^{-1} penicillin and 100 μg ml^{-1} streptomycin, and uveal melanoma cell lines were cultured in RPMI with 10% FBS (GIBCO), 100 U ml^{-1} penicillin and 100 μg ml^{-1} streptomycin. HEK293A cells were utilized for all experiments, unless otherwise noted. All knockout cell lines utilized in this study were previously generated and published in the lab. Cells were transfected with plasmids using PolyJet DNA In Vitro Transfection Reagent (Signagen Laboratories) according to the manufacturer's instructions.

Plasmids and Antibodies

Flag-YAP, Flag-YAP 5SA, GST-YAP were previously generated in the lab. Anti-YAP/TAZ, GAPDH, and actin antibodies were obtained from Santa Cruz Biotechnology. Anti-phospho-YAP (S127), LATS1, phospho-Lats1/2 (Thr 1079/1041), PARP, phospho-Akt (Thr 308), Akt, and HA-HRP antibodies for Western blot, YAP antibody for phostag, and Flag (DYKDDDDK) tag antibodies for IF were obtained from Cell Signaling. Flag-HRP and Flag (M2) for IP were obtained from Sigma-Aldrich. Alexa Fluor 488, 555, and 647-conjugated secondary antibodies for IF were obtained from Invitrogen.

8xTBD assay

YAP reporter assay was performed with a cell line stably engineered to harbor the 8XTBD-driven firefly luciferase gene and TK-driven Renilla luciferase gene as described (Tang et al. Manuscript in preparation).

Western blots

Western blots were performed following standard methods. 7.5% phos-tag gel was used to resolve the phospho-YAP proteins.

Immunofluorescence

Coverslips were pretreated with 2ug/mL Fibronectin solution (Sigma, P4957) in 12-well plates at 37°C overnight and washed with culture media prior to seeding cells. Cells were seeded at 0.3e5 cells/well for transfection or at 0.7e5 cells/well for drug treatments. Cells were fixed in 4% paraformaldehyde for 15 minutes, followed by permeabilization with 0.1% Triton-X for 10 minutes and blocking in 3% BSA for 1 hour. Primary antibody was incubated in 3% BSA overnight at 4°C. Secondary antibodies were diluted in 3% BSA and incubated for 1 hour. Slides were mounted with prolong gold anti-fade reagent with DAPI. Most images were captured with a Nikon Eclipse Ti confocal microscope and then were exported from NIS elements imaging software. Results were quantified in at least 100 randomly chosen cells. Image J was used to merge the signals from channels. For Figure 3A, a Nikon Inverted microscope was used.

Annexin V Staining

Cells were analyzed for phosphatidylserine exposure by an annexin-V FITC/propidium iodide double-staining method using Dead Cell Apoptosis Kit with Annexin V Alexa Fluor™ 488 & Propidium Iodide (PI) obtained from Thermo Fisher. Cells were collected after 48 h of VT01454 treatment and subjected to flow cytometric analysis. A minimum of 5,000 cells were then analyzed by BD FACSAria™ Fusion with FlowJo software for acquisition and analysis.

Soft Agar Colony Assay

A 12-well plate for cell culture was coated with 0.7 ml bottom agar (RPMI containing 10% FBS and 0.8% Difco agar noble). Uveal melanoma cells (4,000 92.1 and 2,000 OCM1 cells per well) were suspended in 1.5 ml top agar (DMEM containing 10% FBS and 0.3% Difco agar noble) in each well. The cells were incubated for 3 weeks and replaced with fresh medium every 3 d. The colonies were stained using 0.05% crystal violet.

2.5 Acknowledgements

I'd like to acknowledge Guang Bo Liu for spearheading the initial chemical library screen for MCB identification, as well as Tracy Tang and Andrei Konradi at Vivace Therapeutics for generously providing the structurally optimized analogs VT01454 and VT01702 and for helpful discussions.

Chapters 2 is currently being prepared for submission for publication of the material. Fu, V., Liu, G-B., Kemper, EK., Li, F-L, Mayfield, JE., Peng, X., Konradi, AW., Tang, TT., Dixon, JE., Cravatt, BF., Gerwick, WH., Guan, K-L. The dissertation author was the primary investigator and author of this material.

Table 2.1: Structures of Compounds Reported to Modulate Hippo Pathway Activity

No.	Compound	Mechanism of Action (MoA)	Institution	References
1	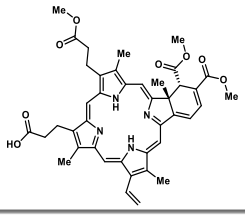	• YAP-TEAD inhibitor • Multiple targets reported, MoA unclear	Bausch + Lomb Verteporfin (Visudyne) is a trademark of Novartis	Liu-Chittenden et al, 2012
2	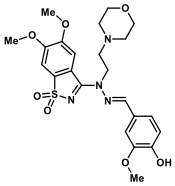	• YAP/TAZ-TEAD inhibitor • MoA unclear from patent	Inventiva	Crawford et al., 2018 (patent review)
3	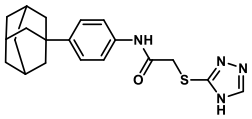	• Targets TEAD palmitoylation pocket • MoA unclear from patent	Mass General Hospital	Mesrouze et al., 2017 Noland et al., 2016 Chan et al., 2016
4	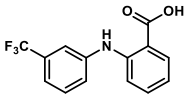	• Targets TEAD palmitoylation pocket • TEAD2-YAP binding is unaffected	A*STAR	Pobbati et al., 2015
5	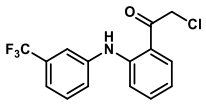	• Targets TEAD palmitoylation pocket • TEAD4-YAP binding is reduced	Indiana University	Bum-Erdene et al., 2018
6	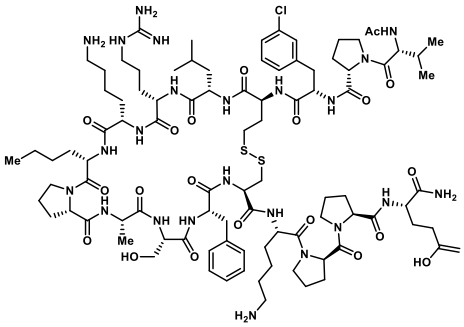	• YAP-TEAD binding competitor • TEAD1-YAP binding is inhibited	Roche	Zhang et al., 2014
7	SVDDHFAKSLGDTWLQIGGSGNPKTANVPQTVPMRLRKLPDSFFKPPE	• YAP-TEAD binding competitor • VGLL4 peptide binds to TEADs • TEAD4-YAP binding is reduced	Chinese Academy of Sciences	Jiao et al., 2014

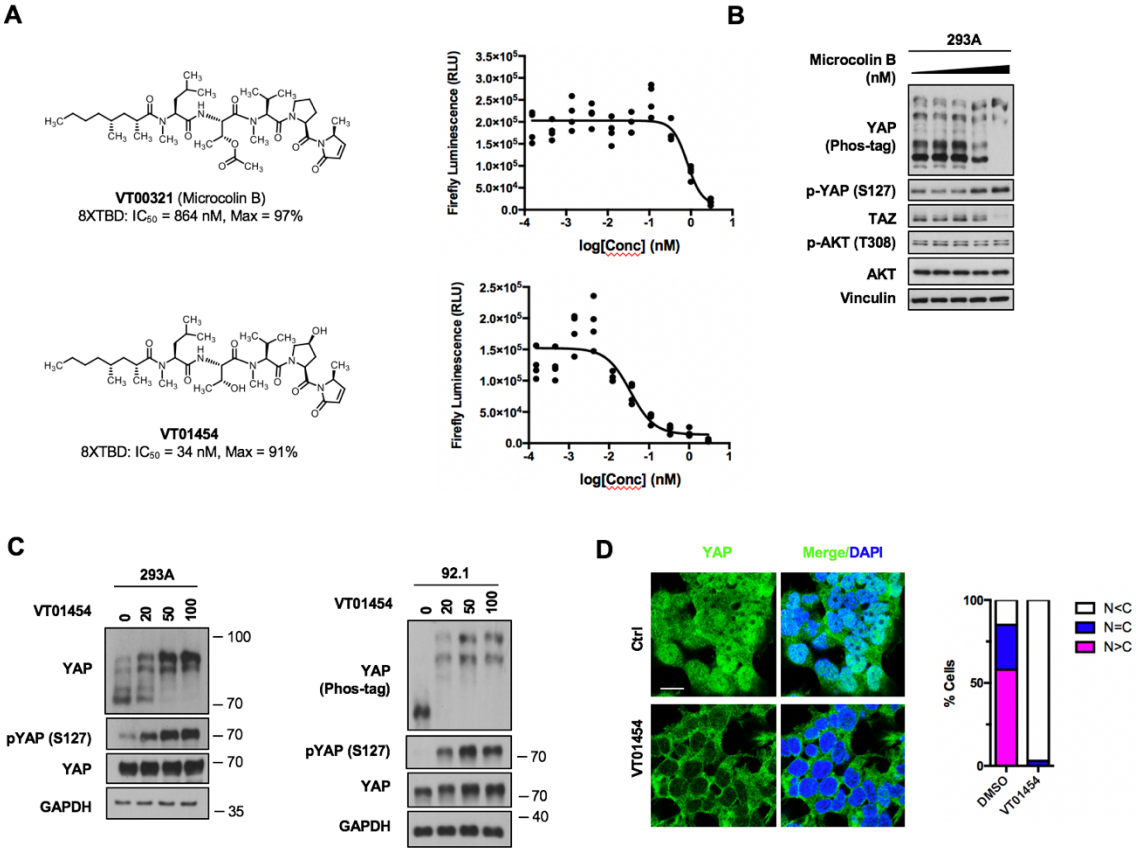

Figure 2.1: Microcolin B is a YAP inhibitor. (A) Structures of Microcolin B and VT01454 with luciferase reporter assays showing their respective effects on TEAD transcriptional activity. An 8xTEAD-Binding Domain (8xTBD) reporter was used. **(B)** Microcolin B induces YAP phosphorylation in a dose-dependent manner. HEK293A cells were treated for 4 hours with the following MCB concentrations: 0, 30, 70, 140, 270nM. **(C)** VT01454 induces YAP phosphorylation in the low nanomolar range. HEK293A and 92.1 cells were treated with the indicated concentrations of VT01454 for 1.5 hours. **(D)** VT01454 induces YAP cytoplasmic translocation. HEK293A cells were treated with DMSO or 50nM VT01454 for 2 hours before immunofluorescence staining of endogenous YAP (green) and 4',6-diamidino-2-phenylindole (DAPI) for DNA (blue). YAP localization was then quantified. Scale bar: 20uM.

Figure 2.2: VT01454 induces YAP phosphorylation through core Hippo pathway components. (A) YAP-5SA overexpression antagonizes MCB effects on YAP phosphorylation. HEK 293A cells were transfected with Flag-YAP wide type or Flag-YAP 5SA plasmids and then treated with 0, 0.15, 0.3 ug/ml MCB for 4 hours. CTL denotes control. **(B) and (C)** MCB induces Lats1 phosphorylation at both the T1079 site, and to a lesser extent, the S909 site. In (B) HEK293A cells were treated without or with 0.2 ug/ml MCB for 2 hours. Immunoprecipitation were performed by Lats1 antibody. Two Lats1 phosphorylated sites (T1079, S909) were tested. In (C) the kinase assays were performed in HEK293A cells with or without 0.2 ug/ml MCB treatment for 2 hours. GST-YAP was used as the Lats1 substrate. **(D) and (E)** MCB requires Lats1/2 to induce YAP phosphorylation and cytoplasmic translocation. 2D HEK293A control (Ctrl), Lats1 knockout (KO), Lats2 knockout (KO) and Lats1/2 double knock out (dKO) cells were treated with 0.15 ug/ml MCB for 2 hours. 2E HEK293A (Ctrl), Lats1 KO, Lats2 KO, and Lats1/2 dKO cells were treated without or with 0.2 ug/ml MCB for 4 hours and YAP localization was determined by immunofluorescence staining for YAP (Green) and 4',6-diamidino-2-phenylindole (DAPI) for DNA (blue). **(F)** VT01454 requires Lats1/2 to induce YAP phosphorylation. HEK293A (Ctrl), Lats1 KO, Lats2 knockout KO, and Lats1/2 dKO cells were treated with the indicated concentrations of VT01454 for 1.5 hours. **(G) and (H)** VT01454 requires both MST1/2 and MAP4K1/2/3/4/6/7 to induce YAP phosphorylation and cytoplasmic translocation. 2G Parental HEK293A and MST1/2/MAP4K1/2/3/4/6/7 knockout (MM-8KO) cells were treated with the indicated concentrations of VT01454 for 1.5 hours. In (H) cells were treated with 50 nM VT01454 for 2hrs and stained with YAP antibody (green) for immunofluorescence.

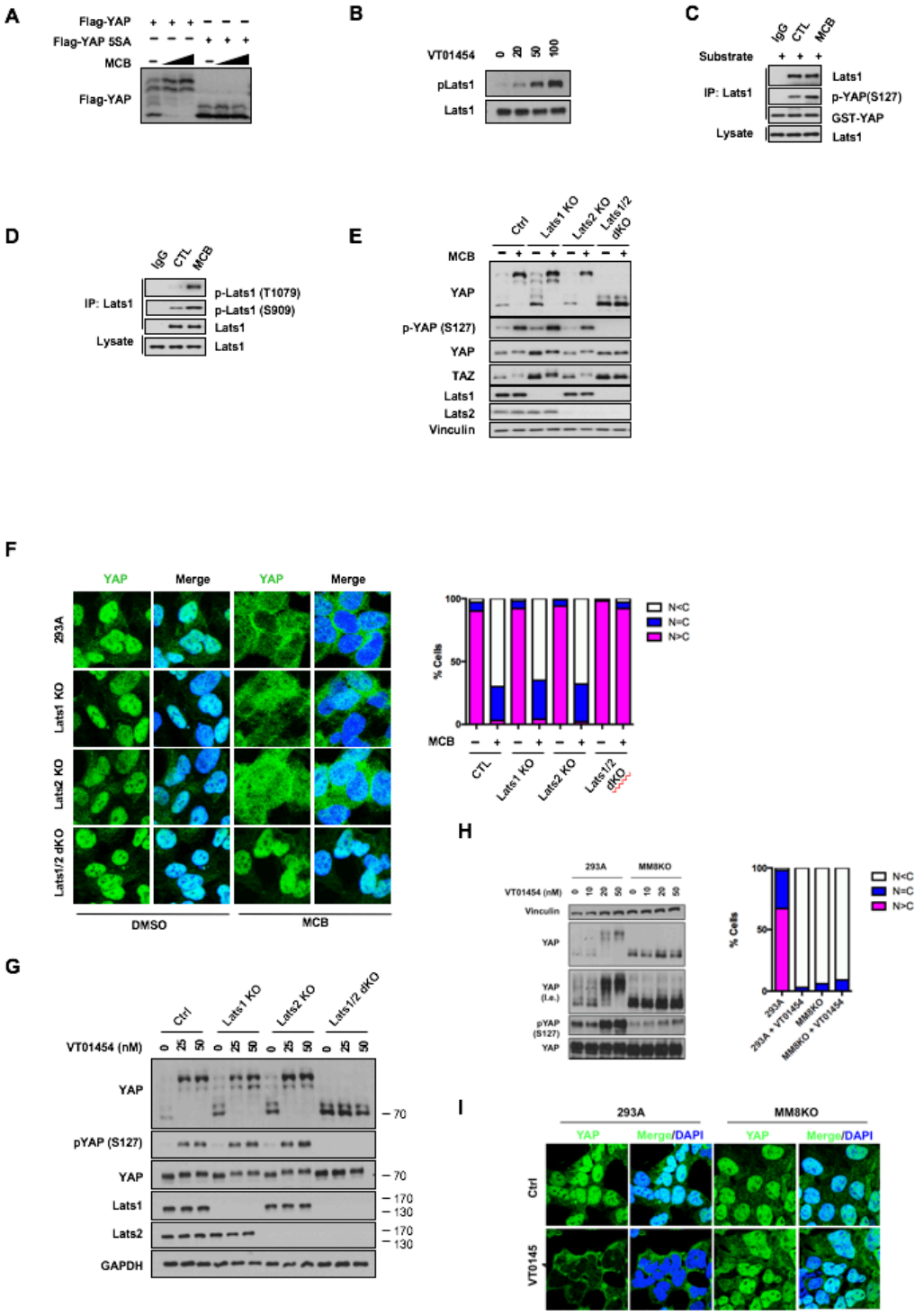
A
Flag-YAP
Flag-YAP 5SA
MCB
Flag-YAP
B
VT01454
0 20 50 100
pLats1
Lats1
C
IgG CTL MCB
Substrate
IP: Lats1
Lats1
p-YAP(S127)
GST-YAP
Lysate
Lats1
D
IgG CTL MCB
IP: Lats1
p-Lats1 (T1079)
p-Lats1 (S909)
Lats1
Lysate
Lats1
E
Ctrl Lats1 KO Lats2 KO Lats1/2 dKO
MCB
YAP
p-YAP (S127)
YAP
TAZ
Lats1
Lats2
Vinculin
F
YAP Merge YAP Merge
293A
Lats1 KO
Lats2 KO
Lats1/2 dKO
DMSO
MCB
% Cells
N<C
N=C
N>C
MCB
CTL
Lats1 KO
Lats2 KO
Lats1/2 dKO
G
Ctrl Lats1 KO Lats2 KO Lats1/2 dKO
VT01454 (nM)
0 25 50 0 25 50 0 25 50 0 25 50
YAP
pYAP (S127)
YAP
Lats1
Lats2
GAPDH
70
70
170
130
170
130
H
293A MM8KO
VT01454 (nM)
0 10 20 50 0 10 20 50
Vinculin
YAP
YAP (l.e.)
pYAP (S127)
YAP
% Cells
N<C
N=C
N>C
293A
293A + VT01454
MM8KO
MM8KO + VT01454
I
293A MM8KO
YAP Merge/DAPI YAP Merge/DAPI
Ctrl
VT0145

Figure 2.3: VT01454 exhibits potent and specific cytotoxicity in YAP-dependent uveal melanoma cell lines. (A) and (B) VT01454 induces apoptosis in uveal melanoma cell lines harboring Gq/11 but not B-raf mutations. 92.1, OMM1, OCM1, OCM8 cells were treated with 50nM VT01454 or 2uM Verteporfin for 24 or 48 hours before capturing brightfield images and trypan blue staining for cell quantification. **(C)** Annexin V staining demonstrates VT01454 induces higher levels of apoptotic induction in Gq/11 but not B-raf mutated UM cells. 92.1, OMM1, OCM1, OCM8 cells were treated with 20 or 50 nM VT01454 for 48 hours. Cell apoptosis were analyzed by flow cytometry using Annexin V/7-AAD staining per manufacturer instructions. **(D)** VT01454 inhibits colony formation in Gq/11 but not B-raf mutated UM cells. 4,000 92.1 and 2,000 OCM1 cells were seeded without or with 50nM VT01454. After 30 days, cells were stained with crystal violet and quantified. **(E) and (F)** MCB induces PARP cleavage in Gq/11 but not B-raf mutated UM cells. 92.1, OMM1, OCM1 and OCM8 cells were treated with 0, 0.2, 0.5, 1, 2, or 4 ug/mL of MCB or VP for 48 hours. Cells were harvested and lysates immunoblotted for PARP expression. **(G)** VT01454 induces PARP cleavage in Gq/11 but not B-raf mutated UM cells. 92.1, OMM1, OCM1 and OCM8 cells were treated with 0, 2.5, 4, 10, 20, or 50 nM VT01454 for 48 hours. Cells were harvested and lysates immunoblotted for PARP expression.

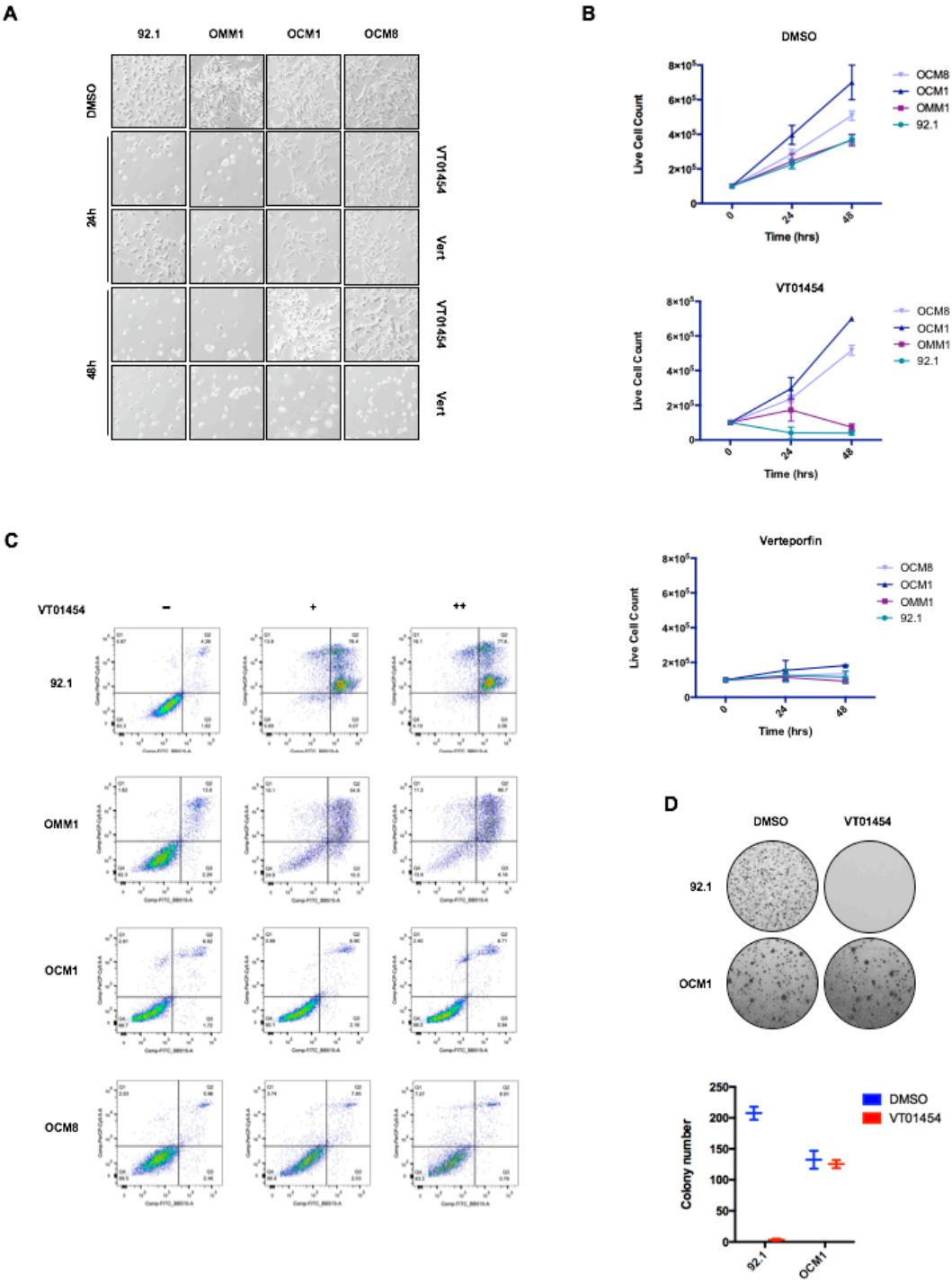
A
92.1
OMM1
OCM1
OCM8
DMSO
24h
48h
VT01454
Vert
VT01454
Vert
B
DMSO
Live Cell Count
Time (hrs)
OCM8
OCM1
OMM1
92.1
VT01454
Verteporfin
C
VT01454
–
+
++
92.1
OMM1
OCM1
OCM8
D
DMSO
VT01454
92.1
OCM1
Colony number
DMSO
VT01454

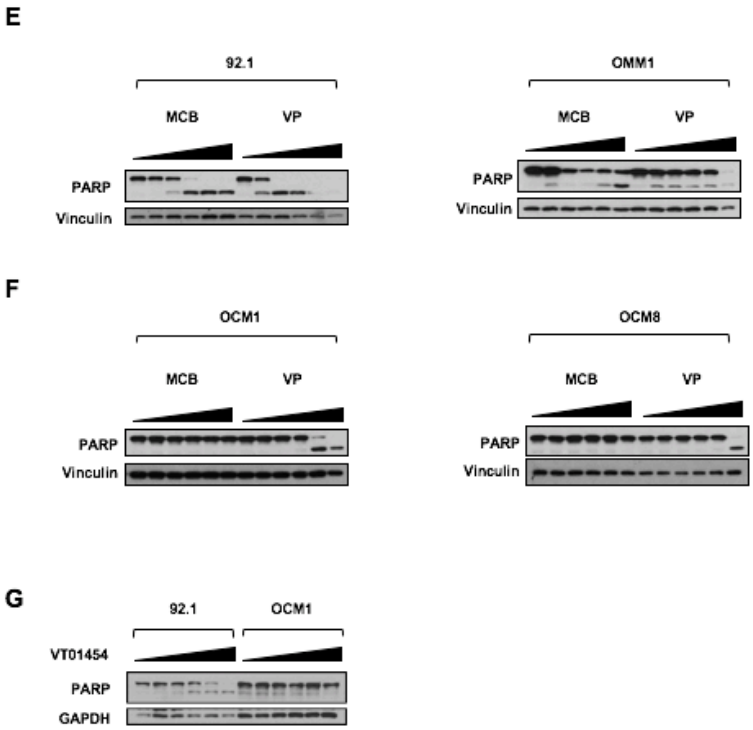

Figure 2.3: VT01454 exhibits potent and specific cytotoxicity in YAP-dependent uveal melanoma cell lines (continued)

Figure S2.1: Chemical library screen for YAP inhibitors. (A) Chemical library screen of marine compounds. HEK 293A cells were treated with 3 ug/ml of different compounds. YAP phosphorylation status was analyzed by immunoblotting. A list of compounds and their corresponding numbers can be found in Table S1 (. **(B)** MCB and VT01454 induce YAP phosphorylation in a time-dependent manner. HEK293A or 92.1 cells were cultured in DMEM supplemented with 10% fetal bovine serum. Cells were seeded at below 80% confluency. HEK293A cells were treated with 0.2 ug/mL MCB or 50 nM VT01454 for the indicated times. 92.1 cells were treated with 0.5 ug/ml MCB for the indicated times. **(C)** Microcolin B induces YAP cytoplasmic translocation. HEK293A cells were treated without or with MCB for 4 hours. Immunofluorescence were performed. YAP (Green), 4',6-diamidino-2-phenylindole (DAPI) for DNA (blue). The localization of YAP was quantified. **(D)** Structures of Microcolin A (1), Microcolin B (2), and their respective derivatives des-acetyl Microcolin A (3) and B (4), dihydro Microcolin B (5), and the doubly-reactive probe (6).

A

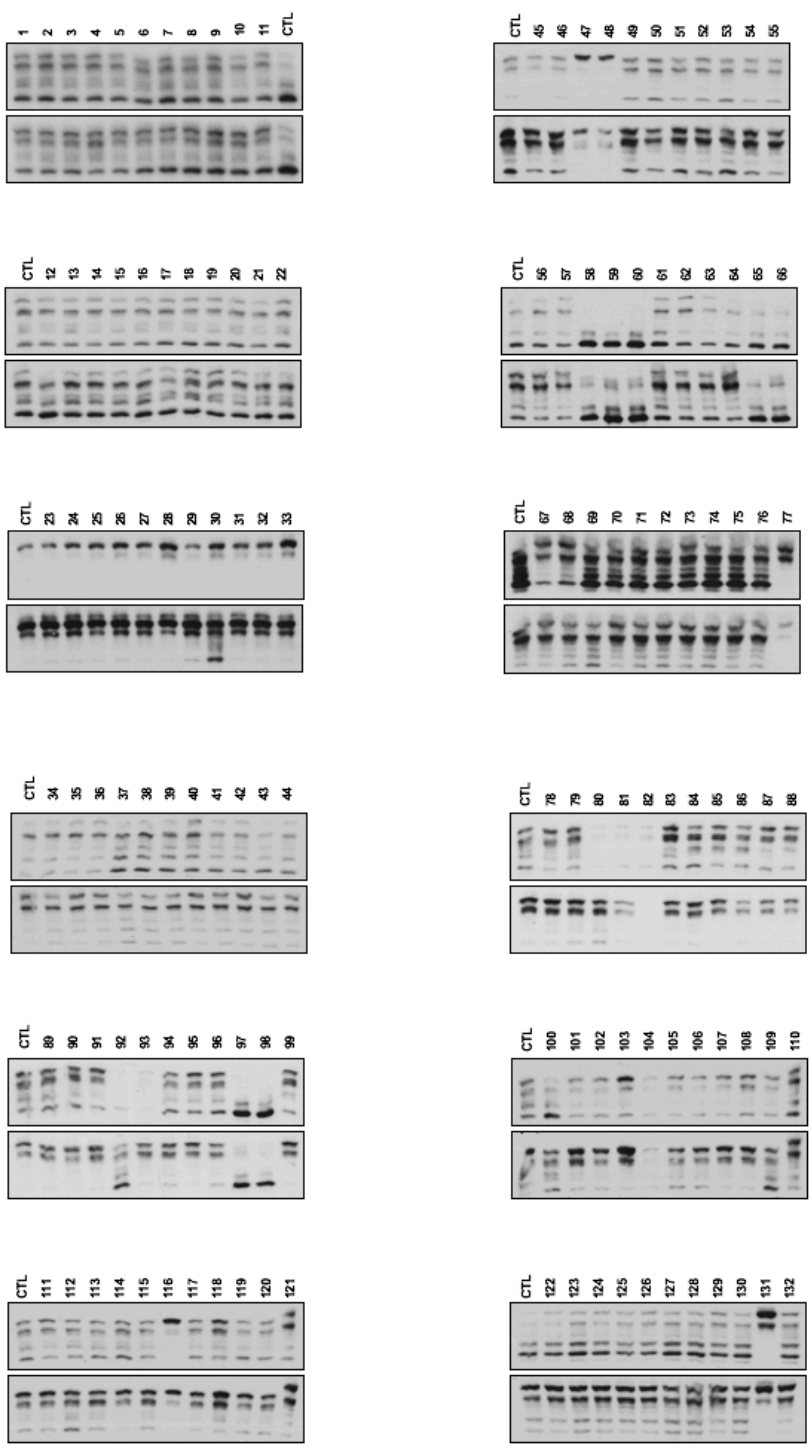
CTL 1 2 3 4 5 6 7 8 9 10 11 CTL
CTL 12 13 14 15 16 17 18 19 20 21 22
CTL 23 24 25 26 27 28 29 30 31 32 33
CTL 34 35 36 37 38 39 40 41 42 43 44
CTL 89 90 91 92 93 94 95 96 97 98 99
CTL 111 112 113 114 115 116 117 118 119 120 121
CTL 45 46 47 48 49 50 51 52 53 54 55
CTL 56 57 58 59 60 61 62 63 64 65 66
CTL 67 68 69 70 71 72 73 74 75 76 77
CTL 78 79 80 81 82 83 84 85 86 87 88
CTL 100 101 102 103 104 105 106 107 108 109 110
CTL 122 123 124 125 126 127 128 129 130 131 132

Figure S2.2: (A) MCB induces apoptosis in uveal melanoma cell lines harboring Gq/11 but not B-raf mutations. 92.1, OMM1, OCM1 and OCM8 cells were treated with 5 ug/ml MCB or 5 ug/ml verteporfin (VP) for 24 or 48 hours. The growth situation was photographed. SRB assay (ask Guangbo) was also performed in the indicated cells by MCB (5 ug/ml) or verteporfin (VP) for different times. All four are uveal melanoma cell lines. 92.1 and OMM1 have activating Gq mutation (so YAP is constitutively active) whereas OCM1 and OCM8 have activating B-Raf mutation (so YAP is not active). **(B)** Annexin V staining demonstrates MCB induces higher levels of apoptotic induction in Gq/11 but not B-raf mutated UM cells. 92.1 and OCM1 cells were treated with 0, 0.5, and 1 ug/ml MCB for 24 hours. Cell apoptosis were analyzed by flow cytometry using Annexin V/7-AAD staining. **(C)** MCB inhibits colony formation in Gq/11 but not B-raf mutated UM cells. 0.3 million 92.1 and OCM1 cells without or with 0.3 ug/ml MCB. After 30 days, Cells were stained by crystal violet and quantified.

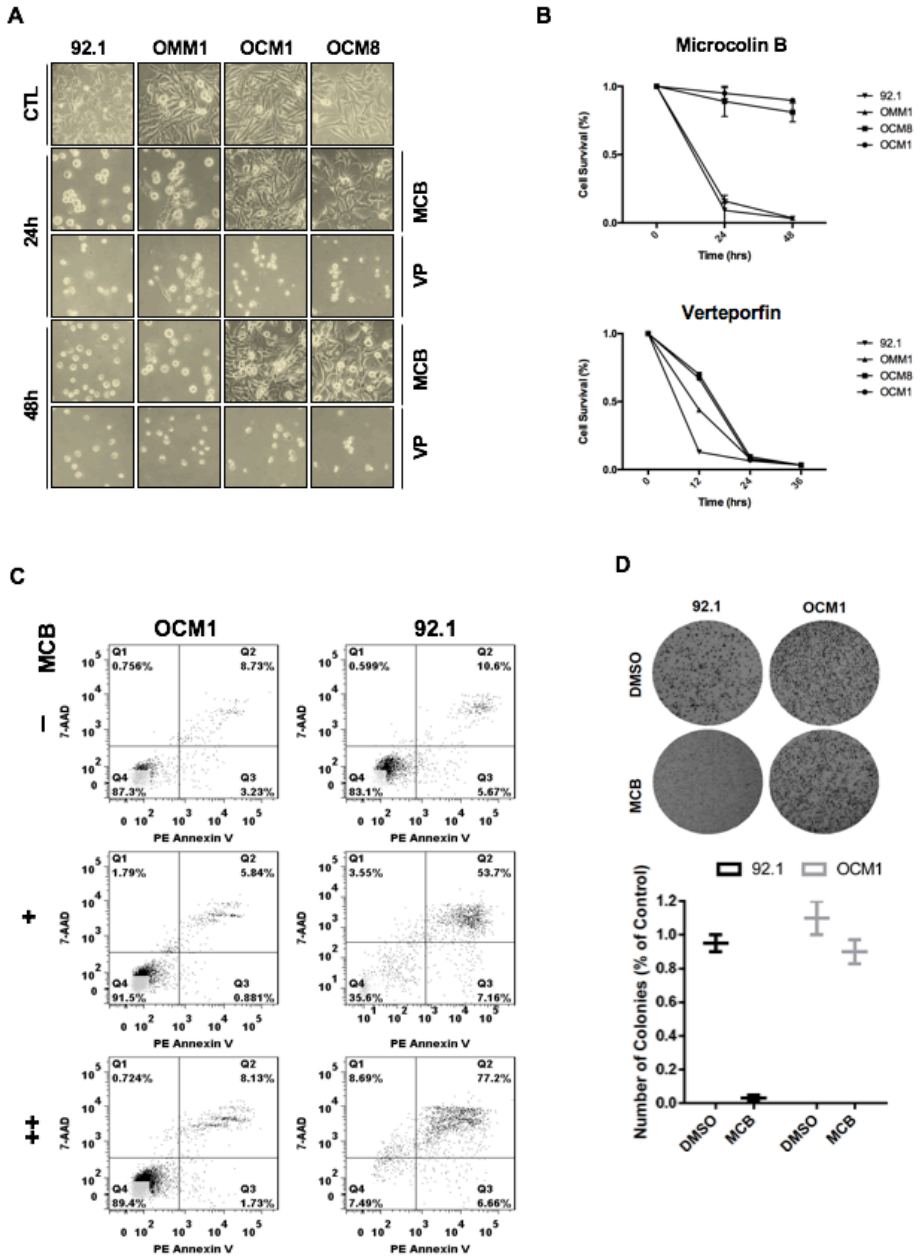
A
92.1
OMM1
OCM1
OCM8
CTL
24h
48h
MCB
VP
MCB
VP
B
Microcolin B
Cell Survival (%)
Time (hrs)
92.1
OMM1
OCM8
OCM1
Verteporfin
Cell Survival (%)
Time (hrs)
92.1
OMM1
OCM8
OCM1
C
MCB
OCM1
92.1
–
+
++
7-AAD
PE Annexin V
Q1 0.756%
Q2 8.73%
Q4 87.3%
Q3 3.23%
Q1 0.599%
Q2 10.6%
Q4 83.1%
Q3 5.67%
Q1 1.79%
Q2 5.84%
Q4 91.5%
Q3 0.881%
Q1 3.55%
Q2 53.7%
Q4 35.6%
Q3 7.16%
Q1 0.724%
Q2 8.13%
Q4 89.4%
Q3 1.73%
Q1 8.69%
Q2 77.2%
Q4 7.49%
Q3 6.66%
D
92.1
OCM1
DMSO
MCB
92.1
OCM1
Number of Colonies (% of Control)
DMSO
MCB
DMSO
MCB

Intermediate **4**

LCMS REPORT

Compound ID : 1
Sample ID : ES2506-970-P1B
Injection Date : 2/27/2017 19:03:19
Injection Vol : 8ul
Location : tray1 vial19
Acq Method : D:\method\5-95AB_1.5MIN_220&254.lcm
Org DataFile : D:\DATA\1702\170227\ES2506-970-P1B.lcd
Instrument & Column: LCMS-S(12#102) : MERCK RP-18e 25-2mm,UM8505/148

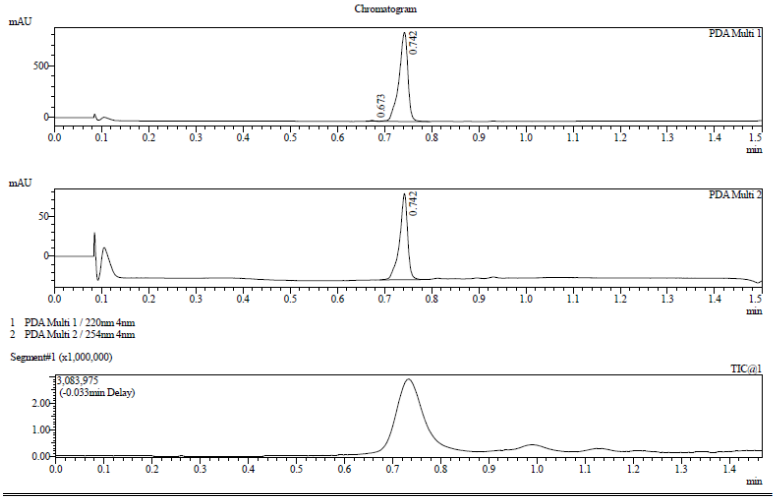

Integration Result

Ch1 220nm 4nm

Peak#	Ret. Time	Height	Height %	USP Width	Area	Area %
1	0.673	9542	1.105	0.015	6324	0.554
2	0.742	853626	98.895	0.032	1135151	99.446

Ch2 254nm 4nm

Peak#	Ret. Time	Height	Height %	USP Width	Area	Area %
1	0.742	105833	100.000	0.029	127882	100.000

Figure S2.3: LCMS Reports of Intermediate 4, Intermediate 5, and Compound 6

Intermediate 4

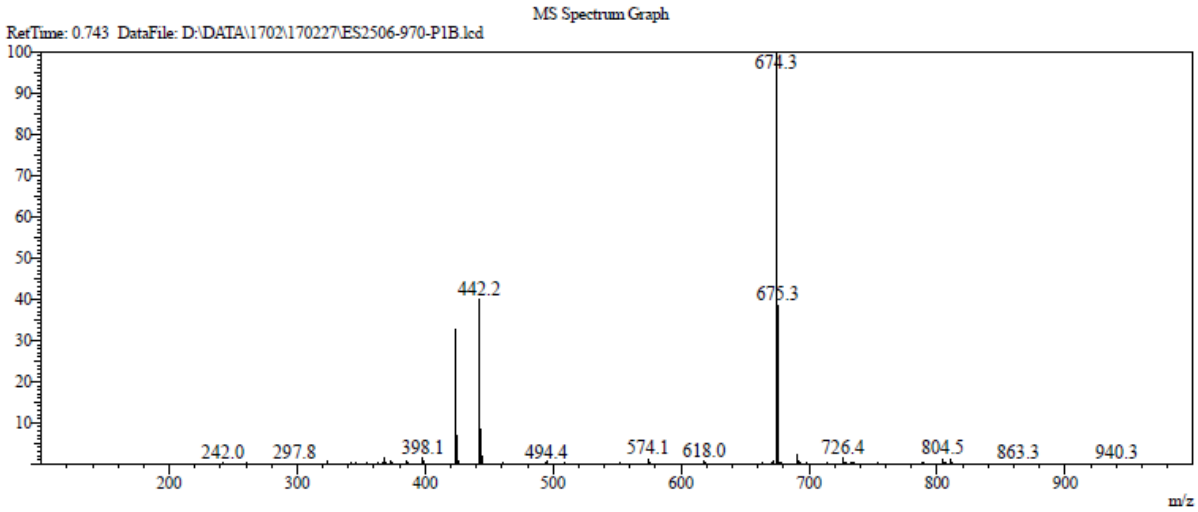

Figure S2.3: LCMS Reports of Intermediate 4, Intermediate 5, and Compound 6 (continued)

Intermediate **5**

LCMS REPORT

Compound ID : 1
Sample ID : ES2506-976-P1B1
Injection Date : 2/27/2017 19:52:01
Injection Vol : 5ul
Location : tray1 vial25
Acq Method : D:\method\5-95AB_1.5MIN_220&254.lcm
Org DataFile : D:\DATA\1702\170227\ES2506-976-P1B1.lcd
Instrument & Column: LCMS-S(12#102) : MERCK RP-18e 25-2mm,UM8505/148

Chromatogram

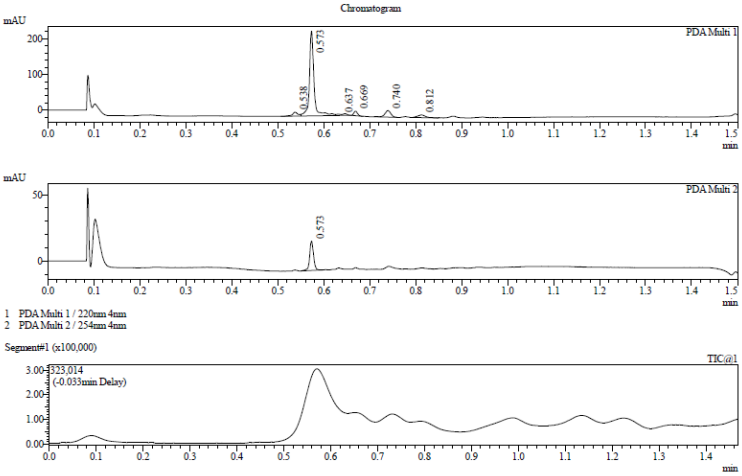

Integration Result

Ch1 220nm 4nm

Peak#	Ret. Time	Height	Height %	USP Width	Area	Area %
1	0.538	10719	4.093	0.020	9987	4.704
2	0.573	211097	80.619	0.016	164891	77.664
3	0.637	3313	1.265	0.037	5818	2.740
4	0.669	12005	4.585	0.015	6818	3.212
5	0.740	17539	6.698	0.023	16160	7.611
6	0.812	7173	2.739	0.032	8639	4.069

Ch2 254nm 4nm

Peak#	Ret. Time	Height	Height %	USP Width	Area	Area %
1	0.573	19478	100.000	0.015	13152	100.000

Figure S2.3: LCMS Reports of Intermediate 4, Intermediate 5, and Compound 6 (continued)

Intermediate 5

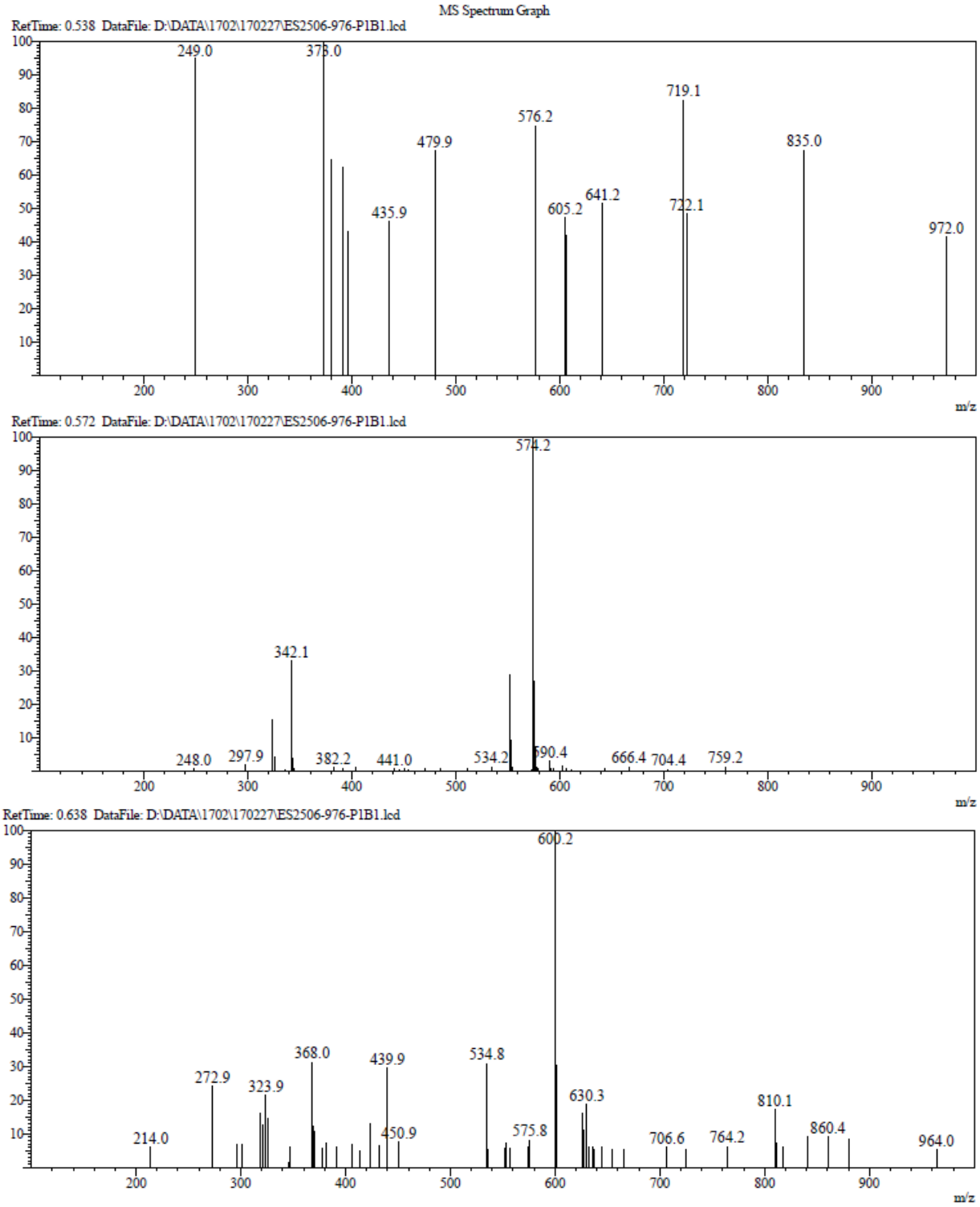

Figure S2.3: LCMS Reports of Intermediate 4, Intermediate 5, and Compound 6 (continued)

Intermediate **6**

LCMS REPORT

Compound ID : WX682
Sample ID : ES2506-978-P1D
Injection Date : 2/28/2017 16:43:25
Injection Vol : 6ul
Location : tray1 vial47
Acq Method : D:\method\5-95AB_1.5MIN_220&254.lcm
Org DataFile : D:\DATA\1702\170228\ES2506-978-P1D.lcd
Instrument & Column: LCMS-S(12#102) : MERCK RP-18e 25-2mm,UM8505/148

Chromatogram

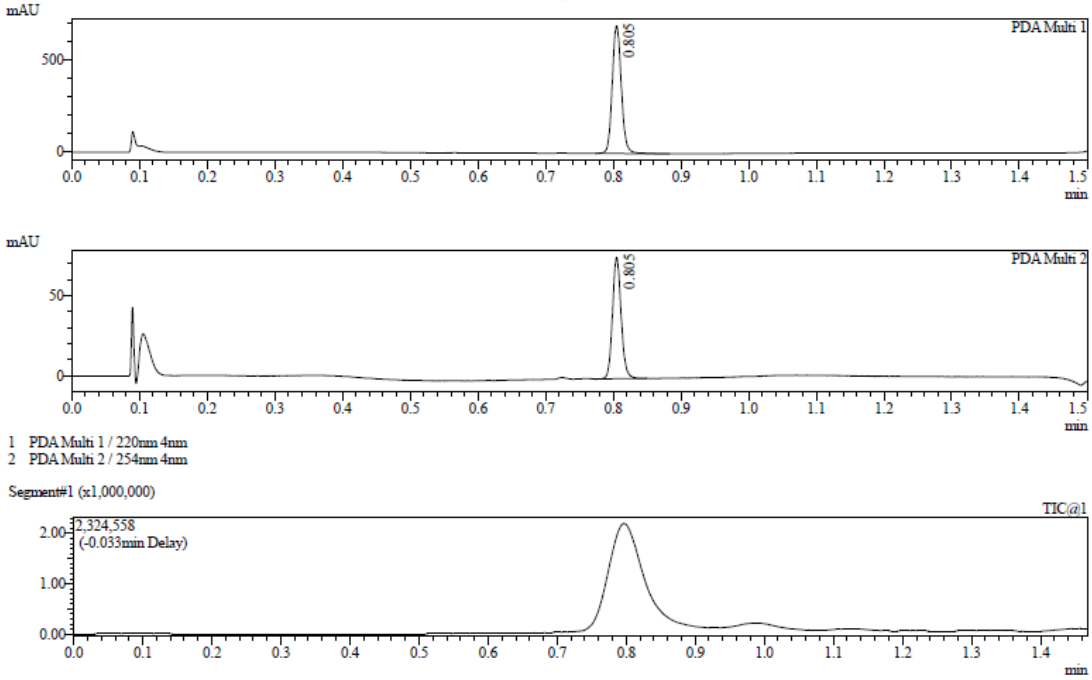

Integration Result

Ch1 220nm 4nm

Peak#	Ret. Time	Height	Height %	USP Width	Area	Area %
1	0.805	687577	100.000	0.024	649471	100.000

Ch2 254nm 4nm

Peak#	Ret. Time	Height	Height %	USP Width	Area	Area %
1	0.805	74464	100.000	0.023	67343	100.000

Figure S2.3: LCMS Reports of Intermediate 4, Intermediate 5, and Compound 6 (continued)

Compound 6

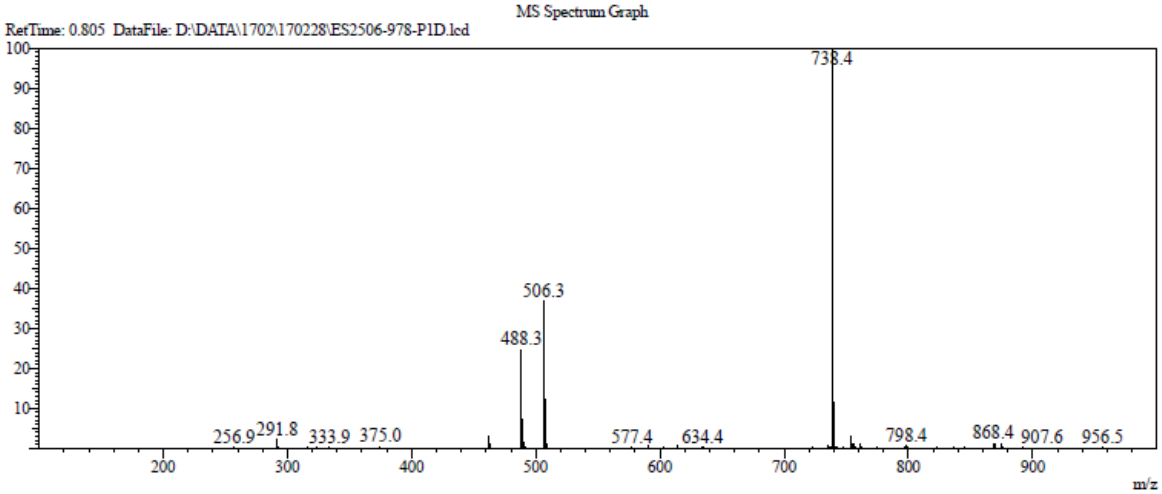

Figure S2.3: LCMS Reports of Intermediate 4, Intermediate 5, and Compound 6 (continued)

2.6 References

ANDRUS, M. B., LI, W. & KEYES, R. F. 1997. Synthesis of microcolin B, a potent new immunosuppressant using an efficient mixed imide formation reaction. ACS Publications: Journal of Organic Chemistry.

BAO, Y., NAKAGAWA, K., YANG, Z., IKEDA, M., WITHANAGE, K., ISHIGAMI-YUASA, M., OKUNO, Y., HATA, S., NISHINA, H. & HATA, Y. 2011. A cell-based assay to screen stimulators of the Hippo pathway reveals the inhibitory effect of dobutamine on the YAP-dependent gene transcription. *J Biochem,* 150**,** 199-208.

BRODOWSKA, K., AL-MOUJAHED, A., MARMALIDOU, A., MEYER ZU HORSTE, M., CICHY, J., MILLER, J. W., GRAGOUDAS, E. & VAVVAS, D. G. 2014. The clinically used photosensitizer Verteporfin (VP) inhibits YAP-TEAD and human retinoblastoma cell growth in vitro without light activation. *Exp Eye Res,* 124**,** 67-73.

BUM-ERDENE, K., ZHOU, D., GONZALEZ-GUTIERREZ, G., GHOZAYEL, M. K., SI, Y., XU, D., SHANNON, H. E., BAILEY, B. J., CORSON, T. W., POLLOK, K. E., WELLS, C. D. & MEROUEH, S. O. 2019. Small-Molecule Covalent Modification of Conserved Cysteine Leads to Allosteric Inhibition of the TEAD·Yap Protein-Protein Interaction. *Cell Chem Biol,* 26**,** 378-389.e13.

CALSES, P. C., CRAWFORD, J. J., LILL, J. R. & DEY, A. 2019. Hippo Pathway in Cancer: Aberrant Regulation and Therapeutic Opportunities. *Trends Cancer,* 5**,** 297-307.

CHAN, P., HAN, X., ZHENG, B., DERAN, M., YU, J., JARUGUMILLI, G. K., DENG, H., PAN, D., LUO, X. & WU, X. 2016. Autopalmitoylation of TEAD proteins regulates transcriptional output of the Hippo pathway. *Nat Chem Biol,* 12**,** 282-9.

CRAWFORD, J. J., BRONNER, S. M. & ZBIEG, J. R. 2018. Hippo pathway inhibition by blocking the YAP/TAZ-TEAD interface: a patent review. *Expert Opin Ther Pat,* 28**,** 867-873.

DASARI, V. R., MAZACK, V., FENG, W., NASH, J., CAREY, D. J. & GOGOI, R. 2017. Verteporfin exhibits YAP-independent anti-proliferative and cytotoxic effects in endometrial cancer cells. *Oncotarget,* 8**,** 28628-28640.

DECICCO, C. P. & GROVER, P. 1996. Total Asymmetric Synthesis of the Potent Immunosuppressive Marine Natural Product Microcolin A. ACS Publications: Journal of Organic Chemistry.

FAN, F., HE, Z., KONG, L. L., CHEN, Q., YUAN, Q., ZHANG, S., YE, J., LIU, H., SUN, X., GENG, J., YUAN, L., HONG, L., XIAO, C., ZHANG, W., LI, Y., WANG, P., HUANG, L., WU, X., JI, Z., WU, Q., XIA, N. S., GRAY, N. S., CHEN, L., YUN, C. H., DENG, X. & ZHOU, D. 2016. Pharmacological targeting of kinases MST1 and MST2 augments tissue repair and regeneration. *Sci Transl Med,* 8**,** 352ra108.

FENG, X., DEGESE, M. S., IGLESIAS-BARTOLOME, R., VAQUE, J. P., MOLINOLO, A. A., RODRIGUES, M., ZAIDI, M. R., KSANDER, B. R., MERLINO, G., SODHI, A., CHEN, Q. & GUTKIND, J. S. 2014. Hippo-independent activation of YAP by the GNAQ uveal melanoma oncogene through a trio-regulated rho GTPase signaling circuitry. *Cancer Cell,* 25**,** 831-45.

FLEMING, J. K., WOJCIAK, J. M., CAMPBELL, M. A. & HUXFORD, T. 2011. Biochemical and structural characterization of lysophosphatidic Acid binding by a humanized monoclonal antibody. *J Mol Biol,* 408**,** 462-76.

GIBAULT, F., CORVAISIER, M., BAILLY, F., HUET, G., MELNYK, P. & COTELLE, P. 2016. Non-Photoinduced Biological Properties of Verteporfin. *Curr Med Chem,* 23**,** 1171-84.

HARVEY, K. F., ZHANG, X. & THOMAS, D. M. 2013. The Hippo pathway and human cancer. *Nat Rev Cancer,* 13**,** 246-57.

JIAO, S., WANG, H., SHI, Z., DONG, A., ZHANG, W., SONG, X., HE, F., WANG, Y., ZHANG, Z., WANG, W., WANG, X., GUO, T., LI, P., ZHAO, Y., JI, H., ZHANG, L. & ZHOU, Z. 2014. A peptide mimicking VGLL4 function acts as a YAP antagonist therapy against gastric cancer. *Cancer Cell,* 25**,** 166-80.

KOEHN, F. E., LONGLEY, R. E. & REED, J. K. 1992. Microcolins A and B, new immunosuppressive peptides from the blue-green alga Lyngbya majuscula. *J Nat Prod,* 55**,** 613-9.

KOEHN, F. E., MCCONNELL, O. J., LONGLEY, R. E., SENNETT, S. H. & REED, J. K. 1994. Analogues of the marine immunosuppressant microcolin A: preparation and biological activity. *J Med Chem,* 37**,** 3181-6.

LIU-CHITTENDEN, Y., HUANG, B., SHIM, J. S., CHEN, Q., LEE, S. J., ANDERS, R. A., LIU, J. O. & PAN, D. 2012. Genetic and pharmacological disruption of the TEAD-YAP complex suppresses the oncogenic activity of YAP. *Genes Dev,* 26**,** 1300-5.

MANDAL, A. K., HINES, J., KURAMOCHI, K. & CREWS, C. M. 2005. Developing microcolin A analogs as biological probes. *Bioorg Med Chem Lett,* 15**,** 4043-7.

MATTERN, R.-H., GUNASEKERA, S. & MCCONNELL, O. 1996. Synthetic Studies of Microcolin B. Elsevier: Tetrahedron.

MATTERN, R. H., GUNASEKERA, S. & MCCONNELL, O. 1997. Synthesis of microcolin analogs using trimethylsilylated lactams. Elsevier: Tetrahedron Letters.

MENG, Z., MOROISHI, T., MOTTIER-PAVIE, V., PLOUFFE, S. W., HANSEN, C. G., HONG, A. W., PARK, H. W., MO, J. S., LU, W., LU, S., FLORES, F., YU, F. X., HALDER, G. & GUAN, K. L. 2015. MAP4K family kinases act in parallel to MST1/2 to activate LATS1/2 in the Hippo pathway. *Nat Commun,* 6**,** 8357.

MESROUZE, Y., BOKHOVCHUK, F., MEYERHOFER, M., FONTANA, P., ZIMMERMANN, C., MARTIN, T., DELAUNAY, C., ERDMANN, D., SCHMELZLE, T. & CHÈNE, P. 2017. Dissection of the interaction between the intrinsically disordered YAP protein and the transcription factor TEAD. *Elife,* 6.

MURPH, M. & MILLS, G. B. 2007. Targeting the lipids LPA and S1P and their signalling pathways to inhibit tumour progression. *Expert Rev Mol Med,* 9**,** 1-18.

NOLAND, C. L., GIERKE, S., SCHNIER, P. D., MURRAY, J., SANDOVAL, W. N., SAGOLLA, M., DEY, A., HANNOUSH, R. N., FAIRBROTHER, W. J. & CUNNINGHAM, C. N. 2016. Palmitoylation of TEAD Transcription Factors Is Required for Their Stability and Function in Hippo Pathway Signaling. *Structure,* 24**,** 179-186.

PLOUFFE, S. W., MENG, Z., LIN, K. C., LIN, B., HONG, A. W., CHUN, J. V. & GUAN, K. L. 2016. Characterization of Hippo Pathway Components by Gene Inactivation. *Mol Cell,* 64**,** 993-1008.

POBBATI, A. V., CHAN, S. W., LEE, I., SONG, H. & HONG, W. 2012. Structural and functional similarity between the Vgll1-TEAD and the YAP-TEAD complexes. *Structure,* 20**,** 1135-40.

SANCHEZ-VEGA, F., MINA, M., ARMENIA, J., CHATILA, W. K., LUNA, A., LA, K. C., DIMITRIADOY, S., LIU, D. L., KANTHETI, H. S., SAGHAFINIA, S., CHAKRAVARTY, D., DAIAN, F., GAO, Q., BAILEY, M. H., LIANG, W. W., FOLTZ, S. M., SHMULEVICH, I., DING, L., HEINS, Z., OCHOA, A., GROSS, B., GAO, J., ZHANG, H., KUNDRA, R., KANDOTH, C., BAHCECI, I., DERVISHI, L., DOGRUSOZ, U., ZHOU, W., SHEN, H., LAIRD, P. W., WAY, G. P., GREENE, C. S., LIANG, H., XIAO, Y., WANG,

C., IAVARONE, A., BERGER, A. H., BIVONA, T. G., LAZAR, A. J., HAMMER, G. D., GIORDANO, T., KWONG, L. N., MCARTHUR, G., HUANG, C., TWARD, A. D., FREDERICK, M. J., MCCORMICK, F., MEYERSON, M., VAN ALLEN, E. M., CHERNIACK, A. D., CIRIELLO, G., SANDER, C., SCHULTZ, N. & NETWORK, C. G. A. R. 2018. Oncogenic Signaling Pathways in The Cancer Genome Atlas. *Cell,* 173**,** 321-337.e10.

SONG, S., XIE, M., SCOTT, A. W., JIN, J., MA, L., DONG, X., SKINNER, H. D., JOHNSON, R. L., DING, S. & AJANI, J. A. 2018. A Novel YAP1 Inhibitor Targets CSC-Enriched Radiation-Resistant Cells and Exerts Strong Antitumor Activity in Esophageal Adenocarcinoma. *Mol Cancer Ther,* 17**,** 443-454.

SORRENTINO, G., RUGGERI, N., SPECCHIA, V., CORDENONSI, M., MANO, M., DUPONT, S., MANFRIN, A., INGALLINA, E., SOMMAGGIO, R., PIAZZA, S., ROSATO, A., PICCOLO, S. & DEL SAL, G. 2014. Metabolic control of YAP and TAZ by the mevalonate pathway. *Nat Cell Biol,* 16**,** 357-66.

TAKAMATSU, S., NAGLE, D. G. & GERWICK, W. H. 2004. Secondary metabolites from marine cyanobacteria and algae inhibit LFA-1/ICAM-1 mediated cell adhesion. *Planta Med,* 70**,** 127-31.

WOJCIAK, J. M., ZHU, N., SCHUERENBERG, K. T., MORENO, K., SHESTOWSKY, W. S., HIRAIWA, M., SABBADINI, R. & HUXFORD, T. 2009. The crystal structure of sphingosine-1-phosphate in complex with a Fab fragment reveals metal bridging of an antibody and its antigen. *Proc Natl Acad Sci U S A,* 106**,** 17717-22.

YU, F. X. & GUAN, K. L. 2013. The Hippo pathway: regulators and regulations. *Genes Dev,* 27**,** 355-71.

YU, F. X., LUO, J., MO, J. S., LIU, G., KIM, Y. C., MENG, Z., ZHAO, L., PEYMAN, G., OUYANG, H., JIANG, W., ZHAO, J., CHEN, X., ZHANG, L., WANG, C. Y., BASTIAN, B. C., ZHANG, K. & GUAN, K. L. 2014. Mutant Gq/11 promote uveal melanoma tumorigenesis by activating YAP. *Cancer Cell,* 25**,** 822-30.

ZHANG, L. H. & LONGLEY, R. E. 1999. Induction of apoptosis in mouse thymocytes by microcolin A and its synthetic analog. *Life Sci,* 64**,** 1013-28.

ZHANG, L. H., LONGLEY, R. E. & KOEHN, F. E. 1997. Antiproliferative and immunosuppressive properties of microcolin A, a marine-derived lipopeptide. *Life Sci,* 60**,** 751-62.

ZHANG, Z., LIN, Z., ZHOU, Z., SHEN, H. C., YAN, S. F., MAYWEG, A. V., XU, Z., QIN, N., WONG, J. C., RONG, Y., FRY, D. C. & HU, T. 2014. Structure-Based Design and Synthesis of Potent Cyclic Peptides Inhibiting the YAP-TEAD Protein-Protein Interaction. *ACS Med Chem Lett,* 5**,** 993-8.

Chapter 3: Target Identification and Mechanism of Action for the YAP Inhibitor VT01454

3.1 Introduction

The mammalian phosphatidylinositol transfer proteins α and β (PITPα/β) are a highly conserved pair of StAR-related lipid transfer (START) proteins that bind and transfer phosphatidylinositol (PI) and phosphatidylcholine (PC) *in vitro* (Yoder et al., 2001, De Vries et al., 1996), and stimulate phosphatidylinositol-4-phosphate (PI4P) production *in vivo* (Ile et al., 2010). Their physiological significance is reflected in the Parkinsonian/neurodegenerative phenotypes of the PITPα-deficient vibrator (vb) mouse (Hamilton et al., 1997), the absent dorsal forebrain in neocortex-conditional *Pitpna/Pitpnb* double knockout mice, and the embryonic lethality of *Pitpna/Pitpnb* double null mice (Xie et al., 2018).

Here, we report a novel role for PITPα/β in regulating the Hippo kinase cascade through the characterization of VT01454, a small-molecule inhibitor and Microcolin B analog which we previously defined as both a potent and specific YAP inhibitor. In the present study, we use bio-orthogonal methods to identify and validate PITPα/β as the protein targets of VT01454, and functionally verify the role of PITPα/β in Hippo signaling by genetic deletion in HEK293A cells. Furthermore, we demonstrate that VT01454 inhibition of PITPα/β regulates the Hippo pathway by modulation of a plasma membrane pool of PI4P, and identify MAP4K6 and MAP4K7 as potential PI4P-interacting proteins in a BioID assay using the PI4P reporter P4M-SidMx2.

3.1.1 Affinity-Based, Bioorthogonal Methods for Small-Molecule Target Deconvolution

Despite the increasing number of target identification techniques developed to date, affinity purification remains the most direct and widely used approach to finding target proteins that bind small molecules of interest. Notably, this approach has been used to identify the targets of many important small-molecule drugs and inhibitors, including FK506 and cyclosporin A (Harding et al., 1989, Takahashi et al., 1989). A target deconvolution project typically begins with structure-activity relationship (SAR) studies where different functional groups on the small molecule of interest are modified or removed to determine their dispensability for drug activity. Sites of negligible impact become points of attachment to an affinity tag

(e.g. biotin) or a solid matrix (e.g. Affinity-Gel agarose beads). Introducing a functional tag into a compound is a challenging task, and for some compounds, the addition of any kind of bulky tag significantly reduces its activity. This problem can be solved through the addition of a small chemical handle (e.g. an alkyne tag) for bioorthogonal chemistry, such as Copper(I)-catalyzed Huisgen-[3 + 2]-azide-alkyne cycloaddition (CuAAC or click chemistry) and Staudinger ligation between azides and triarylphosphine reagents (Prescher and Bertozzi, 2005, Grammel and Hang, 2013). Thus, bioorthogonal approaches minimize structural perturbation and covalently conjugate a functional tag (e.g. biotin-azide, fluorescent-azide) to the compound via 'click' reaction.

Bioorthogonal reactions like CuAAC can easily be conducted in aqueous media, and are typically done in whole cell lysate and occasionally live cells for affinity purification. Furthermore, such bioorthogonal probes (e.g. tag-azides) are often further coupled with a fluorescent or photoreactive group (e.g. benzophenone, diazirine), so-called trifunctional probes (Lapinsky, 2012)that permit photoaffinity reactions that induce covalent cross-linking between compound and target protein. Trifunctional probes have been successfully applied to several drugs including dasatinib, a dual Bcr-Abl and Src family tyrosine kinase inhibitor approved for use in patients with chronic myelogenous leukemia (CML), where trifunctional probe labeling identified several previously unknown targets including several serine/threonine kinases (Shi et al., 2012). Of note, trifunctional probes are widely used for activity-based protein profiling (ABPP), a chemical proteomic approach that globally characterizes enzyme function in living cells (Cravatt et al., 2008).

Following bioorthogonal conjugation, affinity purification is much like immunoprecipitation of specific proteins where the covalently conjugated drugs (e.g. drug-biotin) are incubated with antibody and/or beads (e.g. streptavidin-conjugated beads) in protein extract, followed by extensive washing to remove nonspecifically bound proteins. Finally, the tightly binding proteins are either eluted with excess free drug or under highly denaturing conditions. The eluted proteins are then analyzed by SDS–PAGE and protein bands excised and identified by mass spectrometry (MS). Alternatively, samples are directly processed on beads for total proteome analysis. Given that there are typically many more nonspecific binders than actual drug targets, negative controls such as similarly tagged inactive analogs or more potent analogs (to serve as a 'competitor') of the parental compound are used in parallel whenever possible. One caveat to affinity purification approaches is that most bioactive compounds, especially drugs or drug candidates, bind non-

covalently to their target proteins, and such complexes may not survive the affinity purification process. Once potential targets are identified, subsequent studies must not only confirm direct biochemical binding but demonstrate that the target's modulation leads to the functional effects initially detected in the phenotypic assay. Target "authenticity" can be determined by a host of functional assays, including but not limited to protein overexpression and genetic deletion by RNA interference and CRISPR-based strategies.

Combination with quantitative proteomics

Recent advances in MS technologies have enabled more sensitive and quantitative methods for high-throughput target identification. In particular, studies have effectively coupled affinity purification to stable isotope labeling-based quantitative MS techniques (Rix and Superti-Furga, 2009), such as metabolic labeling (e.g. stable isotope labeling by amino acids [SILAC]) (Ong et al., 2002, Raj et al., 2011), and chemical labeling (e.g. isotope-coded affinity tag [ICAT] (Gygi et al., 1999, Oda et al., 2003) and isobaric tags for relative and absolute quantification [iTRAQ]) (Ross et al., 2004, Huang et al., 2009, Bantscheff et al., 2007). Among these methods, reductive dimethylation (ReDi labeling) has grown increasingly popular as an inexpensive and reliable way of quantifying differences in protein concentration in nearly any sample type (Tolonen and Haas, 2014). ReDi labeling is based on the respective mono- and dimethylation of proline and lysine side chains, using formaldehyde and cyanoborohydride harboring hydrogen atoms in either their natural isotopic distribution ("light") or in deuterated form ("heavy"). Each dimethylated residue on a peptide results in a mass difference of 6.0377 Da between light and heavy forms that is then used by MS to distinguish between the paired samples, and relative peptide abundances are quantified as the ratio of MS1 extracted ion chromatogram areas (i.e. MS1 peak area ratio) of light and heavy versions for each peptide ion pair (Tolonen and Haas, 2014). All of the described approaches directly compare proteins from active probe experiments to proteins from control or negative probe experiments in a quantitative manner, making it possible to cut off nonspecific background signals even under moderate washing conditions.

3.1.2 Introduction to Phosphoinositide Metabolism

Cellular membranes incorporate a diverse repertoire of molecules, including proteins, sterols, and phospholipids. Together, these constituents orchestrate membrane function and consequently establish

and shape membrane identity. One such class of membrane lipids, the phosphatidylinositol phosphates (PIPs), plays a critical role in regulating these processes. Phosphatidylinositol (PI) is made up of 2 fatty acid chains that imbed the lipid in the membrane, a glycerol backbone, and an inositol group facing the cytosol. A highly versatile molecule, PI undergoes phosphorylation and dephosphorylation at the D-3, D-4, and D-5 positions of its inositol ring to generate 7 chemically distinct PIPs: PI 3-phosphate [PI3P], PI 4-phosphate [PI4P], PI 5-phosphate [PI5P], PI 3,4-bisphosphate [PI(3,4)P_2], PI 4,5-bisphosphate [PI(4,5)P_2], PI 3,5-bisphosphate [PI(3,5)P_2], and PI 3,4,5-trisphosphate [PI(3,4,5)P_3], of which PI4P and PI(4,5)P_2 are the most abundant. PIP interconversion is dynamically driven by various kinases and phosphatases, and the precise regulation of their catalytic activity and subcellular localization allows exquisite control of PIPs in cellular space and time (Del Bel and Brill, 2018).

3.1.3 Phosphoinositol-4-Kinase (PI4K) family, the Sac1 phosphatase, and phosphoinositol-4-phosphate (PI4P) metabolism

The conversion of PI to PI4P is a crucial step in the PIP pathway. PI4P is one of the most abundant cellular PIPs and is synthesized by PI4K phosphorylation of PI at the *D*-4 position of its inositol ring (Del Bel and Brill, 2018, Lemmon, 2008). While PI4P serves as a precursor to PI(4,5)P_2 and PI(3,4,5)P_3, it is also a signaling molecule in its own right, playing diverse roles at various endolysosomal membranes in the cell (Balla and Balla, 2006, D'Angelo et al., 2008, Delage et al., 2013, Tan and Brill, 2014). Classically, PI4P regulates Golgi trafficking at the cellular level, a role first evidenced in a yeast study of secretory pathway defects associated with hypomorphic PI4K mutants with compromised PI4P synthesis (Hama et al., 1999, Walch-Solimena and Novick, 1999). A number of PI4P effectors have since been elucidated, all of which function on Golgi membranes to regulate vesicle budding (Wang et al., 2003, Godi et al., 2004), maintenance of Golgi structure (Dippold et al., 2009), and possibly nonvesicular lipid transport (Tóth et al., 2006, D'Angelo et al., 2007). Although canonically enriched at the *trans*-Golgi network (TGN), appreciable levels of PI4P are also found at the PM (GR et al., 2009), early endosomal membranes, late endosomal and lysosomal membranes, and to some extent on most other intracellular membranes (Del Bel and Brill, 2018).

Mammals produce 4 structurally distinct PI4Ks classified into 2 categories: type II PI4Ks (PI4KIIα and PI4KIIβ) and type III PI4Ks (PI4KIIIα and PI4KIIIβ). Type III PI4Ks are largely cytosolic and harbor catalytic domains similar that of the PI 3-kinases (PI3Ks), whereas type II PI4Ks are palmitoylated and contain distinct catalytic domains. PI4KIIIα plays a conserved role in synthesizing plasma membrane (PM) PI4P and has been reported to localize to the PM, ER, among other organelles (Nakatsu et al., 2012). PI4KIIIβ has a conserved role in synthesizing Golgi PI4P, and has been reported to reside at the Golgi (Dumaresq-Doiron et al., 2010), nucleus (Kakuk et al., 2008, Kakuk et al., 2006), ER (Wong et al., 1997) (Balla and Balla, 2006), mitochondria, and lysosomes. PI4KIIα and PI4KIIβ localize to endosomes, where they generate PI4P necessary for endosomal trafficking, and at the trans-Golgi network (TGN), where they facilitate post-Golgi trafficking (Salazar et al., 2005, Clayton et al., 2013). PI4KIIβ is also found at the PM (Wei et al., 2002). Thus, the unique subcellular localization of the PI4Ks generates both spatially and functionally distinct pools of PI4P (Grabon et al., 2019).

Working antagonistically to these PI4Ks is a highly conserved PI 4-phosphatase known as Sac1, which removes phosphate from the *D*-4 position of the inositol ring to replenish PI and restrict PI4P levels. In vitro, human Sac1 dephosphorylates PI4P and to a lesser extent PI3P, while exhibiting no activity towards PI(3,5)P2 as well as PIPs with adjacent phosphate groups (e.g. PI(4,5)P2). Likewise, *in vivo* studies across yeast, *Drosophila,* and mammals have shown that Sac1 far prefers PI4P as a substrate (Foti et al., 2001, Nemoto et al., 2000, Liu et al., 2008, Hughes et al., 2000). Structurally, Sac1 contains 2 conserved transmembrane domains (TMDs) and a SAC domain harboring PIP phosphatase activity, which in and of itself comprises 7 highly conserved catalytic and regulatory motifs, including a catalytic core $CX_5R(T/S)$. Furthermore, mammalian Sac1 harbors a leucine zipper (LZ) motif at its N-terminus and a coat protein I (COPI) binding motif (KEKIDD) at its C-terminus, which are required for Sac1 localization at the Golgi and ER, respectively (Rohde et al., 2003, Blagoveshchenskaya et al., 2008). Sac1 depletion in cells leads to aberrant PI4P accumulation and distribution, suggesting that Sac1 functions to prevent random PI4P dispersal and maintain PI4P pools in specific subcellular locations, thereby preserving the functional identity of intracellular membranes (Tahirovic et al., 2005, Roy and Levine, 2004).

To ensure PIP homeostasis, cellular regulation of Sac1 activity occurs at the levels of gene expression, protein structure or conformation, and localization. Sac1 subcellular localization at the ER,

Golgi and membrane contact sites (MCS) is in turn controlled by its own structural motifs, binding partners, nutrient availability or growth conditions, and PIP levels. Deleting the short C-terminal hydrophobic sequence that localizes Sac1 to the ER renders the enzyme cytoplasmic, and this truncated Sac1 has been effectively harnessed in various ways to acutely deplete different intracellular PI4P pools to study their function in a spatiotemporal manner (Szentpetery et al., 2010).

Viral replication requires PI4P hijacking

Positive-sense RNA viruses such as hepatitis C virus (HCV) hijack cellular PI4P to drive infectious capacity (Altan-Bonnet and Balla, 2012, Bishé et al., 2012). Upon infection, HCV establishes PI4P- and cholesterol-rich "membranous webs" that serve as platforms for viral replication in the host cell; thus, PI4P is upregulated and essential during HCV infection (Hsu et al., 2010, Berger et al., 2011, Reiss et al., 2011). Mechanistically, the HCV nonstructural protein 5a (NS5A) recruits and stimulates PI4KIIIα activity at viral replication sites (Reiss et al., 2011, Berger et al., 2011), while simultaneously removing Sac1 to attenuate PI4P turnover by recruiting the Arf1 GTPase-activating protein (Arf1-GAP) to displace Sac1 from the Golgi (Li et al., 2014). This dual mechanism drives increased PI4P synthesis at viral replication sites.

3.1.4 Phosphoinositide Transfer Proteins alpha and beta (PITPα/β)

PITPs are ancient, eukaryotically conserved proteins classified into two distinct families: the Sec14-PITPs and the StAR-related lipid transfer domain (START)-like PITPs, the latter of which comprise PITPα/β among other lipid transfer proteins (LTPs). PITPα/β are classically defined as transorganelle lipid carriers that supply phosphatidylinositol (PI) from the endoplasmic reticulum (i.e. their site of synthesis) to PtdIns-low membranes involved in phosphoinositide metabolism (Nile et al., 2010). Of note, this inter-membrane lipid transfer is energy-independent, as PITPα/β bind and exchange PI and phosphatidylcholine (PC) in a mutually exclusive manner, showing preference for PI over PC at a 20-fold higher rate of *in vitro* transfer (Wirtz, 1991).

The core START-like PITP consists of four domains: (1) the lipid binding pocket comprising an eight-stranded β sheet, bound by two α helices; (2) an unstructured region referred to as the "regulatory loop"; (3) the C-terminal helix G; and (4) the "lipid exchange loop" that gates the entry to the lipid-binding

pocket (Grabon et al., 2019). It is worth noting that PI and PC bind in nearly identical orientations in the START-like PITP lipid pocket. Both headgroups are sequestered within the cavity β sheet floor, coordinated by four residues (T59, K61, E86, N90 in PITPα) (Tilley et al., 2004, Alb et al., 1995). The G-helix is conformationally dynamic during PITP association with membranes (Tremblay et al., 2005), and molecular dynamics simulations show the G-helix undergoing a localized unfolding (E248) upon PI binding, altering its hydrogen bonding network and therefore its interaction with the A-helix, thus promoting closure of the gate over the lipid binding pocket (Grabon et al., 2017).

Early insights into PITPα/β function in mammalian systems were exclusively gleaned from cell-free or permeabilized cell reconstitution and resolution studies, such as dense core vesicular exocytosis in permeabilized neuroendocrine cells, vesicle budding from the TGN among other Golgi compartments, and scission of coatomer-coated transport vesicles, to name a few (Hay et al., 1995, Hay and Martin, 1993, Ohashi et al., 1995). While these pioneering studies accurately reconstituted PI requirements for each corresponding reaction, the physiological relevance of their projected roles for the PITPs remains unclear (Grabon et al., 2019).

In Vivo PITPα/β Functions in Cell Culture and Vertebrate Models

Initial studies of Class I PITP functions in cellular systems largely used siRNA and overexpression approaches, and quickly made apparent that despite sharing 77% sequence identity, PITPα/β appeared to have functionally distinct cellular and biological roles. Localization studies reported that PITPα resides at the nucleus and the cytoplasm, while PITPβ predominantly resides at the Golgi (Ile et al., 2010, De Vries et al., 1996, Carvou et al., 2010). Overexpression of PITPα appeared to promote the secretion of mitogenic and survival factors, and NIH3T3 fibroblasts overexpressing PITPα exhibited increased survival upon *in vitro* apoptotic induction (Snoek et al., 1999, Bunte et al., 2006). Furthermore, transferring conditioned medium to naive NIH3T3 cells increased proliferation and conferred protection against UV radiation and TNFα treatment (Schenning et al., 2004).

In contrast, an siRNA approach demonstrated that PITPβ is required for cargo transport from the Golgi to the ER in HeLa cells, where transient PITPβ knockdown resulted in Golgi compaction, altered nuclear morphology, reduced intracellular PI4P levels, and strong defects in COPI-mediated Golgi to ER

retrograde trafficking (Carvou et al., 2010). From this study, a lipid-transfer mechanism was proposed in which PITPβ delivers PI from the ER to *cis*-Golgi membranes to make substrate available to PI4KIIβ, which produces PI4P and ultimately affects the actin dynamics that mobilize COPI-coated vesicles (Carvou et al., 2010).

Though PITPs have been traditionally viewed as transmembrane lipid carriers, the first functional analysis of vertebrate PITPβ demonstrated its ability to potentiate PI4K activity, thereby enhancing PI4P production (Ile et al., 2010). This ushered in a new model where PI4Ks are, on their own, biologically insufficient enzymes incapable of producing enough PI4P to overcome the actions of the PI-4-phosphatases. In this model, PITPs act in concert with PI4Ks to produce sufficient levels of PI4P to overcome this regulatory barrier and execute meaningful intracellular signals.

The dramatic effects of PITPβ depletion on the Golgi implicated an important, and perhaps indispensable, role for PITPs in mammalian development. Indeed, PITPα null mice are born alive but exhibit spinocerebellar disease, intestinal and hepatic steatosis, and hypoglycemia before neonatal or perinatal death (Hamilton et al., 1997, Alb et al., 2003). Though *Pitpna* null mice die of multiple systemic failures within a few days of postnatal life (Alb et al., 2002), *Pitpnb* null animals are fertile and exhibit no obvious pathologies as late as 12 months of age (Xie et al., 2018). However, both PITPα/β are required for dorsal forebrain development and full-body deletion of both *Pitpna and Pitpnb* is embryonically lethal, suggesting that PITPα/β are at least partially redundant in embryonic development (Xie et al., 2018).

3.2 Results

3.2.1 Affinity purification/LC-MS/MS identifies PITPα/β as the putative targets of VT01454

To identify the protein targets of VT01454, we used a bioorthogonal labeling strategy followed by affinity purification (Fig 3.1C). To this end, we employed bifunctional probe VT01702, which induces YAP phosphorylation at a lesser potency than VT01454 and harbors an alkyne handle allowing downstream conversion into various tools geared towards target identification (Figure 3.1A, 3.1B). Briefly, HEK293A cells were treated with vehicle or reactive probe VT01702, in the presence or absence of VT01454 to

compete for binding. VT01702 was then conjugated to a fluorescent 545-azide via Copper(I)-catalyzed alkyne-azide cycloaddition (CuAAC) in total cell lysate, and lysates were then resolved on an SDS-PAGE gel and then fluorescently visualized using a Typhoon imager, the idea being that following fluorescent band detection, VT01702 could then be conjugated to a biotin-azide for affinity purification (Figure 3.1C).

The fluorescent 545-conjugated VT01702 consistently yielded an interacting protein that resolved around 37kD and this interaction was suppressed by VT01454 competition, confirming its specificity (Figure 3.1D). To our surprise, no other bands of comparable signal strength resolved in any of the samples. Furthermore, because the samples had been boiled in SDS sample buffer (devoid of β-mercaptoethanol since cysteine residues were prime suspect for target engagement), this indicated that the compound was likely engaging covalently (i.e. irreversibly) with its target. It is also worth noting that no bands at 37kD were resolved upon silver staining (data not shown), a well-established standard for protein abundance prior to mass spectrometric analysis. Based on these preliminary bio-orthogonal experiments, we concluded that: (1) VT01702 was irreversibly engaging a major target at appreciably high specificity, and (2) target identification by total proteome capture could be feasible based on apparently low sample complexity, but a significant increase in sample abundance would be necessary for success in this endeavor.

In order to successfully capitalize on the 37kD band, we needed to optimize a protocol for affinity purification at sufficiently large scale for mass spectrometry detection. To this end, VT01702 was conjugated to a trifunctional 545-biotin-azide (Figure S3.1A) to enable simultaneous streptavidin-biotin affinity purification and fluorescent visualization of its pulldown efficiency (streptavidin antibody detection via Western blot was previously attempted to no success). Using a previously established method with some adaptations (Speers and Cravatt, 2009), affinity purification was conducted at a larger scale and streptavidin pulldown efficiency was validated through Typhoon imaging and silver staining, both of which now resolved the 37kD band of interest (Figure 3.1E). Total proteome capture followed by reductive dimethylation (Tolonen and Haas, 2014) and LC-MS/MS unequivocally revealed Phosphatidylinositol transfer proteins α and β (PITPα/β) as the major targets of VT01454, with a light : heavy (VT01454 : dmso) ratio of 20 (Figure S3.3A). Notably, gel excision samples from the silver stain were submitted in parallel for analysis at an independent facility and PITPα/β were again the most prominently identified proteins, thus corroborating the total proteome data (Figure S3.3B).

PITPs are ancient, eukaryotically conserved proteins classified into two distinct families: the Sec14-PITPs and the StAR-related lipid transfer domain (START)-like PITPs, the latter of which comprise PITPα/β among other lipid transfer proteins (LTPs). PITPα/β are classically defined as transorganelle lipid carriers that supply phosphatidylinositol (PI) from the endoplasmic reticulum (i.e. their site of synthesis) to PtdIns-low membranes involved in phosphoinositide metabolism (Nile et al., 2010). Of note, this inter-membrane lipid transfer is energy-independent, as PITPα/β bind and exchange PI and phosphatidylcholine (PC) in a mutually exclusive manner, showing preference for PI over PC at a 20-fold higher rate of *in vitro* transfer (Wirtz, 1991). Both PITPα/β have a predicted molecular weight of 32 or 35kD – in close alignment with the 37kD band observed in our CuAAC experiments – and share 77% sequence identity while harboring functionally distinct cellular and biological roles.

We used two approaches to biochemically validate the engagement of PITPβ by VT01454. First, we resolved the same affinity purification samples used for MS analysis on an SDS-PAGE gel for immunoblotting with PITPβ antibody. Indeed, the PITPβ antibody detected an enriched signal at 37kD, thus confirming the identity of the long-observed band of interest (Figure 3.1F). Second, we repeated the aforementioned CuAAC experiment using parental or CRISPR-generated PITPβ KO cells, treated with vehicle or with VT01702. Here, we found that the previously resolved 37kD band in the parental cell line had in fact been a doublet all along (Figure 3.1G). The upper band of the doublet was eliminated upon PITPβ deletion, while a fainter lower band remained, which we interpreted as the remaining gene corresponding to PITPα (Figure 3.1G).

3.2.2 VT01702 covalently binds to Cysteine-94 of PITPβ

Subsequent biochemical analysis was conducted to further identify the amino acid residue of target engagement by VT01702. Given that the compound's warhead is an α,β-unsaturated ketone, it was likely acting as a Michael acceptor, making cysteine residues prime candidates for target interaction. PITPβ contains five cysteine residues, of which cysteine-94 was predicted as the most likely site of covalent engagement based on docking simulations generated using the previously reported crystal structure of PITPα (Figure 3.1I) (Tilley et al., 2004). Based on these predictions, wildtype or C94A mutant HA-PITPβ

was overexpressed and immunoprecipitated from 293A cells, and the resulting lysate subjected to CuAAC for fluorescent conjugation and gel imaging, as done previously. Unlike its wildtype counterpart, the C94A mutant was unable to covalently bind VT01702, indicating that cysteine-94 was indeed the residue covalently interacting with VT01702 and analogs (Figure 3.1H).

3.2.3 PITPα/β are novel regulators of the Hippo pathway/YAP phosphorylation

We next aimed to functionally validate PITPα/β as the major effectors of VT01454 regulation of YAP phosphorylation, thereby presenting them as novel regulators of the Hippo pathway. To this end, we generated PITPα/β knockdown (KD) cells by treating PITPβ KO cells with siRNA against PITPα, as previous attempts at generating PITPα/β KO cells were unsuccessful in our hands. PITPα/β KD cells exhibited higher levels of basal YAP phosphorylation compared to their parental counterparts, thus phenocopying the effects of VT01454 and indicating that VT01454 was an inhibitor rather than an agonist (Figure 3.2A). Consistently, basal levels of cytoplasmic YAP were also significantly higher in the PITPα/β KD cells (Figure 3.2B). To confirm that this phenomenon was not an artifact of clonal variation, we repeated the experiment in several other PITPβ KO clones and obtained the same result (data not shown).

Since knocking down PITPα/β led to elevated levels of YAP phosphorylation, we asked whether the converse event of PITPα/β overexpression would inhibit YAP phosphorylation in the presence of VT01454. Consistent with our hypothesis, PITPα/β overexpression antagonized the effects of VT01454 on both YAP phosphorylation and cytoplasmic translocation (Figures 3.2C and 3.2D). Taken together, these experiments suggested that PITPα/β play a previously-unknown role in the Hippo signaling network.

PITPα/β bind and exchange PI and PC in a mutually exclusive manner, thereby allowing energy-independent lipid transport between endomembranes (Grabon et al., 2019). Having shown that VT01454 is a PITP inhibitor and not an agonist, we were curious whether VT01454 treatment inhibited the PI, PC, or both lipid-transfer activities of PITPα/β. To this end, we generated and overexpressed wildtype or PITPβ point mutants K60Q and C94A, which were previously established as PI- and PC-binding deficient mutations, respectively (Carvou et al., 2010, Shadan et al., 2008). The premise of this experiment was that

PITPβ overexpression antagonizes the effects of VT01454 on YAP phosphorylation due to an overflow of PITPβ protein in the cell that overwhelmed the stoichiometric capacity of the compound. If either the PI or PC activity of PITPβ was required to mediate YAP phosphorylation, then its corresponding mutant would be unable to counteract VT01454 when overexpressed in the cell. We found that the K60Q mutant, but not the C94A mutant, was unable to suppress the effects of VT01454 on YAP phosphorylation, indicating that the PI- but not PC-transfer activity of PITPβ was responsible for regulating YAP phosphorylation (Figure 3.2E). One potential argument could be made that the K60Q mutant cannot rescue the YAP effect because it is still capable of binding VT01454, whereas the C94A mutant is by default unable to bind the VT01454 and therefore rescues the YAP effect independently of any actual functional relevance to the Hippo pathway. However, we would like to emphasize that the C94A mutant is only unable to covalently bind to VT01702 (Figure 3.1H). Realistically, *in vivo* VT01454 engagement of PITP requires a slew of hydrophobic and hydrophilic interactions. Thus, the C94A mutant is necessary but not necessarily sufficient for *in vivo* VT01454 binding. It is therefore unlikely that mutating just one site (C94A) would abolish *in vivo* PITP-VT01454 binding altogether.

3.2.4 PITP inhibition by VT01454 leads to depletion of a plasma membrane pool of PI4P

Having established PITPα/β as novel regulators of the Hippo pathway, we next wanted to delineate a mechanism by which PITPα/β inhibition leads to YAP phosphorylation. Since we already established that the PI and not PC transfer activity of PITPβ was required for Hippo pathway modulation, we hypothesized that changes in the levels and/or localization of specific phosphoinositide(s) were mediating Hippo pathway activation and, consequently, YAP phosphorylation.

Mammalian cells synthesize seven chemically distinct phosphatidylinositol phosphates (PIPs): PI 3-phosphate [PI3P], PI 4-phosphate [PI4P], PI 5-phosphate [PI5P], PI 3,4-bisphosphate [PI(3,4)P_2], PI 4,5-bisphosphate [PI(4,5)P_2], PI 3,5-bisphosphate [PI(3,5)P_2], and PI 3,4,5-trisphosphate [PI(3,4,5)P_3], of which PI4P and PI(4,5)P_2 are the most abundant. PIP interconversion is dynamically driven by various kinases and phosphatases, and the precise regulation of their catalytic activity and subcellular localization allows exquisite control of PIPs in cellular space and time (Del Bel and Brill, 2018). Though PITPs have been classically viewed as inter-membrane lipid carriers, the first functional analysis of vertebrate PITPβ

demonstrated that PITPβ could potentiate PI 4-kinase (PI4K) activity to enhance PI4P synthesis (Ile et al., 2010). This ushered in a new model where PI4Ks are, on their own, biologically insufficient enzymes incapable of producing sufficient PI4P to execute meaningful intracellular signals in the face of PIP phosphatase antagonism, requiring the aid of PITPs to boost PI4P production and overcome this stoichiometric barrier.

Based on this rationale, we decided to start by asking whether VT01454 treatment affected PI4P localization in cells transiently expressing the global PI4P reporter GFP-P4M-SidMx2, which has been shown to detect both Golgi and plasma membrane (PM) pools of PI4P (Hammond et al., 2014). Treatment with VT01454 significantly depleted PM but not Golgi PI4P (Figure 3.3A). We confirmed that this phenomenon was indeed due to PITPα/β inhibition by demonstrating that PITPα/β KD cells likewise had significantly reduced levels of PM PI4P compared to their parental, PITPα siRNA KD, and PITPβ KO counterparts (Figure 3.3B). Both results suggested that VT01454 was depleting PM pools of PI4P through its inhibition of PITPα/β. It is worth noting that GFP-p40px and GFP-PLC-δPH (PI3P and PI(4,5)P_2 reporters, respectively) were also tested in parallel, but neither reporter showed noticeable localization changes following VT01454 treatment (Figures S3.2A and S3.2B) and we therefore moved forward with PI4P. Furthermore, the fact that PI4P exhibited significant changes upon VT01454 treatment while PI(4,5)P2 did not, was not of concern. This was due to the fact that, although PI(4,5)P2 is indeed synthesized from PI4P to a certain degree, both PIPs have been reported to operate as independently functioning pools within the cell (Hammond et al., 2012).

3.2.5 Plasma membrane PI4P levels regulate YAP phosphorylation through PI4KIIIα

The conversion of PI to PI4P is a crucial step in the PIP pathway. PI4P is one of the most abundant cellular PIPs and is synthesized by PI4K phosphorylation of PI at the *D*-4 position of its inositol ring (Del Bel and Brill, 2018, Lemmon, 2008). While PI4P serves as a precursor to PI(4,5)P_2 and PI(3,4,5)P_3, it is also a signaling molecule in its own right, playing diverse roles at various endolysosomal membranes in the cell (Balla and Balla, 2006, D'Angelo et al., 2008, Delage et al., 2013, Tan and Brill, 2014). Although canonically enriched at the *trans*-Golgi network (TGN), appreciable levels of PI4P are also found at the PM (GR et al., 2009) and, to some extent, most intracellular membranes (Del Bel and Brill, 2018). Seeing the

effects of VT01454 on PI4P localization, we posited that either: (1) PM PI4P depletion was indeed responsible for inducing YAP phosphorylation, or (2) It was not PI4P depletion, but rather PI accumulation at the ER/Golgi that led to increased YAP phosphorylation (with PM PI4P depletion simply being a side product of this effect). To test the first possibility and account for the second, we needed to acutely deplete intracellular PI4P, ideally from specific subcellular locations.

Sac1 is a highly conserved PI 4-phosphatase that removes phosphate from the D-4 position of the inositol ring, thereby curbing PI4P levels while restoring PI. Sac1 localizes primarily to the ER by virtue of its C-terminal domain, and the replacement of this domain with various molecular modules has rendered Sac1 a widely used and effective tool for spatially specific PI4P depletion (Zewe et al., 2018, Szentpetery et al., 2010). We found that overexpressing a C-terminally-truncated Sac1 (ubiquitously localized throughout the cell) elevated levels of YAP phosphorylation and cytoplasmic translocation, while overexpressing its phosphatase-inactive mutant A442V did not (Figures 3.3C and 3.3D). This suggested that global intracellular PI4P depletion induced Hippo pathway activation.

We next asked whether we could identify a specific PI4P pool (for simplicity, PM versus Golgi PI4P) responsible for inducing YAP phosphorylation. To acutely deplete PI4P from the PM or Golgi, we overexpressed a Myr-Palm-Sac1 construct that localized to the PM or a Sac1-K2A mutant previously reported to accumulate in the Golgi (Blagoveshchenskaya et al., 2008). Golgi localization was confirmed by GM130 staining (Figure S3.2G). Cells overexpressing Myr-Palm-Sac1 but not Sac1-K2A exhibited increased YAP phosphorylation and cytoplasmic translocation (Figures 3.3E and 3.3F). Another Golgi-targeted Sac1 construct, consisting of a C-terminally-truncated Sac1 fused to a GRIP domain (Fuchs et al., 2009), likewise had no effect on YAP phosphorylation (Figure S3.3I). This suggested that a PM but not Golgi pool of PI4P could regulate YAP phosphorylation.

Mammals produce two classes of structurally distinct PI4Ks: type II (PI4KIIα and PI4KIIβ) and type III (PI4KIIIα and PI4KIIIβ) PI4Ks, and their unique subcellular localization generates both spatially and functionally distinct pools of PI4P (Grabon et al., 2019). Of note, PI4KIIIα localizes to and synthesizes PI4P at the plasma membrane, acting as the most immediate control for PI4P signaling at the PM (Nile et al., 2010). Just as observed with Sac1 overexpression, we found that treating cells with established PI4KIIIα inhibitor GSK-A1 (Bojjireddy et al., 2014) likewise induced YAP phosphorylation and cytoplasmic

translocation (Figures 3.3G, 3.3H, and S3.2H). Phenylarsine oxide (PAO) has historically been used as a PI4K inhibitor (Wiedemann et al., 1996), and, as expected, PAO treatment also elevated YAP phosphorylation and cytoplasmic translocation, albeit with far less potency (Figures S6E and S6F). Genetic deletion of PI4KA had only a weak effect on YAP phosphorylation (data not shown), which was not entirely unexpected: since there are four mammalian PI4Ks, eliminating any one of them could very well leave significant amounts of PI4P being generated from the remaining PI4Ks – circumventing this redundancy issue was, in fact, one of the leading premises for designing the recruitable FKBP-Sac1 (Szentpetery et al., 2010). Thus, the lack of YAP phosphorylation changes upon PI4KIIIα deletion was attributed to compensatory mechanisms resulting from sustained rather than acute PI4K and therefore PI4P depletion.

Since depleting PM PI4P induced YAP phosphorylation, we asked whether an increase in PI4P production could protect cells against this effect in the presence of VT01454. Hepatitis C virus (HCV) non-structural protein 5A (NS5A) recruits and activates PI4KIIIα to stimulate local PI4P production during viral replication in host cells, and increased PI4P synthesis is seen in normal cell culture co-expressing NS5A and PI4KIIIα as well (Reiss et al., 2013, Reiss et al., 2011, Hammond et al., 2014). We found that cells co-expressing NS5A and PI4KIIIα indeed exhibited lower levels of YAP phosphorylation and cytoplasmic translocation upon VT01454 treatment, suggesting that increasing PI4P production protects the cells against the effects of VT01454 (Figures S3.3C and S3.3D). Collectively, the data support a model in which VT01454 binds to and inhibits PITPα/β, and the ensuing loss of PI4P at the PM modulates the Hippo pathway and induces YAP phosphorylation.

3.2.6 PI4P binds to MAP4K6 (TNIK) and MAP4K7 (MINK) and regulate their activity towards Lats1/2

Finally, we wanted to elucidate the mechanism by which PI4P depletion at the PM was mediating Hippo kinase activation, and decided to start by screening for potential PI4P-interacting or PI4P-proximal proteins. Proximity-dependent biotin identification (BioID) is a recently developed method for identifying protein–protein interactions, based on proximity-dependent cellular biotinylation by a promiscuous bacterial biotin ligase (Escherichia coli BirA R118G, hereafter called BirA*) fused to a bait protein. Using this method, biotinylated proteins can be selectively isolated by biotin capture methods and identified using mass

spectrometry analysis. The capacity of BioID to identify transient or weak protein-protein interactions *in vivo* provides a major advantage over conventional biochemical analyses (Roux et al., 2012).

Here, we used BioID to identify proteins in close proximity to PI4P-enriched membranes in the presence and absence of VT01454. For the bait protein, we used a tandemly connected P4M-SidMx2 domain from Legionella pneumoniae that specifically binds PI4P and predominantly targets the Golgi and plasma membrane. Cells stably expressing the BirA*P4M-SidMx2 fusion were treated with vehicle or VT01454 before biotin induction and capture. It should be noted that we took this approach and the subsequent data interpretation with caution for the following reasons: (1) BioIDs are rarely conducted for phospholipid-protein interactions, and the only precedent to our knowledge is a recent study identifying phosphatidylserine-binding proteins using a BirA* fused to a tandemly connected pleckstrin homology domain of evectin-2 (Matsudaira et al., 2017); (2) Because P4M-SidMx2 is a PI4P reporter, any protein interactions could potentially be indirect.

Among the most highly ranked candidate proteins from MS analysis, we immediately noted that TNIK/MAP4K7 and MINK1/MAP4K6 were PI4P-proximal proteins (data not shown). This was biochemically confirmed by immunoblotting for MINK1 and TNIK endogenous antibodies (Figure 3.4A), and the interaction was also found to occur in an NF2-dependent manner (Figure 3.4D). Functionally, MAP4K4/6/7 triple knockout (tKO) and MST1/2/MAP4K4/6/7 knockout (MM-5KO) cells exhibited lower levels of YAP phosphorylation in response to VT01454 compared to their parental cells, suggesting that VT01454 inhibited YAP in a MAP4K4/6/7-dependent manner (Figure 3.4B).

Furthermore, total internal reflection fluorescence (TIRF) microscopy was conducted to image the relative localization of TNIK and PI4P at the plasma membrane. Both biomolecules were shown to occupy potentially overlapping regions of the cell, indicating proximity at the very least and potential co-localization, and this overlap was abolished upon PI4P depletion following VT01454 treatment (Figure 3.4C). It is worth noting that confocal microscopy was unable to resolve co-localization between TNIK and PI4P, demonstrating the value of super-resolution imaging in resolving highly localized events at the PM. Taken together, our data delineate a highly speculative model in which VT01454 binds and inhibits PITPα/β, leading to decreased levels of a PM pool of PI4P. PI4P interacts in an inhibitory manner with the MAP4Ks

under basal conditions, and so loss of PI4P at the PM releases the MAP4Ks, allowing them to activate the Hippo pathway, thereby inducing YAP phosphorylation.

3.3 Discussion

We herein describe a novel role for PITPα/β in Hippo pathway regulation through the discovery of a small molecule probe inducing YAP phosphorylation and inhibition. Using a phenotypic screen for inhibitors of the Hippo signaling pathway, we previously identified and characterized Microcolin B (MCB), a naturally synthesized, bioactive lipopeptide with known immunosuppressive and antiproliferative effects (Chapter 2). Treating cells with MCB and its analog VT01454 led to YAP phosphorylation and cytoplasmic translocation in a Lats1/2- and MAP4K-dependent manner (Figure 2.2). Furthermore, MCB and VT01454 induced high levels of cytotoxicity and apoptotic induction in YAP-dependent $G_{q/11}$-mutated but not in B-raf-mutated uveal melanoma cells, demonstrating their high specificity for targeting YAP (Figure 2.3). Multiple approaches validated PITPα/β as the unequivocal biochemical targets of VT01454: (1) bioorthogonal affinity purification using bifunctional probe VT01702, followed by LC-MS/MS analysis of both total proteomic capture and gel excision samples, (2) immunoblotting affinity purified samples using endogenous PITPβ antibody, and (3) CRISPR-mediated genetic deletion of PITPβ. While previous groups have conducted syntheses, structure-activity relationship, and mechanism-of-action studies of the Microcolins and analogs (Koehn et al., 1994, Koehn et al., 1992, Takamatsu et al., 2004, Zhang et al., 1997), ours is the first to not only identify a biological macromolecule with high Microcolin binding affinity, but also a major cell signaling pathway targeted by Microcolin treatment in a potent and specific manner.

While PITPα/β are classically known as Phosphatidylinositol (PI) carriers from its site of synthesis (i.e. the endoplasmic reticulum) to PI-low endomembranes, the last decade of studies proposed a new model in which PITPs potentiate PI4P production by direct PI presentation to PI4Ks. This new system redefines PITPα/β as nanoreactors rather than carriers, allowing diversification of biological outcomes based upon a wide repertoire of PITP-PI kinase combinations (Grabon et al., 2019). Supporting this model include but are not limited to findings that siRNA-knockdown of PITPβ reduces intracellular PI4P levels

(Carvou et al., 2010), and that zebrafish PITPβ stimulates PI4P production in yeast (Ile et al., 2010). Our observations that PITPα/β inhibition, through VT01454 treatment or genetic deletion, reduces intracellular PI4P are consistent with these previous findings and current model.

Much has yet to be uncovered regarding the biological functions of PITPα/β. In addition to its first-identified role in the Vibrator (Vb) mouse, PITPα also mediates netrin-1 induced neurite outgrowth (Xie et al., 2005, Kauffmann-Zeh et al., 1995), whereas at the cellular level, PITPβ is essential for COPI-mediated retrograde transport from the Golgi to the ER (Carvou et al., 2010). Within several days of postnatal life, *Pitpna* null mice die of multiple systemic failures (Alb et al., 2002), while *Pitpnb* null animals are fertile and exhibit no obvious pathologies as late as 12 months of age (Xie et al., 2018). It is also worth noting that both PITPα/β are required for dorsal forebrain development and that full-body deletion of both *Pitpna and Pitpnb* is embryonically lethal (Xie et al., 2018). Though PITPα and PITPβ generally play functionally distinct cellular and biological roles, genetic deletion of both PITPα/β are needed for us to observe a clean upwards mobility shift in a Phostag gel indicative of fully phosphorylated YAP (Figure 3.2A), suggesting that, at least in this context, PITPα/β function similarly in Hippo pathway regulation.

3.4 Future Inquiries

While PI(4,5)P2-dependent recruitment of NF2 has recently been shown to regulate osmotic stress activation of the Hippo pathway (Hong et al., 2020), the role of PI4P specifically in Hippo pathway regulation is unprecedented. Our BioID data utilizing P4M-SidMx2 as 'bait' protein, as well as the biochemical validation following MS analysis, demonstrate that TNIK/MAP4K7 and MINK1/MAP4K6 are potential PI4P-interacting or at the very least PI4P-proximal proteins, and that this interaction or proximity occurs in an NF2-independent manner. We currently propose a model in which PI(4,5)P2 and PI4P respectively regulate NF2 and the MAP4Ks in parallel and in response to non-overlapping extracellular signals. To adequately support this model, several questions must be addressed, including but not limited to the following:

Do MAP4K4/6/7 bind directly to PI4P? Unlike NF2, which contains a known FERM domain, there are not yet any known lipid-binding domains on the MAP4Ks. This question will be addressed using PIP

Strips spotted with PI4P and PI(4,5)P2 at minimum, and any additional PIPs of interest. PIP Strips will be incubated with either (1) total cell lysate from cells overexpressing Flag-MINK1, HA-TNIK, or Flag-MAP4K4, or (2) any of the aforementioned constructs overexpressed then purified from mammalian cells (given their large size, bacterial purification would present additional technical challenges). NF2 binding to PI(4,5)P2 will be used as a positive control. From this experiment, we anticipate at least 3 possible outcomes: (1) The MAP4Ks do not bind PI4P directly, suggesting that PI4P is modulating the Hippo pathway in a less direct manner than we had anticipated; (2) The MAP4Ks exhibit PI4P-specific binding *in vitro*, suggesting for the first time that the MAP4Ks are lipid-binding proteins – an exciting and unprecedented finding that would further support a model in which PI4P directly binds and regulates MAP4K activity; (3) The MAP4Ks bind PI4P along with other PIPs, indicating that MAP4Ks are lipid-binding proteins while necessitating further studies to differentiate the respective roles of PI(4,5)P2 and PI4P in NF2 and MAP4K regulation.

Does VT01454 treatment modulate the kinase activity of MAP4K4/6/7 towards LATS1/2, and furthermore, does this occur in a PI4P-dependent manner? Previous work from our lab has shown that serum starvation, among other signals, induces MST1/2 and MAP4K kinase activity towards LATS2 (Chen et al., 2019). Since VT01454 induces LATS1/2 phosphorylation and MAP4K4/6/7 3-KO cells exhibit a significantly blunted response to VT01454 treatment, it is plausible that VT01454 would induce MAP4K4/6/7 phosphorylation of LATS1/2. This question will be addressed by an *in vitro* kinase assay, using tagged and immuno-purified MAP4Ks and purified LATS2 as a substrate, as previously reported (Chen et al., 2019). From this experiment, we expect at least 2 possible outcomes: (1) VT01454 treatment increases MAP4K activity towards LATS2; or (2) MAP4K kinase activity remains unchanged upon VT01454 treatment, indicating that LATS phosphorylation may be occurring through other mechanisms. If VT01454 induces MAP4K kinase activity, we would further test whether PI4P was involved by repeating the kinase assay in the presence and absence of GSK-A1, a PI4KIIIα inhibitor.

3.5 Experimental Procedures

Cell Culture

All cell lines were cultured at 37 °C with 5% CO_2. HEK293A cells were cultured in DMEM (GIBCO) with 10% FBS (GIBCO), 100 U ml^{-1} penicillin and 100 µg ml^{-1} streptomycin, and uveal melanoma cell lines were cultured in RPMI with 10% FBS (GIBCO), 100 U ml^{-1} penicillin and 100 µg ml^{-1} streptomycin. HEK293A cells were utilized for all experiments, unless otherwise noted. Cells were transfected with plasmids using PolyJet DNA In Vitro Transfection Reagent (Signagen Laboratories) according to the manufacturer's instructions. All knockout cell lines except the PITPβ KO cells were previously generated and published by the lab.

Plasmids, Chemicals, and Antibodies

RFP-Sac1-FKBP, NS5A-mCherry, GFP-SidM-P4Mx2 were generous gifts from Tamas Balla and Gerry Hammond. Flag-Sac1-K2A and GFP-p40px were generous gifts from Seth Field. GFP-C1-PLC-δPH was a gift from T. Meyer (Addgene 21179). Myr-Palm-Sac1 was generated by insertion of a Myr-Palm sequence at the N-terminus of RFP-Sac1-FKBP, and Sac-GRIP was generated by insertion of a GRIP domain at the C-terminus of RFP-Sac1. HA-PITPβ was cloned into pcDNA3.1 (BamH1 and Xba1). All Sac1 and PITPβ point mutants were generated using Q5® Hot Start High-Fidelity 2X Master Mix following standard mutagenesis procedures provided by the manufacturer (NEB #M0494). HA-TNIK, Flag-YAP, and HA-YAP were previously generated and published in the lab. Phenylarsine oxide was obtained from Santa Cruz Biotechnologies, PI4KIIIbeta-IN-10 (HY-100198) was from MedChem Express, and GSK-A1 was purchased from Synkinase (SYN-1219).

PITPβ, MINK1, and TNIK antibodies was obtained from Bethyl Laboratories. Anti-YAP/TAZ, GAPDH, and actin antibodies were obtained from Santa Cruz Biotechnology. Anti-phospho-YAP (S127), LATS1, phospho-Lats1/2 (Thr 1079/1041), and HA-HRP antibodies for Western blot, YAP antibody for phostag, and Flag (DYKDDDDK) tag antibodies for IF were obtained from Cell Signaling. Flag-HRP and Flag (M2) for IP were obtained from Sigma-Aldrich. GM130 was obtained from BD Biosciences. Alexa Fluor 488, 555, and 647-conjugated secondary antibodies for IF were obtained from Invitrogen.

Click Chemistry and Typhoon Imaging

Copper(I)-Catalyzed Alkyne-Azide Cycloaddition (CuAAC) was conducted in total cell lysate using tris-(benzyltriazolylmethyl)amine (TBTA) (Cayman Chemical #18816), sodium ascorbate (Sigma-Aldrich #A7631), copper(II) sulfate pentahydrate (Sigma-Aldrich #209198), and either 545-Azide (Sigma-Aldrich #760757) or biotin azide (Cayman Chemical #13040) or TAMRA-Biotin-Azide (Click Chemistry Tools #1048-5), for 1 hour at room temperature in the dark. For Typhoon imaging, the click reaction was terminated with the addition of 4xSDS sample buffer devoid of beta-mercaptoethanol. TAMRA-BSA (Thermo Fisher #A23016) was used in lieu of regular BSA standards when checking efficiency of affinity purification. Typhoon Imaging was done on an Amersham Biosciences Typhoon 9210 with ImageQuant TL software for image analysis.

Affinity Purification

Cells were treated with 500nM VT01454 (it was recommended the competitor concentration be 10x the probe concentration) and 50nM VT01702 for an hour, then harvested for streptavidin pulldown based on previously established methods (Speers and Cravatt, 2009).

Preparation of labeled proteome for MS-based analysis

Cell pellets were resuspended in 500 µL DPBS with protease inhibitors. Pellets were lysed using a Branson Sonifier probe sonicator (2 x 7 pulses, 40% duty cycle, output setting = 4). Cell lysates were clarified at 12,000 x g for 4 min. Protein concentration was determined using the DC Protein Assay (Bio-Rad) and absorbance was measured using a CLARIOstar microplate reader following manufacturer's instructions. Protein concentrations were normalized to 2 mg/mL in 0.5 mL.

Preparation of isotopically labeled samples for pairwise MS-based analysis

Alkynylated proteins were conjugated to biotin-PEG-N3 using copper-catalyzed azide−alkyne cycloaddition (CuAAC). For isotope dimethyl labeled experiments, samples were prepared as previous reported (Tolonen and Haas, 2014). To 0.5 mL cell lysates in a 1.5 mL Eppendorf tube, 55 µL freshly prepared 'click' mixture (30 µL of 1.7 mM TBTA in 4:1 t-BuOH:DMSO, 10 µL of 50 mM CuSO4 in H2O, 5 µL of 10 mM Biotin-PEG4-azide (ChemPep, cat # 271606) in DMSO, 10 µL of freshly prepared 50 mM

TCEP in H2O) was added and the samples were rotated at room temperature for 1 hour. The reaction was transferred to a 15-mL falcoln tube containing 2.5 mL of 4:1 methanol (MeOH)/chloroform (CHCl3). 1 mL of HPLC water was added, and the resulting cloudy mixture was centrifuged (5,000 x g, 10 min, 4C) to fractionate the protein interphase from the organic and aqueous solvent layers. After washing the protein disc carefully with 4:1 MeOH:CHCl3 (3 mL) followed by sonication in cold 4:1 MeOH:CHCl3 (3 mL) to ensure click reagents were efficiently removed, the remaining precipitate was pelleted by centrifugation (5,000 x g, 15 min, 4C). Remaining solvent was aspirated and protein pellets were resuspended in 1.2% SDS in DPBS by first heating to 95 C for 5 minutes, then probe sonication (10 pulses, 40% duty cycle, output setting = 4). 5 mL of DPBS was added to each sample, and samples were allowed to cool to room temperature before incubation with 50 µL of pre-equilibrated streptavidin agarose resin (1:1 slurry, Pierce) for 3 h at room temperature. Samples were washed 0.2% SDS in DPBS (10 mL, 2x) DPBS (10 mL, 3x), then water (10 mL, 2x). The resin was transferred to Eppendorf tubes and bound proteins were resuspended in 6M urea in DPBS. To this was added 10 mM DTT (25 µL of a 200 mM stock in water) and the beads were incubated at 65°C for 15 min. 20 mM iodoacetamide (25 µL of a 400 mM stock in water) was then added and allowed to react at 37°C for 30 min with shaking. The bead mixture was diluted with 750 µL PBS, pelleted by centrifugation and was resuspended in 200 µL of 100 mM TEAB in water containing 1 µg of sequencing-grade trypsin (20 µg, Promega). Samples were incubated at 37°C with shaking overnight. Peptides were separated from the beads with Micro Bio- Spin columns by centrifugation (800 x g, 2 min). To each digested sample (200 µL), 8 µL of 4% 'light' formaldehyde (Sigma Aldrich, 252549) or 8 µL of 4% 'heavy' formaldehyde-13C, d2 (Sigma Aldrich, 596388) and 8 µL of sodium cyanoborohydride (0.6 M in H2O) were added and the reaction was incubated at room temperature for 1 hour before quenching with 32 µL of 1% NH4OH (in H2O) followed by 16 µL of formic acid. The corresponding 'light' and 'heavy' sample were combined and centrifuged (1,400 x g, 2 min).

Liquid chromatography-mass spectrometry (LC-MS) analysis of probe-labeled proteins

Samples were pressure loaded onto a 250 µm (inner diameter) fused silica capillary columns packed with C18 resin (Aqua 5 µm, Phenomenex) and analyzed on a Finnigan LTQ Orbitrap (Thermo Scientific) coupled to an Agilent 1200- series quaternary pump. The peptides were eluted onto a biphasic

column with a 5 µm tip (100 µm fused silica, packed with C18 (10 cm) and bulk strong cation exchange resin (3 cm, SCX, Phenomenex) in a 5-step MudPIT experiment, using 0%, 25%, 50%, 80%, and 100% salt bumps of 500 mM aqueous ammonium acetate and using a gradient of 5%–100% buffer B in buffer A (buffer A: 95% water, 5% acetonitrile, 0.1% formic acid; buffer B: 5% water, 95% acetonitrile, 0.1% formic acid) as has been described in (Weerapana et al., 2007). Data were collected in data-dependent acquisition mode with dynamic exclusion enabled (20 s, repeat of 2). One full MS (MS1) scan (400-1800 m/z) was followed by 10 MS2 scans (ITMS) of the 10th most abundant ions.

Peptide and protein identification and quantification

The MS2 spectra were extracted from the raw file using RAWconverter (available at http://fields.scripps.edu/rawconv/) with 'select monoisotopic m/z in DDA' enabled. MS2 spectra data were searched using ProLuCID algorithm against a reverse-concatenated, nonredundant variant of the Human UniProt database (2016-07) and filtered using DTASelect 2.0 within the Integrated Proteomics Pipeline (IP2). The precursor ion mass tolerance for a minimum envelop of three isotopic peaks was set to 50 ppm. All cysteines were specified with a static modification for carbamidomethylation (+57.02146) and up to one differential modification was allowed per peptide for either methionine oxidation (+15.994915). For stable isotope dimethyl labeled samples, lysine and N-terminus were also specified with a static modification for demethylation (+28.0313). In addition, peptides were required to have at least one tryptic terminus. Each dataset was simultaneously searched for both 'light' and 'heavy' isotopic labeling by specifying the mass shifts on selected labeled amino acids, specifically, lysine (+8.0142) and arginine (+10.0083) for SILAC samples or lysine (+6.03182) and N-terminus (+6.03182) for 16 dimethyl labeled samples. The minimum peptide length was set to six residues, at least 2 peptides per protein was required and the false-positive rate was set at 1% at spectrum level. Light/Heavy peptide ratios were quantified based on peak areas on MS1 chromatogram with the in-house software (CIMAGE) as previously described. Briefly, MS1 ion chromatograms (±10 ppm) from 'light' and 'heavy' target peptide masses (m/z) were generated using a retention time window (±10 min) centered at the time the peptide ion was selected for MS/MS fragmentation, and subsequently identified. The ratio of 'light' and 'heavy' peptide peak areas are then calculated. To ensure the correct peak-pair is used for quantification, CIMAGE applies a co-elution correlation score filter

(R2 ≥ 0.8) for heavy and light peptide peaks to exclude target peptides with bad co-elution profiles. Furthermore, an 'envelope correlation score' filter is applied to ensure the experimentally observed highresolution MS1 spectrum matches (R2 > 0.8) the predicted isotopic distribution. Peptides detected as singletons, where only the heavy or light isotopically labeled peptide was detected and sequenced, but which passed all other filters described above, were given a standard ratio of 20, which is the maximum SILAC ratio reported here.

Within individual experiment dataset, peptides from the same protein were grouped together and the median ratio from at least two peptides were calculated as the protein ratio if its standard deviation was less than 10; if the standard deviation was greater than 10, the peptide ratio closest to 1 was assigned to the protein ratio. Protein ratios processed as above were then averaged across replicate experiments if their standard deviation is less than 60% of the mean; otherwise the ratio closest to 1 was taken as the final ratio for a protein in certain experiment condition.

Preparation of biotinylated proteome for MS-based analysis

Cell pellets were resuspended in 0.75 mL of lysis buffer (50 mM HEPES pH 7.4, 1% TritonX, 0.2% SDS, 2.5 mM EDTA, 250 mM NaCl, 0.5 mM DTT, 1x Protease Inhibitor Cocktail (Roche). Pellets were lysed using a Branson Sonifier probe sonicator (2 x 7 pulses, 40% duty cycle, output setting = 4). Cell lysates were clarified at 16,000 x g for 10 min at 4 ˚C. 100 µL of pre-equilibrated streptavidin beads were added to each cell pellet. Samples were incubated overnight at 4 ˚C. The next morning, beads were washed 1x with lysis buffer (1 mL), then 2x with lysis buffer with an additional 500 mM NaCl added (1 mL). Samples were washed with 2% SDS in DPBS (1 mL), then 5x times with DPBS (1 mL), then 2x with 2M urea in DPBS (1 mL). Samples were resuspended in 200 µL of 2M urea in DPBS containing 2g sequencing-grade trypsin (20 µg, Promega). To each digested sample (200 µL), 8 µL of 4% 'light' formaldehyde (Sigma Aldrich, 252549) or 8 µL of 4% 'heavy' formaldehyde-13C, d2 (Sigma Aldrich, 596388) and 8 µL of sodium cyanoborohydride (0.6 M in H2O) were added and the reaction was incubated at room temperature for 1 hour before quenching with 32 µL of 1% NH4OH (in H2O) followed by 16 µL of formic acid. The corresponding 'light' and 'heavy' sample were combined and centrifuged (1,400 g, 2 min). Samples were

analyzed by LC-MS/MS as described above in **LC-MS analysis of probe labeled proteins.** Samples were pressure loaded onto a 250 μm (inner diameter) fused silica capillary columns packed with C18 resin (Aqua 5 μm, Phenomenex) and analyzed on a Finnigan LTQ Orbitrap (Thermo Scientific).

Docking Simulation

The PITPα receptor model was prepared from available human structures of PITPα (PDB ID: 1uw5, chain A). The phosphatidylinositol ligand present in the original structure was removed in PyMOL (OpenGL version 2.1). The VT01454 ligand and restraints were prepared using the eLBOW utility in PHENIX (version 1.14-3260). Docking and binding analysis was performed in UCSF Chimera (candidate version 1.11.2, build 41320). Receptor and ligand models were prepared for docking using Dock Prep according to default behavior. The docking was performed in AutoDock Vina according to default behavior. A docking area of interest was selected to include the entire protein monomer and sufficient surrounding space to accommodate ligand. Docking returned eight viable solutions all of which localized to the hydrophobic cavity of the protein. Docks positioning the reactive Michael moiety proximal to cysteine residues were manually selected leaving two viable solutions. The solution with the most favorable Autodock Vina score was chosen for further analysis. The final model was visualized in PyMOL.

siRNA and CRISPR sequences

siRNA knockdown was performed using Lipofectamine RNAiMAX Transfection Reagent (Thermo Fisher #13778030) following manufacturer's instructions, and siRNA sequences used are as follows: siRNA PITPα: rUrUrGrGrArArGrCrArArGrArGrCrArArGrArGrCrUrUrGr

siRNA NF2: rArUrGrArGrCrUrUrCrArGrCrUrCrUrCrUrCrArArGrArGGA

CRISPR genomic editing technology was used for the deletion of genes of interest (Cong et al., 2013). The guide RNA sequences were cloned into the plasmids px459 (Addgene 48319), a gift from Dr. Feng Zhang (Ran et al., 2013). The constructed plasmids were transfected into HEK293A. 24 h after transfection, the transfected cells were enriched by 1 μg ml^{-1} puromycin selection for 3 days and then were sorted onto 96-well plates with only one cell in each well. The clones were screened by Western blot with

gene-specific antibodies and at least two independent clones for each gene deletion were used for each experiment described. The sgRNAs used for the PITPβ KO cell line are as follows:

PITPβ fwd: caccgGCATTCGTGAGGATGATTGC

PITPβ rev: aaacGCAATCATCCTCACGAATGCc

Western blots

Western blots were performed following standard methods. 7.5% phos-tag gel was used to resolve the phosphor-YAP proteins. The detailed information of the antibodies is provided in Supplemental Methods.

Quantitative real-time PCR

Total RNAs were extracted from cells containing PITPα siRNA knockdown using a RNeasy kit (Qiagen). cDNAs were synthesized by reverse transcription using iScript reverse transcriptase (Bio-Rad). cDNAs were then used for quantitative real-time PCR with gene-specific primers and KAPA SYBR FAST qPCR master mix (Kapa Biosystems) using the 7300 Real-time PCR system (Applied biosystems). The relative abundance of mRNAs was calculated by normalizing to GAPDH mRNA. Primers targeting *PITPNA* are as follows: Fwd 5'-CAAGGAGTATCGAGTAATCCTGC-3' and Rev 5'-GCCACCACCCGTTTCATTTT-3'

Immunofluorescence

Coverslips were pretreated with 2ug/mL Fibronectin solution (Sigma, P4957) in 12-well plates at 37°C overnight and washed with culture media prior to seeding cells. Cells were seeded at 0.3e5 cells/well for transfection or at 0.7e5 cells/well for drug treatments. Cells were fixed in 4% paraformaldehyde for 15 minutes, followed by permeabilization with 0.1% Triton-X for 10 minutes and blocking in 3% BSA for 1 hour. Primary antibody was incubated in 3% BSA overnight at 4°C. Secondary antibodies were diluted in 3% BSA and incubated for 1 hour. Slides were mounted with prolong gold anti-fade reagent with DAPI. Most images were captured with a Nikon Eclipse Ti confocal microscope and then were exported from NIS elements imaging software. Results were quantified in at least 100 randomly chosen cells. Image J was used to

merge the signals from channels. For TIRF, cells were seeded onto Nunc Lab Tek II Chambered Coverglass from Thermo Fisher. TIRF images were taken from a NikonA1R confocal STORM microscope.

3.6 Acknowledgements

I'd like to acknowledge Esther Kemper for performing the reductive dimethylation and LC-MS/MS analysis for target identification, Fulong Li for generating the P4M-DisMx2-BirA stable cell line, and Josh Mayfield for contributing the docking simulations.

Chapter 3 is currently being prepared for submission for publication of the material. Fu, V., Liu, G-B., Kemper, E., Li, F-L, Mayfield, J., Tang, T., Meng, ZM., Cravatt, BF., Guan, K-L. The dissertation author was the primary investigator and author of this material.

Figure 3.1: PITPα/ß are the major biochemical targets of VT01454. (A) VT01702 induces YAP phosphorylation in a dose-dependent manner. Cells were treated with the indicated concentrations of VT01702 for 1.5 hours. Accompanying luciferase reporter assays showing VT01702 effects on TEAD transcriptional activity. An 8xTEAD-Binding Domain (8xTBD) reporter was used. **(B)** Chemical structure of VT01702. **(C)** Schematic of target identification workflow. (1) Live cells were treated with 50nM VT01702, (2) click chemistry was performed in total cell lysate to conjugate the target-bound probe to a fluorophore and to biotin, which enabled (3) visualization of the gel band via fluorescent gel scanning and/or (4) affinity purification via streptavidin pulldown. **(D)** Bioorthogonal labeling using fluorescent azide enables visualization of 35kD band following VT01702 treatment. HEK293A cells were pretreated with the indicated concentrations of VT01454 for 30min, then treated with the indicated concentrations of VT01702 for 1 hour prior to cell lysis in what buffer. To conjugate target-bound-VT01702 to a fluorescent 545-azide, click chemistry was performed in total cell lysate for 1 hour at room temperature, samples were run on an SDS-PAGE gel, and the gel was scanned on a Typhoon imager (see Methods section). **(E)** Affinity purification sufficiently enriches target for total proteome capture and reductive dimethylation, followed by LC-MS/MS. Cells were treated for 1 hour with 50nM VT01702 in the presence or absence of 30 min of 500nM VT01454 pre-treatment. Aliquots of affinity-purified lysate were run in parallel on SDS-PAGE gels for Typhoon imaging (upper) and silver staining (lower). Total proteome samples were analyzed by reductive dimethylation/LC-MS/MS, and the silver stain gel band was excised for MS analysis. See Methods for more details on the affinity purification protocol, and LC-MS/MS (IP = immunoprecipitated; SN = supernatant; + = VT01702-treated; c = competitor-treated) **(F)** Endogenous PITPß antibody validates PITPß as a major biochemical target of VT01702. Aliquots of affinity purification samples from 4E were immunoblotted for PITPß expression levels. **(G)** Genetic deletion of PITPß validates PITPß as a major biochemical target of VT01702. HEK293A and PITPα+/-/-/β KO #1.12 cells were treated with the indicated concentrations of VT01702 for 1.5 hours, VT01702- PITPß adducts were conjugated to 545-azide by click chemistry, and lysates were analyzed by SDS-PAGE followed by Typhoon imaging and immunoblotting. **(H)** VT01702 binds to the Cysteine-94 residue of PITPß. Empty vector, HA-tagged Wild-type (WT), or cysteine-94 point-mutated (C94A) PITPß were transfected into HEK293A cells, and immunoprecipitated (IP) 24 hours thereafter using HA antibody. IP samples were analyzed by Typhoon imaging, and all lysates were immunoblotted with the indicated antibodies. **(I)** Docking simulation of VT01454-PITPα predicts C94 as the most likely candidate for covalent attachment. VT01454 (yellow) interaction with PITPα (white) is mediated by three broad structural features:

- The “Hydrophobic Cage” (numbering in blue). The phosphatidylinositol binding cavity of PITP-alpha is lined with multiple hydrophobic residues which stabilize the aliphatic portion of the ligand. VT01454’s peptide like character has multiple aliphatic functional groups which interact via hydrophobic interactions in docking. If true, these interactions likely mediate the majority of VT01454/PITPα association.
- The “Polar Triad” (numbering in red). Derivatization of the lead compound introduced a hydroxyl group to the proline-like residue of VT01454. The hydroxyl interacts with a polar triad (K60, E85, & Y62) in the docked structure. This interaction would increase the affinity relative to a native proline-like residue and may partially explain the demonstrable increase in IC50. These residues also mediate interaction between PITP-alpha and the inositol moiety of physiological ligands, likely contributing to displacement of the ligand.
- The residues involved in “Catalysis” (numbering in yellow). Cysteine 94 is likely the candidate for covalent attachment. Residues surrounding it may facilitate catalysis. K194 is in proximity to interact with the carboxyl group of the reactive moiety via Charge-dipole interaction. This could exaggerate the electron withdrawing effect of the carboxyl group on the attacked carbons and prime the warhead for covalent attachment. A nearby N22 may contribute to alignment/binding by orienting K194 or VT01454. T96 may act as an Acid/Base in the Michael reaction and aid in covalent attachment.

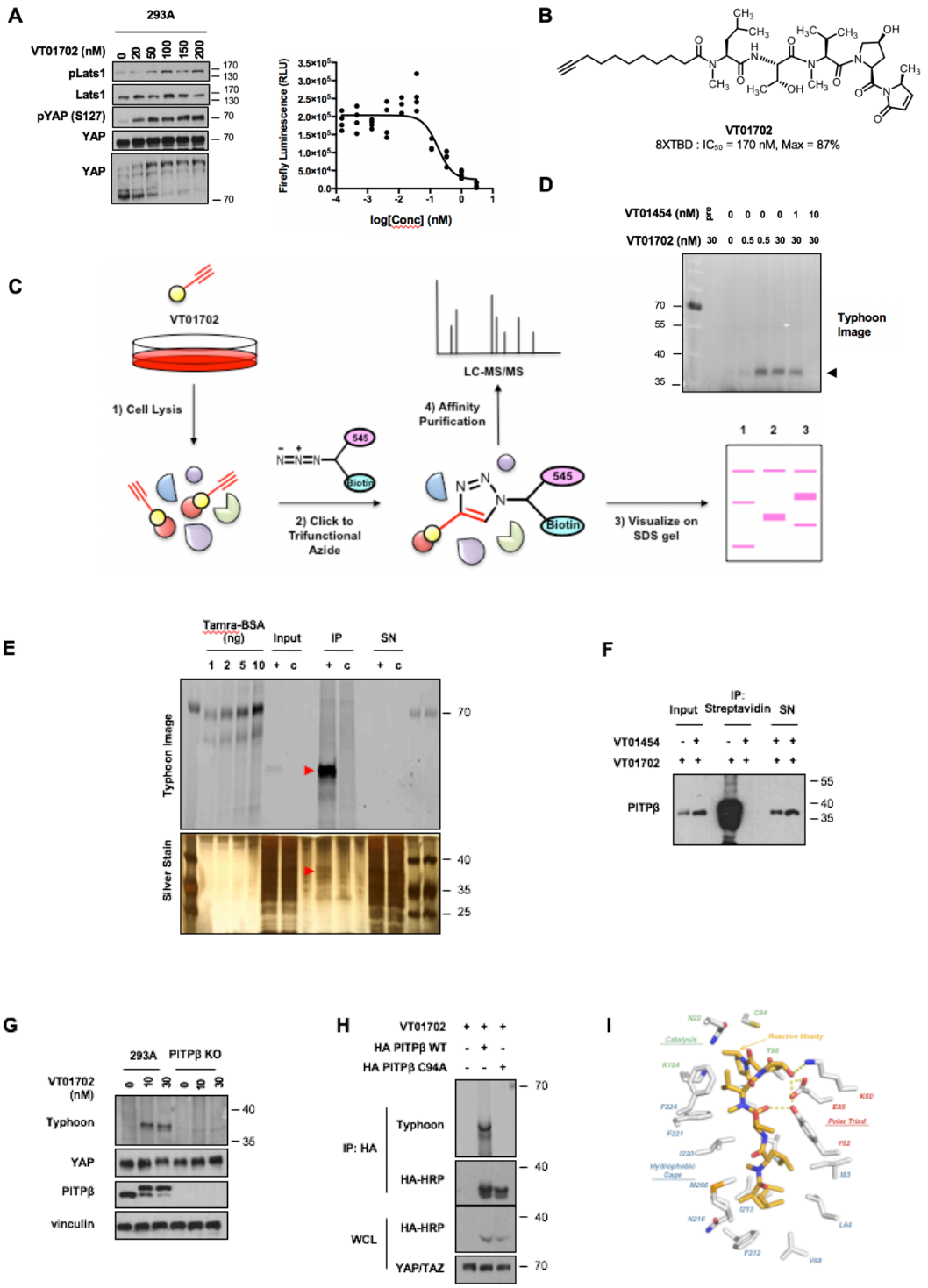
A
293A
VT01702 (nM)
0 20 50 100 150 200
pLats1
Lats1
pYAP (S127)
YAP
YAP
170
130
170
130
70
70
70
Firefly Luminescence (RLU)
log[Conc] (nM)
B
VT01702
8XTBD : IC50 = 170 nM, Max = 87%
C
VT01702
1) Cell Lysis
2) Click to Trifunctional Azide
545
Biotin
4) Affinity Purification
LC-MS/MS
3) Visualize on SDS gel
1 2 3
D
VT01454 (nM) pre 0 0 0 0 1 10
VT01702 (nM) 30 0 0.5 0.5 30 30 30
70
55
40
35
Typhoon Image
E
Tamra-BSA (ng)
1 2 5 10
Input
IP
SN
+ c
Typhoon Image
Silver Stain
70
40
35
25
F
IP: Streptavidin
Input
SN
VT01454
VT01702
PITPβ
55
40
35
G
293A
PITPβ KO
VT01702 (nM)
0 40 30 0 40 30
Typhoon
YAP
PITPβ
vinculin
40
35
H
VT01702
HA PITPβ WT
HA PITPβ C94A
IP: HA
Typhoon
HA-HRP
WCL
HA-HRP
YAP/TAZ
70
40
40
70
I
Catalysis
Reactive Moeity
Polar Triad
Hydrophobic Cage

Figure 3.2: PITPα/ß are the major functional targets of VT01454 that mediate YAP phosphorylation. **(A)** PITPα/ß knockdown induces YAP phosphorylation. Parental 293A or PITPα+/-/-/β KO #1.12 cells were transfected with siRNA targeting PITPα. 48 hours post-transfection, cells were treated with the indicated VT01454 concentrations for 1.5 hours and immunoblotted for the indicated antibodies. **(B)** PITPα/ß knockdown induces YAP cytoplasmic translocation. Parental 293A or PITPα+/-/-/β KO #1.12 cells were transfected with siRNA targeting PITPα and reseeded onto fibronectin-coated coverslips the following day. 48 hours post-transfection, cells were treated with 50nM VT01454 for 2 hours, and stained for immunofluorescence with YAP antibody (green). YAP localization was quantified. **(C)** PITPß overexpression antagonizes the effects of VT01454 on YAP phosphorylation. HEK293A cells were transfected with either Flag-YAP alone or co-transfected with HA- PITPß, treated with the indicated concentrations of VT01454 and harvested 24 hours post-transfection. Flag antibody was used to immunoprecipitate Flag-YAP for immunoblotting detection of phospho-YAP S127. **(D)** PITPß overexpression antagonizes the effects of VT01454 on YAP cytoplasmic translocation. HEK293A cells seeded on fibronectin-coated coverslips were transfected with empty vector or HA-PITPß. 24 hours post-transfection, cells were treated with 50nM VT01454 for 2 hours and stained for immunofluorescence with YAP antibody (green) or HA antibody (red). YAP localization was quantified. **(E)** VT01454 inhibits the phosphotidylinositol (PI) but not phosphotidylcholine (PC) transfer activity of PITPß. HEK293A cells were transfected with wildtype (WT) or point-mutated HA-PITPß (K60Q, C94A). The K60Q mutant is unable to bind PI, while the C94A mutant is unable to bind PC. VT01454 was treated 24 hours post-transfection at the indicated concentrations.

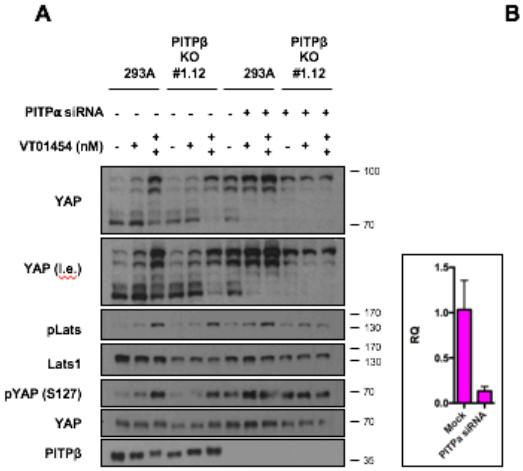
A
293A
PITPβ KO #1.12
293A
PITPβ KO #1.12
PITPα siRNA
VT01454 (nM)
YAP
YAP (l.e.)
pLats
Lats1
pYAP (S127)
YAP
PITPβ
RQ
Mock
PITPα siRNA

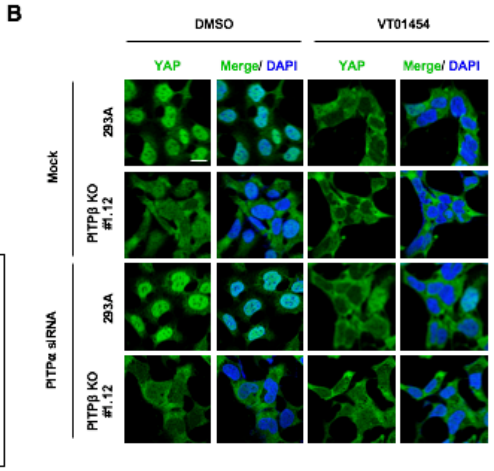
B
DMSO
VT01454
YAP
Merge/ DAPI
YAP
Merge/ DAPI
Mock
293A
PITPβ KO #1.12
PITPα siRNA
293A
PITPβ KO #1.12

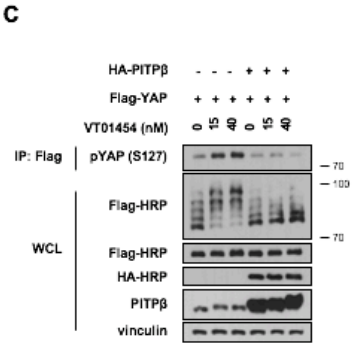
C
HA-PITPβ
Flag-YAP
VT01454 (nM)
IP: Flag
pYAP (S127)
WCL
Flag-HRP
Flag-HRP
HA-HRP
PITPβ
vinculin

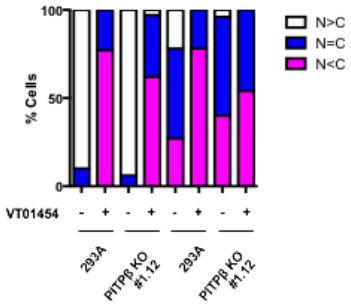
% Cells
N>C
N=C
N<C
VT01454
293A
PITPβ KO #1.12
293A
PITPβ KO #1.12

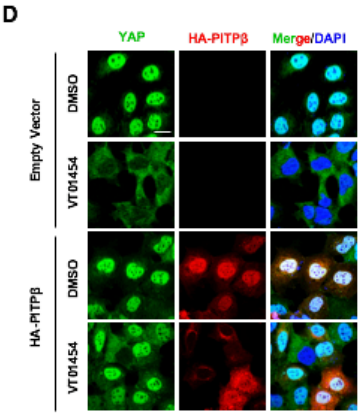
D
YAP
HA-PITPβ
Merge/DAPI
Empty Vector
DMSO
VT01454
HA-PITPβ
DMSO
VT01454

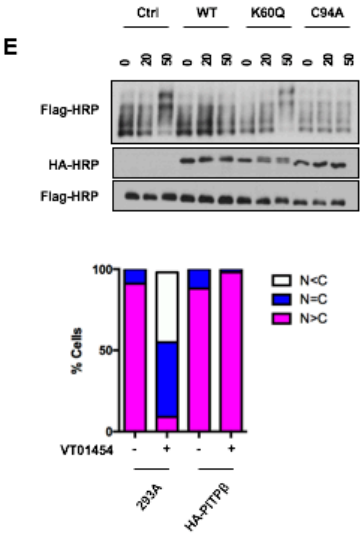
E
Ctrl
WT
K60Q
C94A
Flag-HRP
HA-HRP
Flag-HRP
% Cells
N<C
N=C
N>C
VT01454
293A
HA-PITPβ

Figure 3.3: A plasma membrane pool of PI4P regulates YAP phosphorylation. (A) VT01454 depletes plasma membrane PI4P levels. HEK293A cells seeded on fibronectin-coated coverslips were transfected with the PI4P reporter GFP-P4M-SidMx2, and treated with 50 nM VT01454 for 2 hours 24 hours post-transfection. Cells were stained for immunofluorescence with GM130 antibody (red), a Golgi marker. **(B)** PITPα/ß knockdown depletes plasma membrane PI4P levels. Parental 293A or PITPα+/-/-/β KO #1.12 cells were transfected with siRNA targeting PITPα, and were reverse-transfected with GFP-P4M-SidMx2 and reseeded onto fibronectin-coated coverslips the following day. 48 hours following the initial siRNA transfection, cells were stained for immunofluorescence with GM130 antibody (red). **(C) and (D)** Sac1 overexpression induces YAP phosphorylation and cytoplasmic translocation. **(C)** Cells were co-transfected with Flag-YAP and either RFP-Sac1-FKBP (Sac1) or its phosphatase-inactive mutant (Sac1 A442V) and lysed 24 hours post-transfection for immunoblotting and phos-tag analysis. Both Sac1 constructs are C-terminally truncated, resulting in diffuse cytosolic localization rather than at the ER, their normal site of localization. **(D)** Cells seeded on coverslips were co-transfected with GFP-P4M-SidMx2 (magenta) and either RFP-Sac1-FKBP (Sac1, red) or its phosphatase-inactive mutant (Sac1 A442V, red), and stained with YAP antibody (green) for immunofluorescence 24 hours post-transfection. YAP localization was quantified. **(E) and (F)** Myr-Palm-Sac1 but not Sac1-K2A induces YAP phosphorylation and cytoplasmic translocation. **(E)** Cells seeded on coverslips were co-transfected with GFP-P4M-SidMx2 (magenta) and either Myr-Palm-Sac1 or Sac1-K2A (red), and stained with YAP antibody (green) for immunofluorescence 24 hours post-transfection. YAP localization was quantified. **(F)** Cells were co-transfected with HA-YAP and either Myr-Palm-Sac1 (which targets Sac1 to the plasma membrane) or Sac1-K2A, (which accumulates at the Golgi). Cells were lysed 24 hours post-transfection for immunoblotting and phos-tag analysis. **(G) and (H)** GSK-A1 but not PI4KIIIß-IN-10 induces YAP phosphorylation and cytoplasmic translocation. **(G)** Cells seeded on coverslips were transfected with GFP-P4M-SidMx2 (magenta). 24 hours post-transfection, cells were treated with 20nM GSK-A1 for 10min or 25nM PI4KIIIß-IN-10 for 4 hours, then stained for YAP antibody (green) for immunofluorescence. YAP localization as quantified. **(H)** Cells were treated with the indicated concentrations of GSK-A1 for 10 min and lysed for immunoblot and phos-tag analysis.

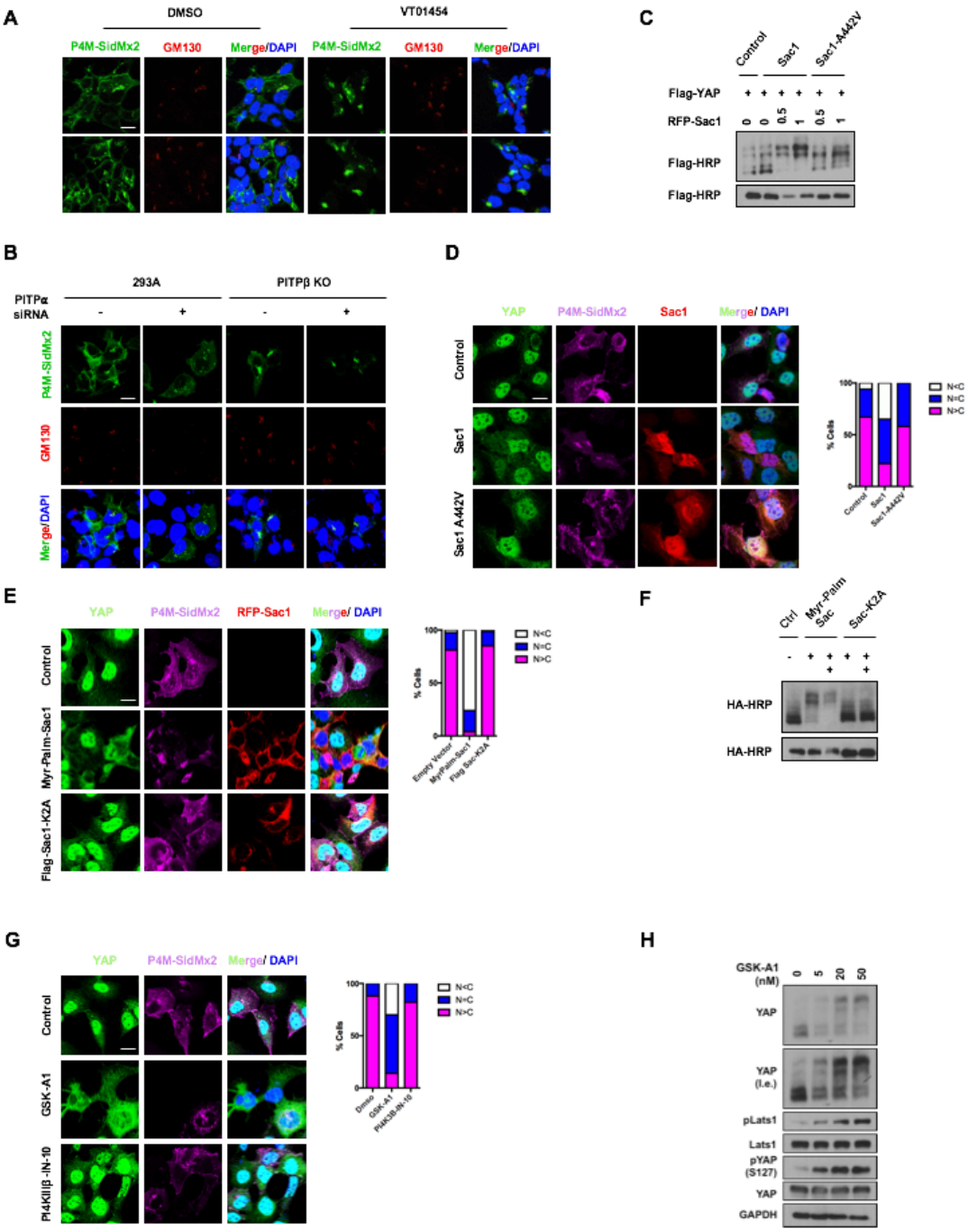
A
DMSO
VT01454
P4M-SidMx2
GM130
Merge/DAPI
B
293A
PITPβ KO
PITPα siRNA
C
Control
Sac1
Sac1-A442V
Flag-YAP
RFP-Sac1
Flag-HRP
D
YAP
P4M-SidMx2
Sac1
Merge/ DAPI
Control
Sac1
Sac1 A442V
% Cells
N<C
N=C
N>C
E
RFP-Sac1
Myr-Palm-Sac1
Flag-Sac1-K2A
F
Ctrl
Myr-Palm Sac
Sac-K2A
HA-HRP
G
GSK-A1
PI4KIIIβ -IN-10
H
GSK-A1 (nM)
YAP (l.e.)
pLats1
Lats1
pYAP (S127)
GAPDH

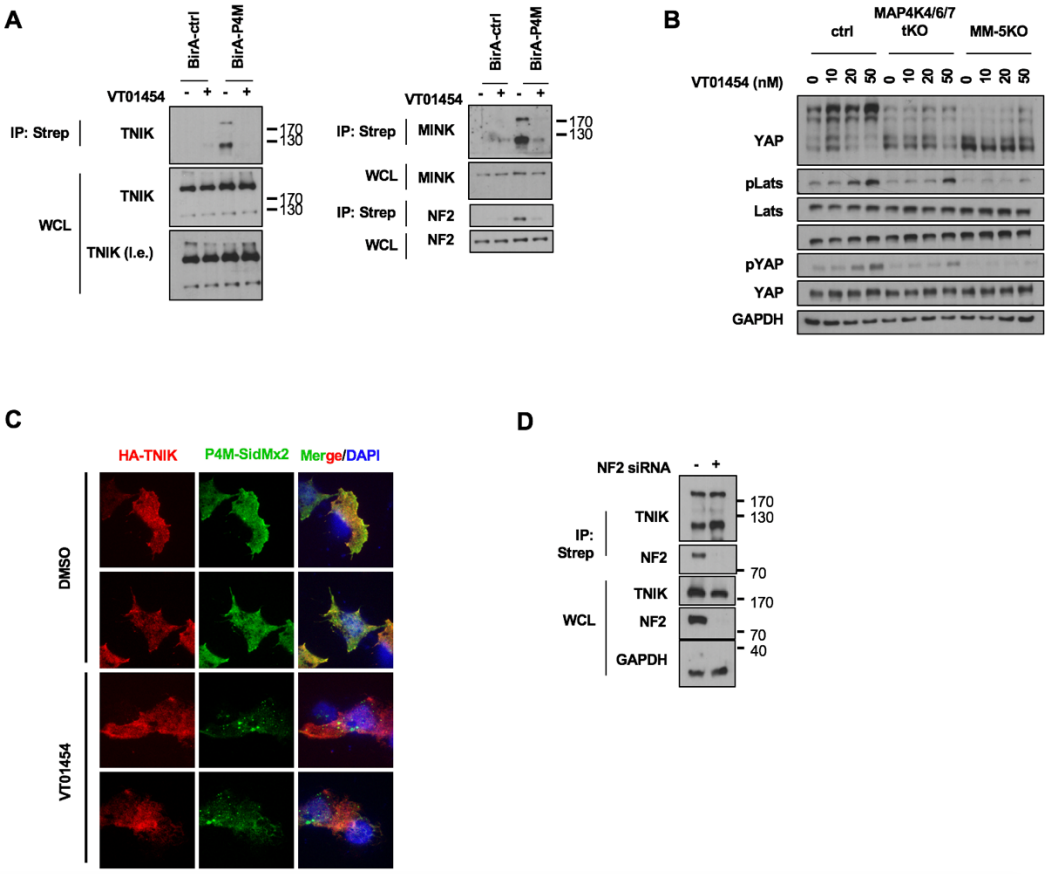

Figure 3.4: BioID using P4M-SidMx2 as bait identifies MAP4K6 and MAP4K7 as PI4P-proximal proteins regulated by VT01454 treatment. (A) Biochemical confirmation of TNIK/MAP4K7 and MINK1/MAP4K6 as PI4P-proximal proteins and abrogation of proximity upon VT01454 treatment. Cells stably expressing BirA-P4M-SidMx2 (BirA-P4M) or a control BirA vector (BirA-ctrl) were treated with 50nM VT01454 for one hour, induced with 1uM biotin for 10 min, then harvested for streptavidin pulldown and subsequent immunoblotting analysis. **(B)** VT01454 induces YAP phosphorylation in a MAP4K4/6/7-dependent manner. Wildtype, MAP4K4/6/7 KO, or MAP4K4/6/7-MST1/2 KO cells were treated the indicated concentrations of VT01454 for one hour, then lysed in sample buffer for immunoblotting analysis. **(C)** TIRF microscopy showing potential co-localization between TNIK and PI4P in the presence and absence of VT01454. Cells were seeded onto 8-well chambered coverglass and treated with 50nM VT01454 for 2 hours before fixation.

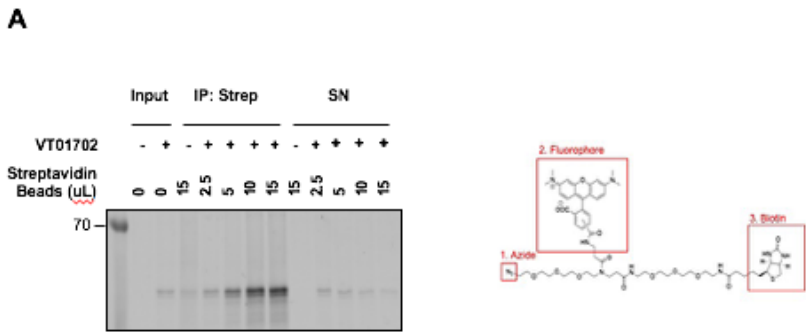

Figure S3.1: (A) Trifunctional 545-biotin-azide click reaction and streptavidin pulldown. Cells were treated with 70nM VT01702, clicked to biotin-azide as previously described, and purified overnight by Streptavidin using the indicated volumes of Streptavidin magnetic beads.

Figure S3.2: VT01454 has no effect on PI3P and PI(4,5)P2 localization. (A) and (B) PI(4,5)P2 reporter GFP-PLC δPH (S6A) and PI3P reporter p40px (S6B) exhibit no significant localization changes upon VT01454 treatment. Cells seeded on coverslips were transfected with GFP-PLC δPH (green) or p40px (red), and fixed for immunofluorescence 24 hours post-transfection.
(C) and (D) PI4KA overexpression antagonizes VT01454 effect on YAP cytoplasmic translocation and phosphorylation. S6C Cells seeded on coverslips were transfected with either Flag-YAP alone or co-transfected with non-structural viral protein 5A (NS5A-Cherry) and Flag-PI4KA. S6D Cells were transfected with either Flag-YAP alone or co-transfected with non-structural viral protein 5A (NS5A-Cherry) and Flag-PI4KA. **(E) and (F)** Phenylarsine oxide (PAO) induces YAP cytoplasmic translocation and phosphorylation. S6E Cells were treated with the indicated concentrations of PAO for 10min, then lysed for immunoblot and phos-tag analysis. S6E Cells seeded on coverslips were treated with 10 uM of PAO for 10 min, then stained for YAP antibody (green) for immunofluorescence. (**G)** Myr-Palm-Sac1 but not Sac1-K2A induces YAP phosphorylation and cytoplasmic translocation, with GM130 co-localization. Cells seeded on coverslips were co-transfected with GFP-P4M-SidMx2 (magenta) and either Myr-Palm-Sac1 or Sac1-K2A (red), and stained with GM130 antibody (green) for immunofluorescence 24 hours post-transfection. **(H)** GSK-A1 but not PI4KIIIß-IN-10 induces YAP phosphorylation and cytoplasmic translocation, with GM130 co-localization. Cells seeded on coverslips were transfected with GFP-P4M-SidMx2 (magenta). 24 hours post-transfection, cells were treated with 20nM GSK-A1 for 10min or 25nM PI4KIIIß-IN-10 for 4 hours, then stained with YAP (green) and GM130 antibody (red) for immunofluorescence. **(I)** Sac1-GRIP (which is targeted to the Golgi) does not induce YAP cytoplasmic translocation. Cells seeded on coverslips were transfected with RFP-Sac1-GRIP (red) and stained for YAP antibody (green) for immunofluorescence.

A

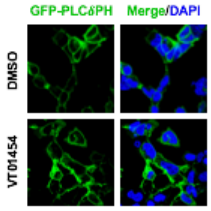
GFP-PLCδPH
Merge/DAPI
DMSO
VT01454

B

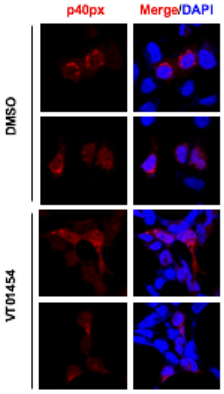
p40px
Merge/DAPI
DMSO
VT01454

C

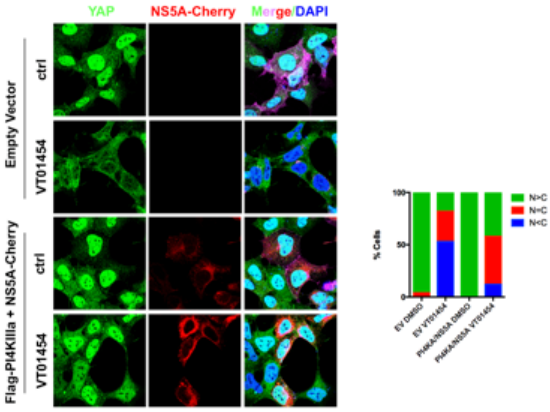
YAP
NS5A-Cherry
Merge/DAPI
Empty Vector
ctrl
VT01454
Flag-PI4KIIIa + NS5A-Cherry
ctrl
VT01454
% Cells
N>C
N=C
N<C
EV DMSO
EV VT01454
PI4KA-NS5A DMSO
PI4KA-NS5A VT01454

D

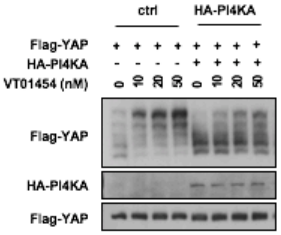
ctrl
HA-PI4KA
Flag-YAP
HA-PI4KA
VT01454 (nM)
0
10
20
50
0
10
20
50
Flag-YAP
HA-PI4KA
Flag-YAP

E

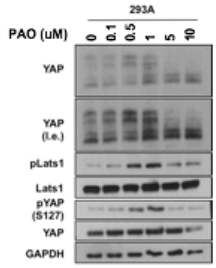
293A
PAO (uM)
0
0.1
0.5
1
5
10
YAP
YAP (l.e.)
pLats1
Lats1
pYAP (S127)
YAP
GAPDH

F

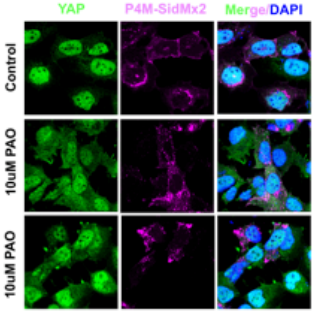
YAP
P4M-SidMx2
Merge/DAPI
Control
10uM PAO
10uM PAO

G

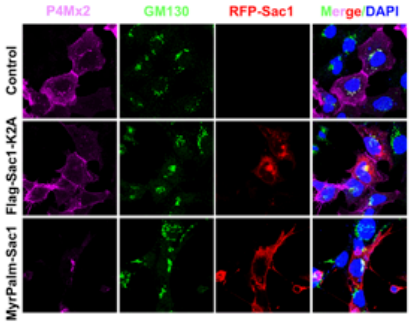
P4Mx2
GM130
RFP-Sac1
Merge/DAPI
Control
Flag-Sac1-K2A
MyrPalm-Sac1

H

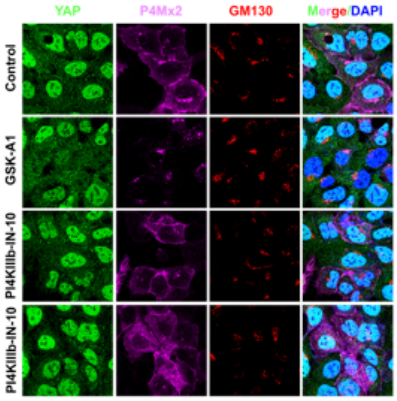
YAP
P4Mx2
GM130
Merge/DAPI
Control
GSK-A1
PI4KIIIb-IN-10
PI4KIIIb-IN-10

I

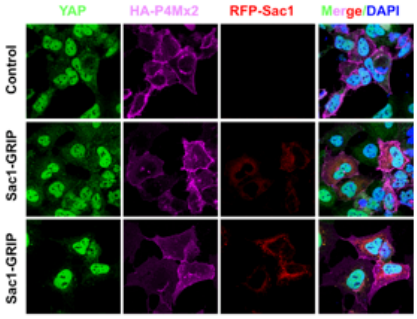
YAP
HA-P4Mx2
RFP-Sac1
Merge/DAPI
Control
Sac1-GRIP
Sac1-GRIP

A

	A	B	C	D	E	F	G	H	I	J	K
1	Accessi	Residue	Description	MaxRat	SpecCo	rep1 (dm	rep2 (di	rep3 (di	average		
2	sp|P11498	0	PC Pyruvate carboxylase, mitochondrial [REVIEWED] ENSG00000173599;IPI00299402;P11498;Q16705	1.38	1767	1.09	1.38	1.16	1.21		Competed
3	sp|Q13085	0	ACACA Acetyl-CoA carboxylase 1 [REVIEWED] ENSG00000132142;IPI00847501;Q13085;B2RP68;Q6KEV6;Q6XDA8;Q7Z2G8;Q7Z561;Q7Z563;Q7Z56	1.41	1206	1.05	1.41	1.31	1.256667		Not competed
4	sp|P04264	0	KRT1 Keratin, type II cytoskeletal 1 [REVIEWED] ENSG00000167768;IPI00220327;P04264;B2RA01;Q14720;Q6GSJ0;Q9H298	4.29	1152	1.16	0.32	4.29	1.923333		
5	sp|P35908	0	KRT2 Keratin, type II cytoskeletal 2 epidermal [REVIEWED] ENSG00000172867;IPI00021304;P35908;Q4VAQ2	8.44	963	1.4	0.15	8.44	3.33		
6	sp|Q96RQ3	0	MCCC1 Methylcrotonoyl-CoA carboxylase subunit alpha, mitochondrial [REVIEWED] ENSG00000078070;IPI00024580;Q96RQ3;Q59ES4;Q9H959;Q	1.33	927	1.12	1.33	1.24	1.23		
7	sp|P13645	0	KRT10 Keratin, type I cytoskeletal 10 [REVIEWED] ENSG00000186395;IPI00009865;P13645;Q14664;Q8N175	10.32	870	1.1	0.17	10.32	3.863333		
8	sp|P05165	0	PCCA Propionyl-CoA carboxylase alpha chain, mitochondrial [REVIEWED] ENSG00000175198;IPI00895869;P05165;B4DKY8;Q15979;Q8WXQ7	1.54	681	1.12	1.54	1.35	1.336667		
9	sp|P48739	0	PITPNB Phosphatidylinositol transfer protein beta isoform [REVIEWED] ENSG00000180957;IPI01014285;P48739;B3KYB8;Q8N5W1	20	678	20	20	20	20		
10	sp|P13647	0	KRT5 Keratin, type II cytoskeletal 5 [REVIEWED] ENSG00000186081;IPI00009867;P13647;Q6PI71;Q6UBJ0;Q8TA91	6.22	348	1.08	0.15	6.22	2.483333		
11	sp|P02538	0	KRT6A Keratin, type II cytoskeletal 6A [REVIEWED] ENSG00000205420;IPI00300725;P02538;A4QPC1;P48667;Q08AR4;Q6NT67;Q96CL4	3.37	330	1.11	0.26	3.37	1.58		
12	sp|P35527	0	KRT9 Keratin, type I cytoskeletal 9 [REVIEWED] ENSG00000171403;IPI00019359;P35527;O00109;Q0IJ47;Q14665	0.66	291	0.52	0.66	0.49	0.556667		
13	sp|O00763	0	ACACB Acetyl-CoA carboxylase 2 [REVIEWED] ENSG00000076555;IPI00157056;O00763;A6NK36;Q16852;Q1HEC1;Q6KE87;Q6KE89;Q6TY48	1.31	258			1.31	1.31		
14	sp|P68371	0	TUBB4B Tubulin beta-4B chain [REVIEWED] ENSG00000188229;IPI00007752;P68371;A2BFA2;P05217	1.13	231	1.13	0.44	1.08	0.883333		
15	sp|P07437	0	TUBB Tubulin beta chain [REVIEWED] ENSG00000229684;ENSG00000232575;ENSG00000235067;ENSG00000196230;ENSG00000227739;ENSG00	1.11	225	1.11	0.45	1.08	0.88		
16	sp|P12035	0	KRT3 Keratin, type II cytoskeletal 3 [REVIEWED] ENSG00000186442;IPI00290857;P12035;A6NIS2;Q701L8	9.24	159		0.26	9.24	4.75		
17	sp|Q71U36	0	TUBA1A Tubulin alpha-1A chain [REVIEWED] ENSG00000167552;IPI00180675;Q71U36;A8K0B8;P04687;P05209	1.29	156	0.78	0.48	1.29	0.85		
18	sp|Q7Z794	0	KRT77 Keratin, type II cytoskeletal 1b [REVIEWED] ENSG00000189182;IPI00376379;Q7Z794;Q7RTS8	20	153	0.93		20	10.465		
19	sp|P02533	0	KRT14 Keratin, type I cytoskeletal 14 [REVIEWED] ENSG00000186847;IPI00384444;P02533;Q14715;Q53XY3;Q9BUE3;Q9UBN2;Q9UBN3;Q9UCY4	1.64	153		0.2	1.64	0.92		
20	sp|P08779	0	KRT16 Keratin, type I cytoskeletal 16 [REVIEWED] ENSG00000186832;IPI00217963;P08779;A8K488;P30654;Q16402;Q9UBG8	1.82	144		0.86	1.82	1.34		
21	sp|Q00169	0	PITPNA Phosphatidylinositol transfer protein alpha isoform [REVIEWED] ENSG00000174238;IPI00216048;Q00169	20	138	20	20	20	20		
22	sp|P08107	0	HSPA1B Heat shock 70 kDa protein 1A/1B [REVIEWED] ENSG00000224501;ENSG00000215328;ENSG00000204389;ENSG00000237724;ENSG0000	1.46	132	1.46	0.34	1.31	1.036667		
23	sp|P60709	0	ACTB Actin, cytoplasmic 1 [REVIEWED] ENSG00000075624;IPI00021439;P60709;P02570;P70514;P99021;Q11211;Q64316;Q75MN2;Q96B34;Q9	1.35	126	1.35	0.39	1.16	0.966667		
24	sp|P68366	0	TUBA4A Tubulin alpha-4A chain [REVIEWED] ENSG00000127824;IPI00007750;P68366;B3KNQ6;P05215	1.22	117		0.51	1.22	0.865		
25	sp|Q13509	0	TUBB3 Tubulin beta-3 chain [REVIEWED] ENSG00000198211;IPI00013683;Q13509;Q9BTZ0;Q9BW10	0.53	81		0.53		0.53		
26	sp|Q9NY65	0	TUBA8 Tubulin alpha-8 chain [REVIEWED] ENSG00000183785;IPI00646909;Q9NY65;B2RCX2;B4DWG3;Q2M3N4	1.36	75			1.36	1.36		
27	sp|Q07020	0	RPL18 60S ribosomal protein L18 [REVIEWED] ENSG00000063177;IPI00215719;Q07020;Q8WTZ6	1.24	66	1.15	1.02	1.24	1.136667		
28	sp|P11142	0	HSPA8 Heat shock cognate 71 kDa protein [REVIEWED] ENSG00000109971;IPI00037070;P11142;Q9H3R6	1.35	54		0.35	1.35	0.85		
29	sp|P04406	0	GAPDH Glyceraldehyde-3-phosphate dehydrogenase [REVIEWED] ENSG00000111640;IPI00219018;P04406;P00354;Q53X65	2.66	51	1.34	0.39	2.66	1.463333		
30	sp|P13639	0	EEF2 Elongation factor 2 [REVIEWED] ENSG00000167658;IPI00186290;P13639;B2RMP5;D6W618;Q58J86	1.47	48	1.35	0.34	1.47	1.053333		
31	sp|Q02878	0	RPL6 60S ribosomal protein L6 [REVIEWED] ENSG00000089009;IPI00790342;Q02878;Q2M3Q3;Q8WW97	1.6	45	1.04	1.02	1.6	1.22		
32	sp|P62241	0	RPS8 40S ribosomal protein S8 [REVIEWED] ENSG00000142937;IPI00216587;P62241;P09058;Q6IRL7	1.11	45	1.11	0.86	1.06	1.01		
33	sp|P19012	0	KRT15 Keratin, type I cytoskeletal 15 [REVIEWED] ENSG00000171346;IPI00290077;P19012;B3KQY1;Q53XV8;Q9BUG4	10.08	36		10.08		10.08		
34	sp|P26373	0	RPL13 60S ribosomal protein L13 [REVIEWED] ENSG00000167526;IPI00465361;P26373;Q3KQT8;Q567Q8;Q9BPX0	1.36	36	1.34	0.69	1.36	1.13		
35	sp|P08238	0	HSP90AB1 Heat shock protein HSP 90-beta [REVIEWED] ENSG00000096384;IPI00414676;P08238;B2R5P0;Q5T9W7;Q9NQW0;Q9NTK6	1.28	36		0.27	1.28	0.775		
36	sp|Q86Y46	0	KRT73 Keratin, type II cytoskeletal 73 [REVIEWED] ENSG00000186049;IPI00878987;Q86Y46;Q32MB2	3.37	33			3.37	3.37		
37	sp|Q7RTS7	0	KRT74 Keratin, type II cytoskeletal 74 [REVIEWED] ENSG00000170484;IPI00329306;Q7RTS7;B5MD61;Q86Y45	3.37	33			3.37	3.37		
38	sp|P61313	0	RPL15 60S ribosomal protein L15 [REVIEWED] ENSG00000174748;IPI00470528;P61313;P39030;P41051;Q5U0C0;Q6IPX6;Q8WYP2;Q96C44;Q9H2	2.12	33	1.06	1.33	2.12	1.503333		

B

	A	B	C	D	E	F	G	H	I	J	K	L
1	Protein Rank	Description	|Log Prob|	Best |Log Prob|	Best score	Total Intensity	# of spectra	# of unique peptides	# of mod peptides	Coverage %	# AA's in protein	Protein DB number
2	1	>sp|P13533|MYH6_HUMAN Myosin-6 OS=Homo sapiens GN=MYH6 PE=1 SV=5	174.74	8.14	618.60	5848920.5	128	51	15	24.96	1939	4870
3	2	>sp|P48739|PIPNB_HUMAN Phosphatidylinositol transfer protein beta isoform OS=Homo	118.15	10.52	786.10	11621923.2	122	39	16	80.44	271	6501
4	3	>sp|P04264|K2C1_HUMAN Keratin, type II cytoskeletal 1 OS=Homo sapiens GN=KRT1 PE=1	94.39	8.97	715.20	5046275.3	64	25	10	35.87	644	4015
5	4	>sp|P13645|K1C10_HUMAN Keratin, type I cytoskeletal 10 OS=Homo sapiens GN=KRT10 P	90.46	9.18	650.30	5709713.6	94	30	12	46.06	584	4882
6	5	>sp|P35908|K22E_HUMAN Keratin, type II cytoskeletal 2 epidermal OS=Homo sapiens GN=	67.28	8.26	793.00	3830104.8	61	24	11	38.50	639	6054
7	6	>sp|P06576|ATPB_HUMAN ATP synthase subunit beta, mitochondrial OS=Homo sapiens GI	62.81	8.23	624.70	1547919.3	30	16	5	33.27	529	4153
8	7	>sp|P68032|ACTC_HUMAN Actin, alpha cardiac muscle 1 OS=Homo sapiens GN=ACTC1 PE=	57.92	5.86	552.00	3502664.4	53	19	7	37.93	377	7481
9	8	>sp|P25705|ATPA_HUMAN ATP synthase subunit alpha, mitochondrial OS=Homo sapiens G	46.29	7.19	598.50	1085188.1	22	12	2	24.23	553	5568
10	9	>sp|P35527|K1C9_HUMAN Keratin, type I cytoskeletal 9 OS=Homo sapiens GN=KRT9 PE=1	35.75	4.74	493.70	1616207.0	42	15	6	28.57	623	6013
11	10	>sp|P13647|K2C5_HUMAN Keratin, type II cytoskeletal 5 OS=Homo sapiens GN=KRT5 PE=1	31.89	4.80	545.50	862023.8	20	11	3	18.14	590	4884
12	11	>sp|P09493|TPM1_HUMAN Tropomyosin alpha-1 chain OS=Homo sapiens GN=TPM1 PE=1	25.26	5.45	509.50	742810.4	16	9	1	31.34	284	4362
13	12	>sp|P08590|MYL3_HUMAN Myosin light chain 3 OS=Homo sapiens GN=MYL3 PE=1 SV=3	24.71	5.66	559.20	691060.8	14	6	1	32.31	195	4296
14	13	>sp|Q99798|ACON_HUMAN Aconitate hydratase, mitochondrial OS=Homo sapiens GN=AC	19.81	5.69	487.60	419058.4	11	7	0	10.77	780	16678
15	14	>sp|P10916|MLRV_HUMAN Myosin regulatory light chain 2, ventricular/cardiac muscle isc	18.51	3.71	456.80	459587.4	14	8	2	31.93	166	4735
16	15	>sp|P12883|MYH7_HUMAN Myosin-7 OS=Homo sapiens GN=MYH7 PE=1 SV=5	17.97	5.90	573.10	572311.7	12	4	0	3.15	1935	4845
17	16	>sp|Q00169|PIPNA_HUMAN Phosphatidylinositol transfer protein alpha isoform OS=Hom	15.21	4.34	462.30	715827.7	18	10	4	37.41	270	7678
18	17	>sp|P40926|MDHM_HUMAN Malate dehydrogenase, mitochondrial OS=Homo sapiens GN	14.84	5.63	498.40	446155.1	11	6	1	21.01	338	6174
19	18	>sp|P04406|G3P_HUMAN Glyceraldehyde-3-phosphate dehydrogenase OS=Homo sapiens	12.54	4.94	404.90	353591.6	11	8	5	21.49	335	4022
20	19	>sp|P02533|K1C14_HUMAN Keratin, type I cytoskeletal 14 OS=Homo sapiens GN=KRT14 P	11.32	4.36	451.50	239907.2	8	5	1	16.10	472	3905
21	20	>sp|P13804|ETFA_HUMAN Electron transfer flavoprotein subunit alpha, mitochondrial OS	11.23	4.37	444.10	376237.2	12	8	3	28.23	333	4902
22	21	>sp|P21796|VDAC1_HUMAN Voltage-dependent anion-selective channel protein 1 OS=Hor	10.87	4.02	487.30	110387.6	4	4	1	16.61	283	5368
23	22	>sp|P22626|ROA2_HUMAN Heterogeneous nuclear ribonucleoproteins A2/B1 OS=Homo sa	10.26	4.81	504.10	153432.2	5	4	0	12.46	353	5421
24	23	>sp|P16615|AT2A2_HUMAN Sarcoplasmic/endoplasmic reticulum calcium ATPase 2 OS=H	10.04	3.60	385.30	236201.8	8	7	0	8.93	1042	5076
25	24	>sp|P48735|IDHP_HUMAN Isocitrate dehydrogenase [NADP], mitochondrial OS=Homo sap	9.67	3.37	379.40	243922.5	7	4	1	9.29	452	6499
26	25	>sp|P06753|TPM3_HUMAN Tropomyosin alpha-3 chain OS=Homo sapiens GN=TPM3 PE=1	8.00	4.37	481.70	190327.6	3	2	1	3.16	285	4168
27	26	>sp|P11498|PYC_HUMAN Pyruvate carboxylase, mitochondrial OS=Homo sapiens GN=PC P	7.20	3.14	479.20	212801.6	5	5	1	5.01	1178	4781
28	27	>sp|P55084|ECHB_HUMAN Trifunctional enzyme subunit beta, mitochondrial OS=Homo sa	6.24	4.09	451.40	135665.9	4	3	0	5.91	474	6983
29	28	>sp|Q9Y623|MYH4_HUMAN Myosin-4 OS=Homo sapiens GN=MYH4 PE=1 SV=2	5.90	5.89	569.30	87129.9	2	1	0	0.67	1939	20876
30	29	>sp|P28331|NDUS1_HUMAN NADH-ubiquinone oxidoreductase 75 kDa subunit, mitochor	5.87	3.18	357.30	74850.5	3	3	0	4.81	727	5675
31	30	>sp|P38117|ETFB_HUMAN Electron transfer flavoprotein subunit beta OS=Homo sapiens G	5.87	3.81	428.10	132643.9	3	2	0	7.84	255	6113
32	31	>sp|Q16134|ETFD_HUMAN Electron transfer flavoprotein-ubiquinone oxidoreductase, mit	5.58	2.72	346.30	69081.5	3	3	0	5.51	617	9109
33	32	>sp|Q02045|MYL5_HUMAN Myosin light chain 5 OS=Homo sapiens GN=MYL5 PE=2 SV=1	5.51	3.68	378.10	51185.8	2	2	1	5.78	173	7775
34	33	>sp|P07195|LDHB_HUMAN L-lactate dehydrogenase B chain OS=Homo sapiens GN=LDHB P	5.49	3.23	401.60	184247.8	5	4	1	13.17	334	4183
35	34	>sp|P07477|TRY1_HUMAN Trypsin-1 OS=Homo sapiens GN=PRSS1 PE=1 SV=1	5.07	2.93	423.60	494726.6	9	5	3	12.15	247	4215

Figure S3.3: Partial List of Mass Spectrometric Analyses for Target Identification and BioID. (A) Partial list of MudPit analysis of total proteome capture. PITPNB and PITPNA are highlighted in green. See Experimental Procedures for details of analysis methods used. **(B)** Partial list of gel excision mass spectrometry analysis. PITPNB and PITPNA are highlighted in yellow as hits of highest abundance.

3.7 References

ALB, J. G., CORTESE, J. D., PHILLIPS, S. E., ALBIN, R. L., NAGY, T. R., HAMILTON, B. A. & BANKAITIS, V. A. 2003. Mice lacking phosphatidylinositol transfer protein-alpha exhibit spinocerebellar degeneration, intestinal and hepatic steatosis, and hypoglycemia. *J Biol Chem,* 278**,** 33501-18.

ALB, J. G., GEDVILAITE, A., CARTEE, R. T., SKINNER, H. B. & BANKAITIS, V. A. 1995. Mutant rat phosphatidylinositol/phosphatidylcholine transfer proteins specifically defective in phosphatidylinositol transfer: implications for the regulation of phospholipid transfer activity. *Proc Natl Acad Sci U S A,* 92**,** 8826-30.

ALB, J. G., PHILLIPS, S. E., ROSTAND, K., CUI, X., PINXTEREN, J., COTLIN, L., MANNING, T., GUO, S., YORK, J. D., SONTHEIMER, H., COLLAWN, J. F. & BANKAITIS, V. A. 2002. Genetic ablation of phosphatidylinositol transfer protein function in murine embryonic stem cells. *Mol Biol Cell,* 13**,** 739-54.

ALTAN-BONNET, N. & BALLA, T. 2012. Phosphatidylinositol 4-kinases: hostages harnessed to build panviral replication platforms. *Trends Biochem Sci,* 37**,** 293-302.

BALLA, A. & BALLA, T. 2006. Phosphatidylinositol 4-kinases: old enzymes with emerging functions. *Trends Cell Biol,* 16**,** 351-61.

BANTSCHEFF, M., EBERHARD, D., ABRAHAM, Y., BASTUCK, S., BOESCHE, M., HOBSON, S., MATHIESON, T., PERRIN, J., RAIDA, M., RAU, C., READER, V., SWEETMAN, G., BAUER, A., BOUWMEESTER, T., HOPF, C., KRUSE, U., NEUBAUER, G., RAMSDEN, N., RICK, J., KUSTER, B. & DREWES, G. 2007. Quantitative chemical proteomics reveals mechanisms of action of clinical ABL kinase inhibitors. *Nat Biotechnol,* 25**,** 1035-44.

BERGER, K. L., KELLY, S. M., JORDAN, T. X., TARTELL, M. A. & RANDALL, G. 2011. Hepatitis C virus stimulates the phosphatidylinositol 4-kinase III alpha-dependent phosphatidylinositol 4-phosphate production that is essential for its replication. *J Virol,* 85**,** 8870-83.

BISHÉ, B., SYED, G. H., FIELD, S. J. & SIDDIQUI, A. 2012. Role of phosphatidylinositol 4-phosphate (PI4P) and its binding protein GOLPH3 in hepatitis C virus secretion. *J Biol Chem,* 287**,** 27637-47.

BLAGOVESHCHENSKAYA, A., CHEONG, F. Y., ROHDE, H. M., GLOVER, G., KNÖDLER, A., NICOLSON, T., BOEHMELT, G. & MAYINGER, P. 2008. Integration of Golgi trafficking and growth factor signaling by the lipid phosphatase SAC1. *J Cell Biol,* 180**,** 803-12.

BOJJIREDDY, N., BOTYANSZKI, J., HAMMOND, G., CREECH, D., PETERSON, R., KEMP, D. C., SNEAD, M., BROWN, R., MORRISON, A., WILSON, S., HARRISON, S., MOORE, C. & BALLA, T. 2014. Pharmacological and genetic targeting of the PI4KA enzyme reveals its important role in maintaining plasma membrane phosphatidylinositol 4-phosphate and phosphatidylinositol 4,5-bisphosphate levels. *J Biol Chem,* 289**,** 6120-32.

BUNTE, H., SCHENNING, M., SODAAR, P., BÄR, D. P., WIRTZ, K. W., VAN MUISWINKEL, F. L. & SNOEK, G. T. 2006. A phosphatidylinositol transfer protein alpha-dependent survival factor protects cultured primary neurons against serum deprivation-induced cell death. *J Neurochem,* 97**,** 707-15.

CARVOU, N., HOLIC, R., LI, M., FUTTER, C., SKIPPEN, A. & COCKCROFT, S. 2010. Phosphatidylinositol- and phosphatidylcholine-transfer activity of PITPbeta is essential for COPI-mediated retrograde transport from the Golgi to the endoplasmic reticulum. *J Cell Sci,* 123**,** 1262-73.

CHEN, R., XIE, R., MENG, Z., MA, S. & GUAN, K. L. 2019. STRIPAK integrates upstream signals to initiate the Hippo kinase cascade. *Nat Cell Biol,* 21**,** 1565-1577.

CLAYTON, E. L., MINOGUE, S. & WAUGH, M. G. 2013. Phosphatidylinositol 4-kinases and PI4P metabolism in the nervous system: roles in psychiatric and neurological diseases. *Mol Neurobiol,* 47**,** 361-72.

CONG, L., RAN, F. A., COX, D., LIN, S., BARRETTO, R., HABIB, N., HSU, P. D., WU, X., JIANG, W., MARRAFFINI, L. A. & ZHANG, F. 2013. Multiplex genome engineering using CRISPR/Cas systems. *Science,* 339**,** 819-23.

CRAVATT, B. F., WRIGHT, A. T. & KOZARICH, J. W. 2008. Activity-based protein profiling: from enzyme chemistry to proteomic chemistry. *Annu Rev Biochem,* 77**,** 383-414.

D'ANGELO, G., POLISHCHUK, E., DI TULLIO, G., SANTORO, M., DI CAMPLI, A., GODI, A., WEST, G., BIELAWSKI, J., CHUANG, C. C., VAN DER SPOEL, A. C., PLATT, F. M., HANNUN, Y. A., POLISHCHUK, R., MATTJUS, P. & DE MATTEIS, M. A. 2007. Glycosphingolipid synthesis requires FAPP2 transfer of glucosylceramide. *Nature,* 449**,** 62-7.

D'ANGELO, G., VICINANZA, M., DI CAMPLI, A. & DE MATTEIS, M. A. 2008. The multiple roles of PtdIns(4)P -- not just the precursor of PtdIns(4,5)P2. *J Cell Sci,* 121**,** 1955-63.

DE VRIES, K. J., WESTERMAN, J., BASTIAENS, P. I., JOVIN, T. M., WIRTZ, K. W. & SNOEK, G. T. 1996. Fluorescently labeled phosphatidylinositol transfer protein isoforms (alpha and beta), microinjected into fetal bovine heart endothelial cells, are targeted to distinct intracellular sites. *Exp Cell Res,* 227**,** 33-9.

DEL BEL, L. M. & BRILL, J. A. 2018. Sac1, a lipid phosphatase at the interface of vesicular and nonvesicular transport. *Traffic,* 19**,** 301-318.

DELAGE, E., PUYAUBERT, J., ZACHOWSKI, A. & RUELLAND, E. 2013. Signal transduction pathways involving phosphatidylinositol 4-phosphate and phosphatidylinositol 4,5-bisphosphate: convergences and divergences among eukaryotic kingdoms. *Prog Lipid Res,* 52**,** 1-14.

DIPPOLD, H. C., NG, M. M., FARBER-KATZ, S. E., LEE, S. K., KERR, M. L., PETERMAN, M. C., SIM, R., WIHARTO, P. A., GALBRAITH, K. A., MADHAVARAPU, S., FUCHS, G. J., MEERLOO, T., FARQUHAR, M. G., ZHOU, H. & FIELD, S. J. 2009. GOLPH3 bridges phosphatidylinositol-4-phosphate and actomyosin to stretch and shape the Golgi to promote budding. *Cell,* 139**,** 337-51.

DUMARESQ-DOIRON, K., SAVARD, M. F., AKAM, S., COSTANTINO, S. & LEFRANCOIS, S. 2010. The phosphatidylinositol 4-kinase PI4KIIIalpha is required for the recruitment of GBF1 to Golgi membranes. *J Cell Sci,* 123**,** 2273-80.

FOTI, M., AUDHYA, A. & EMR, S. D. 2001. Sac1 lipid phosphatase and Stt4 phosphatidylinositol 4-kinase regulate a pool of phosphatidylinositol 4-phosphate that functions in the control of the actin cytoskeleton and vacuole morphology. *Mol Biol Cell,* 12**,** 2396-411.

FUCHS, Y. F., EISLER, S. A., LINK, G., SCHLICKER, O., BUNT, G., PFIZENMAIER, K. & HAUSSER, A. 2009. A Golgi PKD activity reporter reveals a crucial role of PKD in nocodazole-induced Golgi dispersal. *Traffic,* 10**,** 858-67.

GODI, A., DI CAMPLI, A., KONSTANTAKOPOULOS, A., DI TULLIO, G., ALESSI, D. R., KULAR, G. S., DANIELE, T., MARRA, P., LUCOCQ, J. M. & DE MATTEIS, M. A. 2004. FAPPs control Golgi-to-cell-surface membrane traffic by binding to ARF and PtdIns(4)P. *Nat Cell Biol,* 6**,** 393-404.

GR, H., G, S. & RF, I. 2009. Immunocytochemical techniques reveal multiple, distinct cellular pools of PtdIns4P and PtdIns(4,5)P2. Biochem J.

GRABON, A., BANKAITIS, V. A. & MCDERMOTT, M. I. 2019. The interface between phosphatidylinositol transfer protein function and phosphoinositide signaling in higher eukaryotes. *J Lipid Res,* 60**,** 242-268.

GRABON, A., ORŁOWSKI, A., TRIPATHI, A., VUORIO, J., JAVANAINEN, M., RÓG, T., LÖNNFORS, M., MCDERMOTT, M. I., SIEBERT, G., SOMERHARJU, P., VATTULAINEN, I. & BANKAITIS, V. A. 2017. Dynamics and energetics of the mammalian phosphatidylinositol transfer protein phospholipid exchange cycle. *J Biol Chem,* 292**,** 14438-14455.

GRAMMEL, M. & HANG, H. C. 2013. Chemical reporters for biological discovery. *Nat Chem Biol,* 9**,** 475-84.

GYGI, S. P., RIST, B., GERBER, S. A., TURECEK, F., GELB, M. H. & AEBERSOLD, R. 1999. Quantitative analysis of complex protein mixtures using isotope-coded affinity tags. *Nat Biotechnol,* 17**,** 994-9.

HAMA, H., SCHNIEDERS, E. A., THORNER, J., TAKEMOTO, J. Y. & DEWALD, D. B. 1999. Direct involvement of phosphatidylinositol 4-phosphate in secretion in the yeast Saccharomyces cerevisiae. *J Biol Chem,* 274**,** 34294-300.

HAMILTON, B. A., SMITH, D. J., MUELLER, K. L., KERREBROCK, A. W., BRONSON, R. T., VAN BERKEL, V., DALY, M. J., KRUGLYAK, L., REEVE, M. P., NEMHAUSER, J. L., HAWKINS, T. L., RUBIN, E. M. & LANDER, E. S. 1997. The vibrator mutation causes neurodegeneration via reduced expression of PITP alpha: positional complementation cloning and extragenic suppression. *Neuron,* 18**,** 711-22.

HAMMOND, G. R., FISCHER, M. J., ANDERSON, K. E., HOLDICH, J., KOTECI, A., BALLA, T. & IRVINE, R. F. 2012. PI4P and PI(4,5)P2 are essential but independent lipid determinants of membrane identity. *Science,* 337**,** 727-30.

HAMMOND, G. R., MACHNER, M. P. & BALLA, T. 2014. A novel probe for phosphatidylinositol 4-phosphate reveals multiple pools beyond the Golgi. *J Cell Biol,* 205**,** 113-26.

HARDING, M. W., GALAT, A., UEHLING, D. E. & SCHREIBER, S. L. 1989. A receptor for the immunosuppressant FK506 is a cis-trans peptidyl-prolyl isomerase. *Nature,* 341**,** 758-60.

HAY, J. C., FISETTE, P. L., JENKINS, G. H., FUKAMI, K., TAKENAWA, T., ANDERSON, R. A. & MARTIN, T. F. 1995. ATP-dependent inositide phosphorylation required for Ca(2+)-activated secretion. *Nature,* 374**,** 173-7.

HAY, J. C. & MARTIN, T. F. 1993. Phosphatidylinositol transfer protein required for ATP-dependent priming of Ca(2+)-activated secretion. *Nature,* 366**,** 572-5.

HONG, A. W., MENG, Z., PLOUFFE, S. W., LIN, Z., ZHANG, M. & GUAN, K. L. 2020. Critical roles of phosphoinositides and NF2 in Hippo pathway regulation. *Genes Dev*.

HSU, N. Y., ILNYTSKA, O., BELOV, G., SANTIANA, M., CHEN, Y. H., TAKVORIAN, P. M., PAU, C., VAN DER SCHAAR, H., KAUSHIK-BASU, N., BALLA, T., CAMERON, C. E., EHRENFELD, E., VAN KUPPEVELD, F. J. & ALTAN-BONNET, N. 2010. Viral reorganization of the secretory pathway generates distinct organelles for RNA replication. *Cell,* 141**,** 799-811.

HUANG, S. M., MISHINA, Y. M., LIU, S., CHEUNG, A., STEGMEIER, F., MICHAUD, G. A., CHARLAT, O., WIELLETTE, E., ZHANG, Y., WIESSNER, S., HILD, M., SHI, X., WILSON, C. J., MICKANIN, C., MYER, V., FAZAL, A., TOMLINSON, R., SERLUCA, F., SHAO, W., CHENG, H., SHULTZ, M.,

RAU, C., SCHIRLE, M., SCHLEGL, J., GHIDELLI, S., FAWELL, S., LU, C., CURTIS, D., KIRSCHNER, M. W., LENGAUER, C., FINAN, P. M., TALLARICO, J. A., BOUWMEESTER, T., PORTER, J. A., BAUER, A. & CONG, F. 2009. Tankyrase inhibition stabilizes axin and antagonizes Wnt signalling. *Nature,* 461**,** 614-20.

HUGHES, W. E., WOSCHOLSKI, R., COOKE, F. T., PATRICK, R. S., DOVE, S. K., MCDONALD, N. Q. & PARKER, P. J. 2000. SAC1 encodes a regulated lipid phosphoinositide phosphatase, defects in which can be suppressed by the homologous Inp52p and Inp53p phosphatases. *J Biol Chem,* 275**,** 801-8.

ILE, K. E., KASSEN, S., CAO, C., VIHTEHLIC, T., SHAH, S. D., MOUSLEY, C. J., ALB, J. G., HUIJBREGTS, R. P., STEARNS, G. W., BROCKERHOFF, S. E., HYDE, D. R. & BANKAITIS, V. A. 2010. Zebrafish class 1 phosphatidylinositol transfer proteins: PITPbeta and double cone cell outer segment integrity in retina. *Traffic,* 11**,** 1151-67.

KAKUK, A., FRIEDLÄNDER, E., VEREB, G., KÁSA, A., BALLA, A., BALLA, T., HEILMEYER, L. M. & GERGELY, P. 2006. Nucleolar localization of phosphatidylinositol 4-kinase PI4K230 in various mammalian cells. *Cytometry A,* 69**,** 1174-83.

KAKUK, A., FRIEDLÄNDER, E., VEREB, G., LISBOA, D., BAGOSSI, P., TÓTH, G. & GERGELY, P. 2008. Nuclear and nucleolar localization signals and their targeting function in phosphatidylinositol 4-kinase PI4K230. *Exp Cell Res,* 314**,** 2376-88.

KAUFFMANN-ZEH, A., THOMAS, G. M., BALL, A., PROSSER, S., CUNNINGHAM, E., COCKCROFT, S. & HSUAN, J. J. 1995. Requirement for phosphatidylinositol transfer protein in epidermal growth factor signaling. *Science,* 268**,** 1188-90.

KOEHN, F. E., LONGLEY, R. E. & REED, J. K. 1992. Microcolins A and B, new immunosuppressive peptides from the blue-green alga Lyngbya majuscula. *J Nat Prod,* 55**,** 613-9.

KOEHN, F. E., MCCONNELL, O. J., LONGLEY, R. E., SENNETT, S. H. & REED, J. K. 1994. Analogues of the marine immunosuppressant microcolin A: preparation and biological activity. *J Med Chem,* 37**,** 3181-6.

LAPINSKY, D. J. 2012. Tandem photoaffinity labeling-bioorthogonal conjugation in medicinal chemistry. *Bioorg Med Chem,* 20**,** 6237-47.

LEMMON, M. A. 2008. Membrane recognition by phospholipid-binding domains. *Nat Rev Mol Cell Biol,* 9**,** 99-111.

LI, H., YANG, X., YANG, G., HONG, Z., ZHOU, L., YIN, P., XIAO, Y., CHEN, L., CHUNG, R. T. & ZHANG, L. 2014. Hepatitis C virus NS5A hijacks ARFGAP1 to maintain a phosphatidylinositol 4-phosphate-enriched microenvironment. *J Virol,* 88**,** 5956-66.

LIU, Y., BOUKHELIFA, M., TRIBBLE, E., MORIN-KENSICKI, E., UETRECHT, A., BEAR, J. E. & BANKAITIS, V. A. 2008. The Sac1 phosphoinositide phosphatase regulates Golgi membrane morphology and mitotic spindle organization in mammals. *Mol Biol Cell,* 19**,** 3080-96.

MATSUDAIRA, T., MUKAI, K., NOGUCHI, T., HASEGAWA, J., HATTA, T., IEMURA, S. I., NATSUME, T., MIYAMURA, N., NISHINA, H., NAKAYAMA, J., SEMBA, K., TOMITA, T., MURATA, S., ARAI, H. & TAGUCHI, T. 2017. Endosomal phosphatidylserine is critical for the YAP signalling pathway in proliferating cells. *Nat Commun,* 8**,** 1246.

NAKATSU, F., BASKIN, J. M., CHUNG, J., TANNER, L. B., SHUI, G., LEE, S. Y., PIRRUCCELLO, M., HAO, M., INGOLIA, N. T., WENK, M. R. & DE CAMILLI, P. 2012. PtdIns4P synthesis by PI4KIIIα at the plasma membrane and its impact on plasma membrane identity. *J Cell Biol,* 199**,** 1003-16.

NEMOTO, Y., KEARNS, B. G., WENK, M. R., CHEN, H., MORI, K., ALB, J. G., DE CAMILLI, P. & BANKAITIS, V. A. 2000. Functional characterization of a mammalian Sac1 and mutants exhibiting substrate-specific defects in phosphoinositide phosphatase activity. *J Biol Chem,* 275**,** 34293-305.

NILE, A. H., BANKAITIS, V. A. & GRABON, A. 2010. Mammalian diseases of phosphatidylinositol transfer proteins and their homologs. *Clin Lipidol,* 5**,** 867-897.

ODA, Y., OWA, T., SATO, T., BOUCHER, B., DANIELS, S., YAMANAKA, H., SHINOHARA, Y., YOKOI, A., KUROMITSU, J. & NAGASU, T. 2003. Quantitative chemical proteomics for identifying candidate drug targets. *Anal Chem,* 75**,** 2159-65.

OHASHI, M., JAN DE VRIES, K., FRANK, R., SNOEK, G., BANKAITIS, V., WIRTZ, K. & HUTTNER, W. B. 1995. A role for phosphatidylinositol transfer protein in secretory vesicle formation. *Nature,* 377**,** 544-7.

ONG, S. E., BLAGOEV, B., KRATCHMAROVA, I., KRISTENSEN, D. B., STEEN, H., PANDEY, A. & MANN, M. 2002. Stable isotope labeling by amino acids in cell culture, SILAC, as a simple and accurate approach to expression proteomics. *Mol Cell Proteomics,* 1**,** 376-86.

PRESCHER, J. A. & BERTOZZI, C. R. 2005. Chemistry in living systems. *Nat Chem Biol,* 1**,** 13-21.

RAJ, L., IDE, T., GURKAR, A. U., FOLEY, M., SCHENONE, M., LI, X., TOLLIDAY, N. J., GOLUB, T. R., CARR, S. A., SHAMJI, A. F., STERN, A. M., MANDINOVA, A., SCHREIBER, S. L. & LEE, S. W. 2011. Selective killing of cancer cells by a small molecule targeting the stress response to ROS. *Nature,* 475**,** 231-4.

RAN, F. A., HSU, P. D., WRIGHT, J., AGARWALA, V., SCOTT, D. A. & ZHANG, F. 2013. Genome engineering using the CRISPR-Cas9 system. *Nat Protoc,* 8**,** 2281-2308.

REISS, S., HARAK, C., ROMERO-BREY, I., RADUJKOVIC, D., KLEIN, R., RUGGIERI, A., REBHAN, I., BARTENSCHLAGER, R. & LOHMANN, V. 2013. The lipid kinase phosphatidylinositol-4 kinase III alpha regulates the phosphorylation status of hepatitis C virus NS5A. *PLoS Pathog,* 9**,** e1003359.

REISS, S., REBHAN, I., BACKES, P., ROMERO-BREY, I., ERFLE, H., MATULA, P., KADERALI, L., POENISCH, M., BLANKENBURG, H., HIET, M. S., LONGERICH, T., DIEHL, S., RAMIREZ, F., BALLA, T., ROHR, K., KAUL, A., BÜHLER, S., PEPPERKOK, R., LENGAUER, T., ALBRECHT, M., EILS, R., SCHIRMACHER, P., LOHMANN, V. & BARTENSCHLAGER, R. 2011. Recruitment and activation of a lipid kinase by hepatitis C virus NS5A is essential for integrity of the membranous replication compartment. *Cell Host Microbe,* 9**,** 32-45.

RIX, U. & SUPERTI-FURGA, G. 2009. Target profiling of small molecules by chemical proteomics. *Nat Chem Biol,* 5**,** 616-24.

ROHDE, H. M., CHEONG, F. Y., KONRAD, G., PAIHA, K., MAYINGER, P. & BOEHMELT, G. 2003. The human phosphatidylinositol phosphatase SAC1 interacts with the coatomer I complex. *J Biol Chem,* 278**,** 52689-99.

ROSS, P. L., HUANG, Y. N., MARCHESE, J. N., WILLIAMSON, B., PARKER, K., HATTAN, S., KHAINOVSKI, N., PILLAI, S., DEY, S., DANIELS, S., PURKAYASTHA, S., JUHASZ, P., MARTIN, S., BARTLET-JONES, M., HE, F., JACOBSON, A. & PAPPIN, D. J. 2004. Multiplexed protein quantitation in Saccharomyces cerevisiae using amine-reactive isobaric tagging reagents. *Mol Cell Proteomics,* 3**,** 1154-69.

ROUX, K. J., KIM, D. I., RAIDA, M. & BURKE, B. 2012. A promiscuous biotin ligase fusion protein identifies proximal and interacting proteins in mammalian cells. *J Cell Biol,* 196**,** 801-10.

ROY, A. & LEVINE, T. P. 2004. Multiple pools of phosphatidylinositol 4-phosphate detected using the pleckstrin homology domain of Osh2p. *J Biol Chem,* 279**,** 44683-9.

SALAZAR, G., CRAIGE, B., WAINER, B. H., GUO, J., DE CAMILLI, P. & FAUNDEZ, V. 2005. Phosphatidylinositol-4-kinase type II alpha is a component of adaptor protein-3-derived vesicles. *Mol Biol Cell,* 16**,** 3692-704.

SCHENNING, M., VAN TIEL, C. M., VAN MANEN, D., STAM, J. C., GADELLA, B. M., WIRTZ, K. W. & SNOEK, G. T. 2004. Phosphatidylinositol transfer protein alpha regulates growth and apoptosis of NIH3T3 cells: involvement of a cannabinoid 1-like receptor. *J Lipid Res,* 45**,** 1555-64.

SHADAN, S., HOLIC, R., CARVOU, N., EE, P., LI, M., MURRAY-RUST, J. & COCKCROFT, S. 2008. Dynamics of lipid transfer by phosphatidylinositol transfer proteins in cells. *Traffic,* 9**,** 1743-56.

SHI, H., ZHANG, C. J., CHEN, G. Y. & YAO, S. Q. 2012. Cell-based proteome profiling of potential dasatinib targets by use of affinity-based probes. *J Am Chem Soc,* 134**,** 3001-14.

SNOEK, G. T., BERRIE, C. P., GEIJTENBEEK, T. B., VAN DER HELM, H. A., CADEÉ, J. A., IURISCI, C., CORDA, D. & WIRTZ, K. W. 1999. Overexpression of phosphatidylinositol transfer protein alpha in NIH3T3 cells activates a phospholipase A. *J Biol Chem,* 274**,** 35393-9.

SPEERS, A. E. & CRAVATT, B. F. 2009. Activity-Based Protein Profiling (ABPP) and Click Chemistry (CC)-ABPP by MudPIT Mass Spectrometry. *Curr Protoc Chem Biol,* 1**,** 29-41.

SZENTPETERY, Z., VÁRNAI, P. & BALLA, T. 2010. Acute manipulation of Golgi phosphoinositides to assess their importance in cellular trafficking and signaling. *Proc Natl Acad Sci U S A,* 107**,** 8225-30.

TAHIROVIC, S., SCHORR, M. & MAYINGER, P. 2005. Regulation of intracellular phosphatidylinositol-4-phosphate by the Sac1 lipid phosphatase. *Traffic,* 6**,** 116-30.

TAKAHASHI, N., HAYANO, T. & SUZUKI, M. 1989. Peptidyl-prolyl cis-trans isomerase is the cyclosporin A-binding protein cyclophilin. *Nature,* 337**,** 473-5.

TAKAMATSU, S., NAGLE, D. G. & GERWICK, W. H. 2004. Secondary metabolites from marine cyanobacteria and algae inhibit LFA-1/ICAM-1 mediated cell adhesion. *Planta Med,* 70**,** 127-31.

TAN, J. & BRILL, J. A. 2014. Cinderella story: PI4P goes from precursor to key signaling molecule. *Crit Rev Biochem Mol Biol,* 49**,** 33-58.

TILLEY, S. J., SKIPPEN, A., MURRAY-RUST, J., SWIGART, P. M., STEWART, A., MORGAN, C. P., COCKCROFT, S. & MCDONALD, N. Q. 2004. Structure-function analysis of human [corrected] phosphatidylinositol transfer protein alpha bound to phosphatidylinositol. *Structure,* 12**,** 317-26.

TOLONEN, A. C. & HAAS, W. 2014. Quantitative proteomics using reductive dimethylation for stable isotope labeling. *J Vis Exp*.

TREMBLAY, J. M., UNRUH, J. R., JOHNSON, C. K. & YARBROUGH, L. R. 2005. Mechanism of interaction of PITPalpha with membranes: conformational changes in the C-terminus associated with membrane binding. *Arch Biochem Biophys,* 444**,** 112-20.

TÓTH, B., BALLA, A., MA, H., KNIGHT, Z. A., SHOKAT, K. M. & BALLA, T. 2006. Phosphatidylinositol 4-kinase IIIbeta regulates the transport of ceramide between the endoplasmic reticulum and Golgi. *J Biol Chem,* 281**,** 36369-77.

WALCH-SOLIMENA, C. & NOVICK, P. 1999. The yeast phosphatidylinositol-4-OH kinase pik1 regulates secretion at the Golgi. *Nat Cell Biol,* 1**,** 523-5.

WANG, Y. J., WANG, J., SUN, H. Q., MARTINEZ, M., SUN, Y. X., MACIA, E., KIRCHHAUSEN, T., ALBANESI, J. P., ROTH, M. G. & YIN, H. L. 2003. Phosphatidylinositol 4 phosphate regulates targeting of clathrin adaptor AP-1 complexes to the Golgi. *Cell,* 114**,** 299-310.

WEI, Y. J., SUN, H. Q., YAMAMOTO, M., WLODARSKI, P., KUNII, K., MARTINEZ, M., BARYLKO, B., ALBANESI, J. P. & YIN, H. L. 2002. Type II phosphatidylinositol 4-kinase beta is a cytosolic and peripheral membrane protein that is recruited to the plasma membrane and activated by Rac-GTP. *J Biol Chem,* 277**,** 46586-93.

WIEDEMANN, C., SCHÄFER, T. & BURGER, M. M. 1996. Chromaffin granule-associated phosphatidylinositol 4-kinase activity is required for stimulated secretion. *EMBO J,* 15**,** 2094-101.

WIRTZ, K. W. 1991. Phospholipid transfer proteins. *Annu Rev Biochem,* 60**,** 73-99.

WONG, K., MEYERS DDR & CANTLEY, L. C. 1997. Subcellular locations of phosphatidylinositol 4-kinase isoforms. *J Biol Chem,* 272**,** 13236-41.

XIE, Y., DING, Y. Q., HONG, Y., FENG, Z., NAVARRE, S., XI, C. X., ZHU, X. J., WANG, C. L., ACKERMAN, S. L., KOZLOWSKI, D., MEI, L. & XIONG, W. C. 2005. Phosphatidylinositol transfer protein-alpha in netrin-1-induced PLC signalling and neurite outgrowth. *Nat Cell Biol,* 7**,** 1124-32.

XIE, Z., HUR, S. K., ZHAO, L., ABRAMS, C. S. & BANKAITIS, V. A. 2018. A Golgi Lipid Signaling Pathway Controls Apical Golgi Distribution and Cell Polarity during Neurogenesis. *Dev Cell,* 44**,** 725-740.e4.

YODER, M. D., THOMAS, L. M., TREMBLAY, J. M., OLIVER, R. L., YARBROUGH, L. R. & HELMKAMP, G. M. 2001. Structure of a multifunctional protein. Mammalian phosphatidylinositol transfer protein complexed with phosphatidylcholine. *J Biol Chem,* 276**,** 9246-52.

ZEWE, J. P., WILLS, R. C., SANGAPPA, S., GOULDEN, B. D. & HAMMOND, G. R. 2018. SAC1 degrades its lipid substrate PtdIns4. *Elife,* 7.

ZHANG, L. H., LONGLEY, R. E. & KOEHN, F. E. 1997. Antiproliferative and immunosuppressive properties of microcolin A, a marine-derived lipopeptide. *Life Sci,* 60**,** 751-62.

Chapter 4: Conclusion

4.1 Conclusion and Future Directions

Two decades of intense research has established the Hippo pathway as a cardinal regulator of organ size and tissue homeostasis, and expanded its core kinase cascade into a complex signaling network integrating a diverse repertoire of extracellular inputs (Yu and Guan, 2013). The Hippo pathway is recognized as among the top ten most somatically altered signaling pathways in cancer (Sanchez-Vega et al., 2018), and continuing to decode the front lines of its molecular regulation is an area of considerable basic and translational interest. While several studies have identified various components of the peripheral Hippo network, the upstream regulation of MST1/2 and the MAP4Ks remains an ongoing area of inquiry. The work described in this thesis details both the target identification of a small molecule YAP inhibitor and the discovery of a novel PI4P-mediated regulatory mechanism modulating Hippo pathway activity.

Our work first identifies Microcolin B (MCB), a bioactive lipopeptide with known immunosuppressive and antiproliferative effects (Zhang et al., 1997), as a novel molecule targeting the Hippo pathway, through a phenotypic screen for compounds inducing YAP phosphorylation. We describe the structural optimization of MCB to yield its more potent analog VT01454 and demonstrate the specific cytotoxicity of VT01454 towards uveal melanoma cell lines harboring YAP-dependent mutations, as opposed to their YAP-independent counterparts. We subsequently describe a novel role for PITPα/β in Hippo pathway regulation resulting from an unbiased target identification, validating PITPα/β as the unequivocal biochemical targets of VT01454 through a combination of bioorthogonal and molecular biology approaches. Though various groups have previously conducted syntheses, structure-activity relationship, and mechanism-of-action studies of the Microcolins and their analogs (Koehn et al., 1994, Koehn et al., 1992, Takamatsu et al., 2004, Zhang et al., 1997), our study is the first to not only identify a biological macromolecule with high Microcolin binding affinity, but also a major cell signaling pathway specifically and potently modulated by Microcolin treatment.

Our observations that depletion of plasma membrane PI4P induces YAP phosphorylation suggests that PI4P normally regulates the Hippo pathway in an inhibitory manner (Figure 4.1). Modulation of the

Hippo pathway by intracellular PI4P levels is a previously unknown mechanism, and provides new clues in decoding the complex regulation of MST1/2 and the MAP4Ks. In light of another recent finding from our lab that PI(4,5)P2-dependent recruitment of NF2 regulates osmotic stress-induced activation of the Hippo pathway (Hong et al., 2020), it will be both interesting and imperative to explore how these dual mechanisms (i.e. Hippo pathway-inhibitory PI4P and Hippo pathway-activating PI(4,5)P2 regulation) act in concert with one another to jointly modulate Hippo pathway activation. Our BioID data utilizing P4M-SidMx2 as 'bait' protein, as well as the biochemical validation following MS analysis, demonstrate that TNIK/MAP4K7 and MINK1/MAP4K6 are potential PI4P-interacting or at the very least PI4P-proximal proteins. Given that this interaction or proximity occurs in an NF2-independent manner, one plausible model would be that PI(4,5)P2 and PI4P respectively regulate NF2 and the MAP4Ks in parallel, and in response to distinct extracellular signals.

Our collective findings present intriguing new prospects for the Hippo signaling research field. First, the identification and characterization of MCB provides proof-of-concept of YAP's druggability in cancers exhibiting YAP hyperactivity and YAP dependence, and suggests potential clinical implications of future optimization of the Microcolins as anticancer therapeutic strategies. Second, the successful target identification of VT01454 reveals an unprecedented PITP-PI4P signaling axis modulating Hippo pathway activation, providing novel insights into the still-unclear mechanisms of MST1/2 and MAP4K regulation. Finally, the burgeoning concept of a phospholipid-regulated Hippo pathway opens up a new perspective of phospholipids in tissue homeostasis, and raises the possibility of YAP as a druggable node in cancers exhibiting lipid kinase hyperactivity as well as diseases characterized by phospholipid dysregulation; and, conversely, lipid kinases as novel therapeutic targets in YAP-driven cancers.

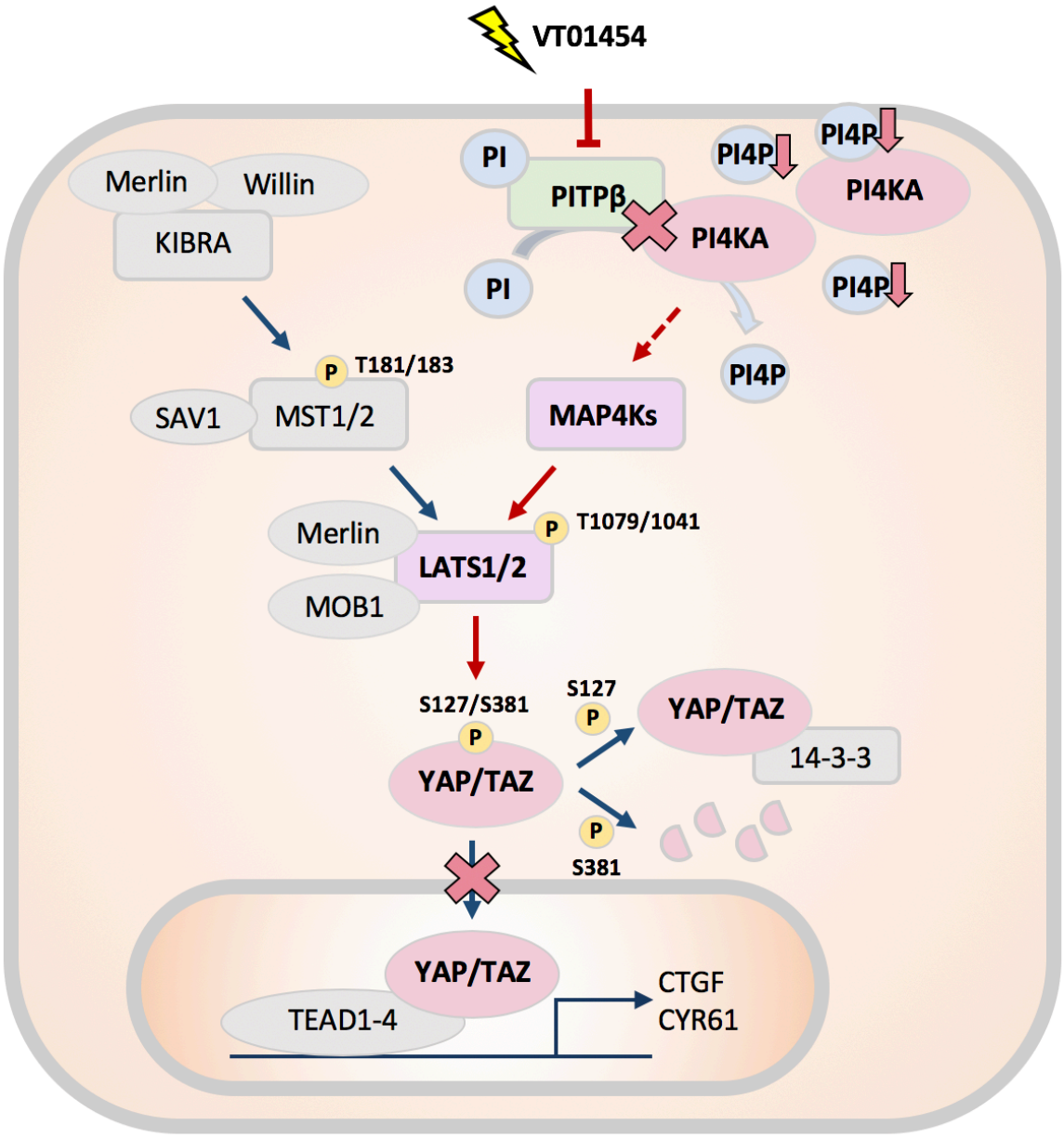

Figure 4.1: Summarizing Model Depicting Mechanism of Action for a Novel YAP Inhibitor. VT01454 inhibits PITPβ, inhibiting its presentation of PI to PI4KA and thereby reducing PI4P at the plasma membrane. PI4P depletion induces Lats1/2 and YAP phosphorylation, and we currently hypothesize that PI4P binds to the MAP4Ks in an inhibitory manner, releasing the MAP4Ks upon VT01454 treatment to allow activation and phosphorylation of Lats1/2.

4.2 References

HONG, A. W., MENG, Z., PLOUFFE, S. W., LIN, Z., ZHANG, M. & GUAN, K. L. 2020. Critical roles of phosphoinositides and NF2 in Hippo pathway regulation. *Genes Dev*.

KOEHN, F. E., LONGLEY, R. E. & REED, J. K. 1992. Microcolins A and B, new immunosuppressive peptides from the blue-green alga Lyngbya majuscula. *J Nat Prod,* 55**,** 613-9.

KOEHN, F. E., MCCONNELL, O. J., LONGLEY, R. E., SENNETT, S. H. & REED, J. K. 1994. Analogues of the marine immunosuppressant microcolin A: preparation and biological activity. *J Med Chem,* 37**,** 3181-6.

SANCHEZ-VEGA, F., MINA, M., ARMENIA, J., CHATILA, W. K., LUNA, A., LA, K. C., DIMITRIADOY, S., LIU, D. L., KANTHETI, H. S., SAGHAFINIA, S., CHAKRAVARTY, D., DAIAN, F., GAO, Q., BAILEY, M. H., LIANG, W. W., FOLTZ, S. M., SHMULEVICH, I., DING, L., HEINS, Z., OCHOA, A., GROSS, B., GAO, J., ZHANG, H., KUNDRA, R., KANDOTH, C., BAHCECI, I., DERVISHI, L., DOGRUSOZ, U., ZHOU, W., SHEN, H., LAIRD, P. W., WAY, G. P., GREENE, C. S., LIANG, H., XIAO, Y., WANG, C., IAVARONE, A., BERGER, A. H., BIVONA, T. G., LAZAR, A. J., HAMMER, G. D., GIORDANO, T., KWONG, L. N., MCARTHUR, G., HUANG, C., TWARD, A. D., FREDERICK, M. J., MCCORMICK, F., MEYERSON, M., VAN ALLEN, E. M., CHERNIACK, A. D., CIRIELLO, G., SANDER, C., SCHULTZ, N. & NETWORK, C. G. A. R. 2018. Oncogenic Signaling Pathways in The Cancer Genome Atlas. *Cell,* 173**,** 321-337.e10.

TAKAMATSU, S., NAGLE, D. G. & GERWICK, W. H. 2004. Secondary metabolites from marine cyanobacteria and algae inhibit LFA-1/ICAM-1 mediated cell adhesion. *Planta Med,* 70**,** 127-31.

YU, F. X. & GUAN, K. L. 2013. The Hippo pathway: regulators and regulations. *Genes Dev,* 27**,** 355-71.

ZHANG, L. H., LONGLEY, R. E. & KOEHN, F. E. 1997. Antiproliferative and immunosuppressive properties of microcolin A, a marine-derived lipopeptide. *Life Sci,* 60**,** 751-62.